NTNU
Norwegian University of
Science and Technology

Compositional Simulation of Tertiary Gas Injection Experiments

Investigating the Effects of Capillary Pressure

Sunniva Bjerkehagen Smeland

Summary

Tertiary gas injection is an enhanced oil recovery method, which aims for reducing residual oil in a reservoir by gas injection. Tertiary gas injection induces a system of three-phase where water, oil and gas flow simultaneously in a porous medium. Three-phase flow increases the complexity of a system, as dynamic rock properties such as capillary pressure and especially relative permeability are difficult to measure. Because of the insecurities related to measured three-phase relative permeability, mathematical and empirical models are often used to calculate three-phase relative permeability rather than implementing experimentally obtained data.

Datasets from two tertiary gas injection experiments conducted on Bentheimer sandstone cores are studied. Equilibrium gas to the existing oil was injected in Experiment 1, while dry separator gas was injected in Experiment 2. Experiment 1 was kept under certain conditions to avoid mass transfer between components. In Experiment 2 mass transfer through vaporization was present and an additional water recovery was observed in the experimental production data.

In this study the mentioned tertiary gas injection experiments are simulated and history matched with a compositional model applying a three-phase relative permeability model called Extended Stone model 1. The overall goal of this study is to achieve a satisfactory match for all fluid recoveries with an emphasis on capillary pressure effects. The extra water recovery observed in Experiment 2 is attempted history matched by applying gas-water capillary pressure data, which is usually not implemented in a typical simulation model applying Extended Stone model 1. In addition to the simulation

study, the current thesis contains a comprehensive literature review on three-phase relative permeability and tertiary gas injection publications.

A match of all fluid recoveries is achieved for both experiments. Extended Stone model 1 together with applying gas-water capillary pressure data seem to be sufficient for history matching the two different tertiary gas injection experiments where one include mass transfer and one does not. The match of Experiment 2 is however not perfect, which indicates that Extended Stone model 1 is not ideal for simulation of mass transfer experiments on a component level. However, the simulations show promising results and can be an indicator for future developments of simulation of three-phase flow.

Sammendrag

Tertiær gassinjeksjon er en økt oljeutvinningsmetode som reduserer residuell olje i et reservoar ved gassinjeksjon. Tertiær gassinjeksjon introduserer et trefasesystem hvor vann, olje og gass strømmer samtidig i et porøst medium. Trefasestrømning øker kompleksiteten til et system ved at dynamiske bergparametre som kapillærtrykk og spesielt relativ permeabilitet blir vanskeligere å måle. Grunnet usikkerhetene ved målte trefase relative permeabiliteter, blir matematiske og empiriske modeller ofte brukt for å regne ut threefase relativ permeabilitet istedenfor å implementere eksperimentelle oppnådde data.

Datasett fra to tertiære gassinjeksjonseksperimenter utført på Bentheimer sandsteinkjerner er studert. Likevektsgassen til den eksisterende oljen ble injisert i Eksperiment 1, mens tørr seperatorgass ble injisert i Eksperiment 2. Eksperiment 1 ble holdt under visse betingelser for å unngå masseovergang mellom komponenter. I Eksperiment 2 skjedde masseovergang gjennom vaporisering og en ekstra vannproduksjon ble observert i de eksperimentelle produksjonsdataene.

I dette studiet blir de nevnte tertiære gassinjeksjonseksperimentene simulert og historietilpasset med en komposisjonell modell med bruk av en trefase relativitetsmodell kalt Extended Stone model 1. The overordnede målet til studiet er å oppnå en tilpasning for all fluidproduksjonene med ekstra vekt på kapillærtrykkseffekter. Den ekstra vannproduksjonen observert i Eksperiment 2 er forsøkt historietilpasset ved å anvende gassvannkapillærtrykk som vanligvis ikke er brukt i typiske simuleringsmodeller som anvender Extended Stone model 1. I tillegg til simuleringstudiet, inneholder denne mas-

iv

teroppgaven et omfattende litteraturgjennomgang på trefase relative permeabilitetsmodeller og tertiær gassinjeksjon.

En historietilpasning for alle fluidproduksjoner er oppnådd for begge eksperimenter. Extended Stone model 1 sammen med anvendelse av gass-vann kapillærtrykksdata virker tilstrekkelig for å historietilpasse to forskjellige tertiære gassinjeksjonseksperimenter hvor den ene opplever masseoverføring og den andre gjør ikke. Tilpasningen til Eksperiment 2 er likevel ikke perfekt, noe som indikerer at Extended Stone model 1 ikke er ideell for å simulere masseoverføringseksperimenter på komponentnivå. Likevel viser simuleringene lovende resultater og kan være en indikator for videre utvikling av simulering på trefasestrømning.

Preface

This thesis is written as the final project of my master's degree in Petroleum Engineering and Geoscience at the Norwegian University of Science and Technology in Trondheim, Norway. The work behind this thesis is done during the spring semester of 2018 with preliminary studies conducted the previous semester, fall of 2017.

The work is intended for people interested in simulation of tertiary gas injection and especially for those with particular interest in handling three-phase data. Basic knowledge of reservoir simulation is recommended, but not required.

Trondheim, June 11, 2018

Sunniva Bjerkehagen Smeland

Acknowledgment

I would like to thank my supervisor Professor Odd Steve Hustad for supporting me during the work of this thesis. He has always helped me along the way while encouraging me to find the answers myself. This is very much appreciated!

Further, I would like to thank my fellow student, Anton Lindahl, who has conducted a similar study as me. He has contributed with great discussions and input in times of frustration.

<div align="right">S.B.S.</div>

Contents

List of Figures

List of Tables

Chapter 1

Introduction

1.1 Background

Enhanced oil recovery (EOR) methods are widely used in the petroleum industry to-
day. The goal of EOR is to increase oil recovery after primary and secondary recovery
processes. Tertiary gas injection is a central EOR method which reduces residual oil by
convective flow and mass transfer.

Tertiary gas injection induces a system of three-phase flow where water, oil and gas
flow simultaneously in a porous medium. As a consequence, prediction of tertiary gas
injection efficiency becomes very complex as three-phase flow is not understood in all
details with high insecurities in experimental three-phase data. In addition, if compo-
sitional effects are present during a displacement process, a black oil model will not
suffice for simulation and a compositional model is necessary. This is a more complex
model as it requires fluid properties for each associated hydrocarbon.

There are many studies on simulation of tertiary gas injection experiments in the liter-
ature. A shared issue of several of these studies is the emphasis/focus of three-phase
relative permeability data. Studies on three-phase relative permeability was first pub-
lished in 1941 when Leverett and Lewis (1941) conducted a study on experimentally ob-
tained three-phase data. What most authors of this subject have concluded is the high

insecurity of experimentally obtained three-phase relative permeability data of the intermediate phase. Because of this, mathematical models are used instead to calculate three-phase relative permeability. Two of the most famous models are the ones from Stone which he developed in 1970 and 1973.

Hustad and Holt (1992) did a study on tertiary gas injection where they conducted two different immiscible vertical displacement experiments on Bentheimer cores. The cores were waterflooded down to residual oil saturation before gas was injected into the cores. The experiments included different types of injection gas. In Experiment 1, the equilibrium gas to the oil is injected and a dry separator gas is injected in Experiment 2. Hustad and Holt (1992) observed how displacement mechanisms contributed to oil recovery.

Hustad and Holt (1992) simulated the experiments. The simulation models were compositional applying a three-phase relative permeability model. The authors initially applied the models of Stone to simulate the experiments, but the models proved inapplicable. The simulation results deviated from the experimental production data, and a new and improved model was necessary. Hustad developed a modified version of the first Stone model, Extended Stone model 1, which was successful and history matched Experiment 1 very well. However, the authors still had issues with Experiment 2, especially for the water recovery.

Because the injection gas in Experiment 2 was dry, vaporization effects were present during the displacement. This can been seen as an additional water recovery in the experimental production data. Extended Stone model 1 was unable to capture the extra water recovery and a match between simulated and experimental water recovery was not achieved. Hustad later suspected that the simulation model was unable to history match the experiment because it did not apply gas-water capillary pressure data. This hypothesis is tested out in the current study on Hustad and Holt's experiments. By applying gas-water capillary pressure at a time vaporization effects are present, can a water match be obtained? In addition to matching the water recovery, effort is also given to the oil and gas match.

Because the experiments are a case of three-phase flow, there is a choice whether the intermediate-wet phase relative permeability should be entered in the model with experimentally obtained values or calculated. Because three-phase relative permeability is difficult to measure, three-phase relative permeability models are often used instead. The Stone models are two of those models. The literature study in this thesis focuses on the different established three-phase relative permeability models and their assumptions. Tertiary gas injection and two field cases are also presented to enlighten the potential of this EOR method.

1.2 Objectives

The main objectives of this Master's thesis are:

1. History match Hustad and Holt's Experiment 1 and 2.

2. Investigate the effects of capillary pressure on fluid recovery.

3. Confirm the reliability on relative permeability data:

    (a) Experimentally obtained two-phase relative permeability.

    (b) Calculated three-phase relative permeability.

1.3 Limitations

This study involves simulation of three-phase flow. The major limitation will be the insecurity related to three-phase relative permeability and the chosen three-phase relative permeability model, Extended Stone model 1. As mentioned, three-phase flow has been highly discussed in the literature as it is not completely understood. These insecurities can lead to simulation errors.

Another limitation is the amount of available data. As the simulation models are compositional, there is a higher complexity within the input data than in a black oil model. Experiment 1, where there are no vaporization effects, could be modelled by the black

oil model. However, the available data is not sufficient for constructing a black oil
model for Experiment 1, and can then not be made for a comparison study.

1.4   Approach

To history match Experiment 1 and 2, simulation models for each respective experi-
ment are constructed for the compositional simulation tool, Eclipse. Prior to achiev-
ing a match for Experiment 2, a match of Experiment 1 is obtained to establish cor-
rect dynamic rock properties such as relative permeability and oil-water capillary pres-
sure curve level. When Experiment 1 is matched, Experiment 2 is matched with the
gas-water capillary pressure curve joined at the oil-water curve at the water saturation
where vaporization effects are suspected to be present. Experiment 1 is then simu-
lated with the joined capillary pressure curve to observe whether this has an effect on
the fluid recovery match. Ideally the joining will not affect Experiment 1 as the joining
should occur at a water saturation never reached by Experiment 1.

1.5   Structure of the Report

The report is structured as follows:

- Chapter 2: Literature study on tertiary gas injection.

- Chapter 3: Literature study on reservoir simulation. General description of im-
  portant factors in reservoir simulation and a thorough study on three-phase rel-
  ative permeability, equation of state and other important factors such as hystere-
  sis. (The theory described in this chapter is not directly used in this study.)

- Chapter 4: Detailed description of Hustad and Holt's experiments (the experi-
  ments which this thesis is based on). Provide experimental data and simulation
  results of the past study.

- Chapter 5: Description of theory which is directly used in this thesis. The theory
  in this chapter is a continuation of the theory presented in Chapter 3.

- Chapter 6: This chapter explains the process of achieving a match of Experiment 1 and 2. A surprising obstacle is included and discussed.

- Chapter 7: This chapter presents the results of the experiments, saturation profiles at different times and a sensitivity study.

- Chapter 8: This chapter provides a thorough discussion of all aspects of the project. How can the changes to input data be justified, the reliability of the chosen model, were the objectives reached?

- Chapter 9: This chapter sums up the results and includes the conclusion.

- Chapter 10: Provide suggestions for further work.

Chapter 2

Tertiary Gas Injection

"Enhanced oil recovery (EOR) is oil recovery by the injection of materials not normally present in the reservoir" (Lake, 1996). EOR consists of many categories where tertiary gas injection falls into one of them. Not surprisingly, tertiary gas injection involves injection of gas into a reservoir that has experienced a secondary waterflood. Tertiary gas injection can either be a miscible or immiscible process depending on the type of injection gas. Some tertiary gas injections processes are the Double Displacement Process (DDP), Second Contact Water Displacement (SCWD) and Water-Alternating-Gas (WAG). This chapter will limit itself to immiscible processes as the experiments simulated in this study is considered immiscible. Although studies show immiscible gas injection processes perform better Taheri2013, it is not always possible to achieve an immscible process because of the required pressure, minimum miscibility pressure.

There lies a great potential for increased oil recovery when applying tertiary gas injection. Laboratory studies conducted by Kantzas et al. (1988) show that tertiary gas injection can increase oil recovery from 40% - 60% after a waterflood to almost 100% in the presence of connate water. Field studies have reported oil recoveries from 85% - 95% (Carlson, 1988), (Fassihi and Gillham, 1993).

Establishment of an oil bank is an important feature during an immiscible tertiary gas injection process. Several factors on both a macro- and microscopic level affect the

displacement efficiency and the formation of the oil bank. Injection and production
rates, reservoir dip angle and three-phase relative permeability are examples on fac-
tors affecting the system on a macroscopic level. Wettability, capillary pressure and the
spreading coefficient affect the system on a microscopic pore level.

2.1   Macroscopic Mechanisms

Because the water, oil and gas have different densities, they will naturally segregate be-
cause of gravity. This can potentially lead to poor sweep efficiency during gas injection
if the gas simply avoids displacing the oil by flowing above it. This will be a problem in
horizontal reservoirs where the gas will be allowed to flow above the oil. If gas is injected
from the top in a vertical reservoir, the gas is forced to "touch" the oil and possibly dis-
place it if the operational parameters are optimal. Gas can also be injected from the
bottom and push the oil upwards naturally by the assistance of gravity.

Ren et al. (2005) conducted a simulation study on gravity assisted tertiary gas injection
where they investigated the effects of injection and production rates, dip angle and oil
relative permeability on an East Fault Block of Hawkins Oilfield. They concluded that
a high dipping reservoir is favorable because in addition to less phase-segregation is-
sues, a higher dipping angle increase the optimal injection rate. A higher injection rate
reduces the production time, which is a crucial aspect in the petroleum industry. Too
high injection rate can lead to fingering of the gas, and should therefore be carefully
decided.

Ren et al. also looked at oil relative permeability. Because the system becomes three-
phase when gas is injected, the oil relative permeability is a three-phase parameter.
Instead of using unreliable experimentally obtained three-phase data, a model based
on two-phase data was used to calculate the oil relative permeability in the simulation
model. Ren et al. tested four different three-phase relative permeability models: Stone
model 1 and 2 proposed by Stone (1970, 1973) and the Linear Isoperm Model and the
Segregated Model both developed by Baker (1988). Ren et al. found that Stone model 2

was the most suited correlation for the tertiary gas injection experiment because of its ability to show gradually decreasing oil saturation in the region above the established oil bank and a longer transition zone (Ren et al., 2005). Comparing the different models and what oil relative permeability the models yield, Ren et al. (2005) could conclude how different oil relative permeabilities result in different oil recovery.

2.2 Microscopic Mechanisms

Ren et al. (2005) investigated microscopic mechanisms such as wettability and the spreading coefficient. The authors observed how a water-wet reservoir was beneficial because water will occupy the smaller pores leaving the oil in the bigger pores. The spreading coefficient is in relation to the formation of a continuous oil film, which will connect residual oil blobs left in the water swept region to the oil bank and consequently lead to higher oil recovery. The spreading coefficient is defined by the interfacial tension between the present phases. The spreading coefficient for oil over water is defined as:

$$S_{o/w} = \sigma_{gw} - \sigma_{go} - \sigma_{ow}$$

Where σ_{gw}, σ_{go}, σ_{ow} are the interfacial tensions between gas-water, gas-oil and oil-water respectively. Ren et al. concluded that a positive spreading coefficient was favorable as it will make the oil spread as a thin film between the gas and water phase during injection of gas. Figure 2.1 illustrates the establishment of an continuous oil film when gas enters a pore.
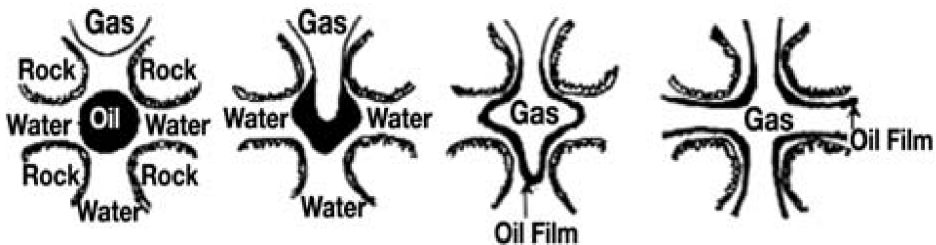
Figure 2.1: Spreading of oil phase, (Ren et al., 2005)

2.3   Case A: Abu Dhabi

The following case comes from the conference paper: "24 years of successful EOR through Immiscible Tertiary Gas Injection" by Madathil et al. (2015).

During the production life of a reservoir, the water cut can eventually reach unacceptable values. If the water cut is considered too high and improving the oil mobility is deemed necessary, an EOR method applied to the reservoir could be beneficial. This was the case for the company Total and two of their offshore reservoirs in Abu Dhabi (Madathil et al., 2015). After several laboratory and simulation studies, it was decided that immiscible injection of natural gas was the best choice to enhance the recovery. This was partly supported because of available lean gas from a deeper located reservoir in the same field. The field consists of five reservoirs in total, but only two of them were subjected to EOR.

The two reservoirs come from the same carbonate field, but they have different properties. One reservoir has pressure support from an aquifer and good vertical communication. From this point on, this reservoir is called reservoir #3 (similar to the original report). The other reservoir consists of 14 layers from 3 to 20 meters thick separated by anhydrite layers with no aquifer support. This reservoir will be called reservoir #2.

Conducting Special Core Analysis Laboratory (SCAL) and Pressure-Volume-Temperature (PVT) experiments showed how hydrocarbon gas injection could induce a swelling effect in the undersaturated oil in reservoir #3. The volume increase of oil could lead to an oil relative permeability increase of 16.0% while also reduce the oil viscosity (Pearce et al., 2013). This was promising results for the initially good reservoir that had suddenly experience a rapid increase in water cut. To verify the laboratory results, they conducted a field study using a pilot well injecting from the bottom.

The main goal of the pilot well was to prove the effect of dry gas injection in reservoir #3 and provide a performance plan for further installment of other injection wells. In addition, the pilot well was installed to gather field data to improve the tuning of

the Equation of State (EOS) for the compositional simulator chosen for the simulation study. Because of the updip location of the nearby production wells, the gas migrated naturally towards them. However, only one of the nearby producers experienced gas breakthrough. This was later concluded to be a cause of a high permeability streak. Because of this streak, another pilot well was necessary to obtain enough data to develop a full field EOR plan. The second pilot well resulted in gas breakthrough in all nearby producers and a better understanding of gas migration was possible.

Considering the performance of the pilot wells and other simulation studies, the oil increment was estimated to be 2% - 3% of initial oil in place (Pearce et al., 2013). The benefits of gas injection were swelling effect, reduction of residual saturation, stripping of lighter components from oil and reduction of the bottom hole pressure value due to more gas in the well column (Pearce et al., 2013). Madathil et al. (2015) also illustrates microscopic mechanisms showing the same spreading tendency of the oil phase described by Ren et al. (2005). As gas enters a water-wet pore with an oil bubble in the center, oil spreads between the gas- and water-phase and connects to other oil-phase regions. Also in agreement with Ren et al. (2005), a low injection rate improves the sweep efficiency by avoiding fingering effects.

After several years of production with injection of gas from below in reservoir #3, the recovery surpassed 50% with still an ongoing effect (Madathil et al., 2015), (Pearce et al., 2013). This was very good results considering the reservoir in question was carbonate. After 15 years of applying immiscible gas injection, 3% of the original oil in place had been additionally recovered. Full field gas injection in reservoir #2 was still under evaluation at the time the report was published. All in all, the authors concluded immiscible tertiary gas injection was successful for reservoir #3.

The authors observed how severe heterogeneity caused problems for the gas as it is much more sensitive to it than water. This is partly the reason why reservoir #3 showed better results than the more heterogeneous reservoir #2. Based on this case study, immiscible tertiary gas injection is a favorable choice if the target reservoir is not severely heterogeneous, it has good vertical communication and with a gas source nearby.

2.4   Case B: California

The following case comes from the conference paper: "A Case History on California Immiscible Gas Injection, Elk Hills Field" by Kostelnik et al. (2017).

The Elk Hills field has a long history of production since its discovery in 1919. Because of pressure support from a salt water aquifer in the Eastern Shallow Oil Zone, pressure maintenance lasted long. When the pressure eventually depleted, further drive mechanisms were supported by gravity drainage and gas cap expansion applying updip gas injection. Widespread immiscible gas injection started in 2005.

The structure of the field is dominated by an anticline with a flat crest and dipping flanks. The area discussed in the report is situated at the northern flank where the downdip aquifer is located. The double displacement process was applied and resulted in an incremental recovery of 12% to date (2017). Because of the heterogeneity of the reservoir, further recovery is expected if the gas injection keeps progressing through other intervals of the reservoir (Kostelnik et al., 2017).

Before the full field gas injection project initiated in 2005, the reservoir had been subjected to gas injection to offer pressure support. However, analyses showed that the gas recovered additional oil and reduced the residual oil to water from 20% to 10% to gas (Kostelnik et al., 2017). Because of this observation, immiscible gas injection was considered a favorable choice for enhanced oil recovery in 2005.

In the early stages of the production life, pressure depletion was the main drive mechanism of the reservoir. However, when the pressure dropped significantly, aquifer influx controlled the production. To prevent the aquifer from moving past the producers, gas injection/recycling was introduced. Even though the gas injection/recycling increased the oil recovery, the gas rate was below the voidage rate and stable injection rate. The engineering team decided to strip the injection gas from nitrogen to introduce an immiscible displacement process. As a result, the oil-water contact moved down-dip and the reservoir pressure increased.

Similarly to the case study by Madathil et al. (2015), heterogeneity is considered unfavorable in an immiscible gas injection process. It can lead to earlier gas breakthrough and reduce sweep efficiency. However, the other benefits of the immiscible displacement in this study overshadowed this weakness and the project is considered a success.

2.5 Lessons Learned

The case studies show the potential of a successful immiscible tertiary gas injection process. Problems can occur with severe heterogeneity. It seems from the case of Kostelnik et al. (2017) that injection rate increased when the displacement was made immiscible. Higher injection rate is more stable, but other studies also shows a better formation of the oil bank (Ren et al., 2005). Immiscible gas injection can either be updip or downdip. If there was/is available pressure support from a nearby water aquifer downdip, updip gas injection can be a good solution to lower the oil-water contact.

While laboratory studies have showed oil recoveries up to 100%, field studies have not yet reached those levels.

Chapter 3

Reservoir Simulation

Because this thesis is mainly a simulation study, this chapter will present different aspects of reservoir simulation and how one build a simulation model before the actual work of this study is presented in Chapter 6.

Reservoir simulation plays an important part in the oil and gas industry today. The goal of reservoir simulation is to predict the performance of porous media or reservoirs, and optimize the development of a potential field. Reservoir simulation is the application of a physical and mathematical model that will estimate the behavior of reservoir fluids by a set of equations with certain assumptions. Reservoir simulation is either on full field scale or on laboratory core scale.

Reservoir simulation is not the only method of predicting reservoir performance. Other ways are analogy, conducting experiments and pure mathematical methods. An analogical approach to predicting performance consists of comparing a mature reservoir to the target reservoir. The two reservoirs are considered having similar features, which make the behavior of the mature reservoir a possible forecast to the target reservoir. An experimental method involves measuring physical properties in a laboratory, such as pressure and saturation, to later scale the properties up to reservoir standards. Lastly, the mathematical method involves using equations to predict performance. This method is an integral part of reservoir simulation.

An applicable and ready reservoir simulation model has gone through several steps before it is considered a valid model. Prior to constructing the simulation model, physical reservoir data is gathered and validated. With the necessary physical data at hand, a mathematical model is constructed consisting of a system of partial differential equations. The physical and mathematical models are then discretized to obtain a numerical model, which will be developed into computer codes and algorithms to solve the system. When such a model is constructed, it can be history matched to already existing production data and physical properties to tune the simulation model to predict performance more accurately. Figure 3.1 illustrates the steps of building a reservoir simulation model.
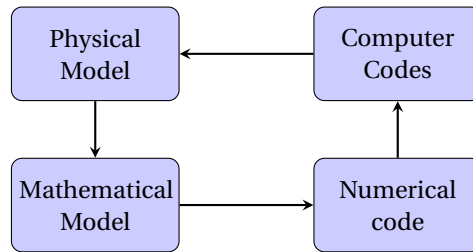
Figure 3.1: Reservoir Simulation Steps, (Chen, 2007).

A simulation model consists of keywords with corresponding input data, and it is the keywords that order the computer to treat the data in a specific way. This means that the physical reservoir data, the inputs to the model, can be handled in many different ways depending on the chosen keywords. This chapter will go through different reservoir classifications, rock properties, fluid properties and history matching.

3.1   Reservoir Classifications

Classification of the reservoir is very important as there are many different ways to construct a fitting simulation model. Typical reservoir classifications include, among others, what type of fluid is present and recovery process, number of dimensions, number of phases, coordinate system and rock structure. These distinct characteristics are im-

portant to specify as they have a large impact on simulation of fluid recovery.

3.1.1 Fluid Model

The type of fluid model will affect the performance of a reservoir and it is important to the construction of a model. The fluid models model the dynamic behavior of the hydrocarbons and other fluids during the life of the field, (Schlumberger, 2016b). Commercial simulators, such as Eclipse, will have an option to specify this, such as black oil, thermal and compositional. A black oil model is used when there are no compositional effects during production of a reservoir. This means there is no mass transfer between fluids and this model is considered conventional. In a black oil model there is a liquid oil phase and a vapor gas phase. A compositional model, on the other hand, consider compositional effects. This increases the complexity of the system because this type of model incorporates molecular data for each individual hydrocarbon which is controlled by an equation of state (EOS). A thermal model allows the temperature and pressure to vary during a simulation.

3.1.2 Model Dimensions

The number of dimensions of the reservoir is connected to the grid system of the reservoir. The grid system can either be zero-, one-, two- or three-dimensional and this affects the directions the fluids are allowed to flow.

In a zero-dimensional system, 0D, the model consists of one cell or block. This kind of system cannot distinguish flow directions, but it can determine fluid production, initial fluid distribution, pressure and average saturation.

In a one-dimensional system, 1D, the model allows for flow in only one direction. This makes a 1D model unequipped for representing a reservoir field. It is however very useful on laboratory scale representing smaller cores.

A two-dimensional system, 2D, is better when representing areal flooding. It allows for flow in two directions. A three-dimensional model, 3D, is a more recent development

as an effect of more powerful computers. 3D allows for full field simulation.

3.1.3   Coordinate System

The coordinate system is also linked to the grid system. The coordinate system can either be rectangular, cylindrical or spherical depending on what kind of flow system the reservoir has.

3.1.4   Number of Phases

Number of phases (one, two or three) and phase behavior is also an important aspect of reservoir simulation. Incorrect modelling of the interaction between the phases and the properties of the phases themselves can possibly yield great erroneous predictions. Number of phases and phase behavior is controlled by a set of equations, called equations of state. This will be discussed further later in this chapter.

3.1.5   Rock Structure and Response

The rock structure and the rock response are also features that needs to be addressed in a simulation model. The reservoir can be single porosity, dual porosity or dual porosity/permeability. Not having a single porosity system is only an option when the reservoir is fractured.

3.2   Rock Properties

Rock properties in reservoir engineering can be divided into two groups: static and dynamic. Static rock properties are porosity, pore size, rock compressibility and permeability. Dynamic properties are fluid saturation, wettability, relative permeability and capillary pressure (Satter and Iqbal, 2015).

Two of the most important dynamic rock properties in a simulation model are relative permeability and capillary pressure. Relative permeability and capillary pressure are treated simultaneously in a simulation model as they both are functions of phase saturations. The number of phases of the system has great impact of the treatment of

relative permeability and capillary pressure data.

To make it more structural, the explanation of the treatment of relative permeability and capillary pressure will be divided into separate sections below. Capillary pressure is not discussed in similar detail as relative permeability.

3.2.1   Relative Permeability

When there are several phases flowing in a porous medium, it is termed as a multiphase flow system. In such a system, the relative permeability is a dimensionless measure of the effective permeability of one of the present phases. Relative permeability indicates the ability of a fluid to flow in the presence of other fluids. The relative permeability is the ratio between the effective permeability of one particular phase at a certain saturation and the absolute permeability to that phase at 100% saturation. Effective permeability is a measure of the preferentially flow of a particular fluid when there are other fluids present. Absolute permeability is a measure of the ability to flow through a porous medium when there is only one phase present. The term is devised from Darcy's equation to fit multiphase flow conditions (PERM Inc, a). Relative permeability can be expressed as such:

$$k_{ri} = \frac{k_i}{k}$$

Where i=w, g, o and k_i is the effective permeability of phase i and k is absolute permeability.

Relative permeability is a function of phase saturation. The phase saturations are linked by one important equation, $S_w + S_o + S_g = 1$. In a two-phase system, the properties (i.e. relative permeability etc) are one-dimensional and there is only one independent saturation. One-dimensional means the property (relative permeability) is a function of one phase-saturation only. In a simulation model, if there is zero gas saturation, $S_g = 0$, properties are either functions of water saturation, S_w, or oil saturation, $S_o = 1 - S_w$. In a three-phase system there are two independent saturations and the properties can be

either one- or two-dimensional. Properties are two-dimensional if they are functions of two phase-saturations.

Applying relative permeability data in reservoir simulation is important because relative permeability represents the flow of the different fluids in a reservoir. There are however multiple ways of treating this kind of data, and the chosen method will have an effect on prediction of fluid production. As mentioned, relative permeability is a function of phase-saturations. Because of this, relative permeability is entered in a simulation model using saturation functions. Relative permeability can then, dependent on which saturation function one implements, be either dependent on one or two phase-saturations, making them either one- or two-dimensional. These dimensions are not to be confused with grid dimensions discussed earlier. The saturation functions inserted in a simulation model are tables of phase saturations with corresponding relative permeability data (and capillary pressure).

There is typically more than one phase present in a hydrocarbon reservoir, making it necessary to measure relative permeabilities. There are several established methods of measuring two-phase relative permeability data that are considered to yield valid data. However, for a three-phase system, the process of measuring is not fully understood because of the system's complexity. To compensate for the poor measurement methods, mathematical and empirical correlations based on two-phase data are used instead.

Consider a water-wet three-phase system where there is no contact between gas and water. In such a system, the water- and gas relative permeability are commonly assumed to be a function of their own saturation only. The oil relative permeability would, on the other hand, be a function of both water and gas saturation. Because the water- and gas relative permeability are functions of a single saturation, they can be measured as they would be in a two-phase system. The oil relative permeability cannot.

It is common to illustrate three-phase oil relative permeability in a triangular graph to show the dependencies on both saturations. Figure 3.2 illustrates typical tendencies of three-phase oil relative permeabilities. The figure shows an area where the oil is mo-

bile, and it is in this area one can plot the oil relative permeability as oil isoperms (lines of constant relative permeability). Because of the experimental difficulties with three-phase flow, a simulation model often implements a method of calculating three-phase oil relative permeability instead of inserting experimentally obtained data.
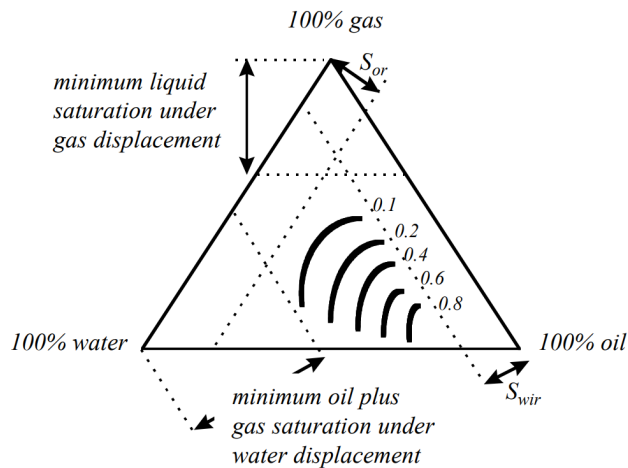
Figure 3.2: Oil isoperms in a ternary diagram, (Kleppe, 2017)

3.2.1.1 Calculating Three-Phase Oil Relative Permeability

Calculating three-phase oil relative permeability, k_{ro}, can be done according to many different models. The simplest method is to say that k_{ro} is the product of the oil relative permeability in water, k_{row}, and the oil relative permeability in gas, k_{rog}. However, this is not very representative as limiting saturations are not necessarily the same in two- and three-phase flow, (Kleppe, 2017).

Through time, many different studies have been conducted trying to estimate, and maybe more important, understand three-phase relative permeability. Some studies are solely an investigation on three-phase relative permeability, while other studies provided correlations and models for estimating three-phase relative permeability. Corey et al. (1956) were the first to publish a three-phase relative permeability model in 1956, soon to be followed by others like Naar and Wygal (1961), Land (1968) and Stone (1970, 1973). What the authors all have in common is that they try to understand how three-

phase relative permeability curves behave in different wettability systems. From this basis they construct correlations to calculate three-phase relative permeability when measuring three-phase data, particularly the oil relative permeability, is a challenge. What these authors agree on is the assumption that in a water-wet system, the wetting (water)- and non-wetting (gas) phases are only functions of their own saturations, not affected by other phases present. Oil, the intermediate phase, is however dependent on both the wetting- and the non-wetting phase. This assumption is however contradicted in other early literature like Leverett and Lewis (1941) and Spronsen (1982).

Leverett and Lewis (1941) conducted a study on three-phase relative permeability in 1941. They concluded, in contrast to later assumptions just mentioned, that both oil- and gas relative permeability are affected by other phase saturations than their own. However, in agreement with later models, the three-phase water relative permeability is concluded to only be a function of its own phase saturation. They saw that the minimum water saturation was similar for displacement experiments in a two- and three-phase systems. They also discovered, when plotting three-phase relative permeability data in a ternary diagram, a three-phase flowing region. Their research was tremendously important for the following three-phase relative permeability investigations. Leverett & Lewis did however not consider hysteresis effects, making their two-phase data not suited for later use for estimation of three-phase oil relative permeability.

As briefly mentioned, Corey et al. (1956) published their investigations on three-phase relative permeability in water-wet systems in 1956. Similarly to other authors, they displayed their findings in ternary diagrams, but also presented ways of calculating both water- and oil relative permeability based on experimentally obtained gas relative permeability. Unlike Leverett and Lewis (1941), they did not ignore hysteresis effects. Instead they overcame it by using different core specimens for each saturation point (Manjnath and Honarpour, 1984). They concluded that gas relative permeability curves obtained when water was present were identical when water was absent. Because gas relative permeability is independent of other phases, gas isoperms are straight curves parallel to the gas iso-saturation values. Three-phase water relative permeability was

assumed to be independent of other phases than its own.

Saraf and Fatt (1967) used in 1967 nuclear magnetic resonance to measure both two- and three-phase relative permeability. They arrived at the same conclusion as Leverett and Lewis (1941) and Corey et al. (1956) that three-phase water relative permeability is a function only of its own phase saturation and that three-phase oil relative permeability is dependent on both water and oil saturations (thus also gas saturation). Three-phase gas was found to depend on total liquid saturation, thus saying the gas isoperms should be straight lines, just like Corey et al. (1956) concluded as well. However, the experimental error to gas was high because of very low relative permeability values and caution should therefore be given to the conclusions made.

Spronsen (1982) came to a conclusion different from the authors just mentioned. He did agree that three-phase oil relative permeability is a function of all present phases, but what differs him from the others is that he concluded the same for water. Spronsen applied the centrifuge method to measure three-phase relative permeability data, which he concluded was a reliable method of measuring three-phase data. His study only focused on water and oil, so gas measurements were not a part of his study. Spronsen's conclusion on three-phase water relative permeability dependency is agreed by other authors like Caudle et al. (1951), Reid (1956) and Donaldson et al. (1966). These conclusions can be found in the comparison study conducted by Manjnath and Honarpour (1984).

What Leverett and Lewis (1941), Corey et al. (1956), Saraf and Fatt (1967) and Spronsen (1982) concluded was taken into account when others constructed correlations and models for estimating three-phase relative permeability. However, most of the models disregard Spronsen's conclusion on water relative permeability, and a common assumption is that three-phase oil relative permeability is the only phase dependent on other phases.

Today, the models proposed by Stone (1970, 1973) are popular among the reservoir engineers. The simulation model in this report applies a modified version of the first Stone

model, and because of this, the Stone models, along with the modified version, will be discussed and explained so the reader will understand how the three-phase oil relative permeability is treated. The modified version will be discussed in a separate chapter.

3.2.1.2 Stone Model 1

This section is rewritten material from the article "Probability Model for Estimating Three-Phase Relative Permeability" written by Stone in 1970, (Stone, 1970).

Stone model 1 is the first model given by Herbert L. Stone for calculating three-phase oil relative permeability. He saw the need for determining this kind of data mathematically as the established experimental procedures for measuring three-phase data were deemed unreliable.

Stone suggested the use of two sets of two-phase data to obtain oil relative permeability. By interpolating between these two data sets, one can reach a region of three-phase. The method was verified by observing how interpolated values agreed with available experimental three-phase data. Stone limited himself to a water-wet system, although his findings could be said to regard oil-wet systems as well.

The data required to calculate three-phase oil relative permeability, k_{ro}, is from two sets of two-phase data: oil-water and oil-gas. From this data one has oil relative permeability in water, k_{row}, water relative permeability, k_{rw}, oil relative permeability in gas, k_{rog}, and gas relative permeability, k_{rg}. Hysteresis effects are taken into account by switching between drainage and imbibition curves if necessary. There are however limitations to handle complex saturation histories.

The model is based on the channel flow theory. The channel flow theory states that in any flow channel there is at most only one mobile fluid. The wetting phase of the system occupies the smaller pores of the system, while the non-wetting phase is located in the bigger ones. The intermediate phase separates the two phases. As a consequence, this theory also says that at equal water saturations, the microscopic fluid distribution at the

oil-water interface will be identical in a water-oil system and in a water-oil-gas system as long as change in water saturation is the same in both cases (increasing/decreasing). What does this imply? This means that the water relative permeability, k_{rw}, and the water-oil capillary pressure, P_{cow}, in a three-phase system is only a function of water saturation and that they are the same for both a three- and two-phase system. This also extends to the oil-gas relationship.

Stone treats connate water and residual oil as immobile fluids. With this, normalized fluid saturations are defined as:

$$S_o^* = \frac{S_o - S_{om}}{1 - S_{wc} - S_{om}}$$ (3.1)

(for $S_o > S_{om}$)

$$S_w^* = \frac{S_w - S_{wc}}{1 - S_{wc} - S_{om}}$$ (3.2)

(for $S_w > S_{wc}$)

$$S_g^* = \frac{S_g}{1 - S_{wc} - S_{om}}$$ (3.3)

Where,

- S_i^* = normalized saturations, i = o, g, w

- S_{om} = minimum value of residual oil saturation

- S_{wc} = connate water saturation

If S_o^* is 100%, k_{ro} is also 100%. If S_o^* is decreasing, k_{ro} also decreases, but in greater degree. To make sure k_{ro} decreases in a non-proportional manner, a factor, β, is multiplied with the normalized saturation. Whether k_{ro} is decreasing due to increased water or gas, is controlled by having β as two separate and independent functions of water, $\beta_w = \beta_w(S_w)$, and gas, $\beta_g = \beta_g(S_g)$. The relationship then becomes:

$$k_{ro} = S_o^* \cdot \beta_w \cdot \beta_g$$

Where β_w and β_g are as follows:

$$\beta_w = \frac{k_{row}}{1 - S_w^*} \tag{3.4}$$

$$\beta_g = \frac{k_{rog}}{1 - S_g^*} \tag{3.5}$$

A special case occurs when $S_w \leq S_{wc}$. In this situation, k_{ro}, is defined to be a unique function of gas saturation regardless of the water saturation. Physically this means that the oil saturation needs to behave like the connate water, thus being immobile at a certain level. If this is the case, gas-oil relative permeability data measured in the absence of connate water can be used to determine β_g.

There is a limitation to the original Stone models that others have tried to fix. This modification has improved Stone model 1 and 2 in such a way that when people refer to the Stone models today in reservoir simulation, it is actually the modified versions of Aziz (1979). Aziz modified both Stone models.

The limitation is as follows: Only if endpoint relative permeabilities are equal to one, the original models reduce to the two-phase data. To overcome this issue and to create a smooth transition to two-phase data, Aziz suggested the use of absolute permeability as the basis for calculating oil relative permeability, and the modification to Stone model 1 can be formulated as equation 3.6:

$$k_{ro} = k_{rowc} \cdot S_o^* \cdot \{\frac{k_{row}/k_{rowc}}{(1 - S_w^*)}\} \cdot \{\frac{k_{rog}/k_{rowc}}{(1 - S_g^*)}\} = k_{rowc} \cdot S_o^* \cdot F_w \cdot F_g \tag{3.6}$$

With:

$$F_w = \frac{\beta_w}{k_{rowc}} = \frac{k_{row}}{k_{rowc} \cdot (1 - S_w^*)}$$

$$F_g = \frac{\beta_g}{k_{rowc}} = \frac{k_{rog}}{k_{rowc} \cdot (1 - S_g^*)}$$

Where k_{rowc} is the value of the oil relative permeability in the presence of connate water only. Equation 3.6 is the one used for simulations with Stone's first model in Eclipse Simulation Tool.

3.2.1.3   Stone Model 2

This section is rewritten material from the article "Estimation of Three-Phase Relative Permeability and Residual Oil Data" written by Stone in 1973, (Stone, 1973).

Stone model 1 certainly has shortcomings, resulting in a revised version Stone came up with himself three years later after he published Stone model 1. Stone claims this version improves the estimation of three-phase oil relative permeability data with the same basis of two sets of two-phase relative permeability data. An advantage of Stone model 2 is how it can provide estimates of oil residuals in the three-phase region, not needing this data as an input as Stone model 1 do.

Stone claims this new and improved model provides estimates in better agreement with experimental data, especially in the region of low oil saturation. Similarly to Stone model 1, this method is also regarded applicable to an oil-wet system where water is the intermediate phase, thus making water the targeted relative permeability to estimate. Stone model 2 is also based on the channel flow theory discussed earlier.

This second model offers a new relationship between three-phase relative permeability and two-phase data:

$$k_{ro} + k_{rw} + k_{rg} = (k_{row} + k_{rwo}) \cdot (k_{rog} + k_{rgo}) \tag{3.7}$$

As for Stone model 1, relative permeability data for water and gas is the same for a two- and three-phase system. Rearranging equation 3.7, the oil relative permeability in a three-phase system can be calculated:

$$k_{ro} = (k_{row} + k_{rw}) \cdot (k_{rog} + k_{rg}) - k_{rw} - k_{rg} \tag{3.8}$$

If this equation yields a negative k_{ro}, it implies complete blockage of oil, simply indicating $k_{ro} = 0$.

Aziz (1979) also developed a modified version of Stone model 2 with the use of absolute permeability. Again, Aziz' formula is the one used for Stone's second model in Eclipse Simulation Tool. The formulation for three-phase oil relative permeability becomes equation 3.9:

$$k_{ro} = k_{rowc} \left[\left(\frac{k_{row}}{k_{rowc}} + k_{rwo} \right) \cdot \left(\frac{k_{rog}}{k_{rowc}} + k_{rgo} \right) - k_{rw} - k_{rg} \right] \tag{3.9}$$

3.2.1.4   Recent Three-Phase Relative Permeability Model Studies

A more recent study on three-phase relative permeability is the one by Pejic and Maini (2003). In 2003, Pejic and Maini conducted a comprehensive study on experimental and theoretical developments on three-phase relative permeability. The authors have compared several models of estimating the oil relative permeability in a three-phase system.

A reoccurring issue with evaluating three-phase relative permeability models are the insecurities in obtained experimental data. To overcome this, Pejic and Maini have screened different data sets for reliability and completeness to ensure representative data. Pejic and Maini found that no models predicted three-phase oil relative permeability with high accuracy, however there are some models that are better than others.

To see whether the models could predict reasonable three-phase oil relative permeabilities, Pejic and Maini needed four relative permeability curves from two-phase oil-water and oil-gas displacements: k_{row}, k_{rwo}, k_{rog} and k_{rgo}. Not all published experimental data sets consisted of the necessary curves, making the works of Maini et al. (1990), Oak (1990) and Donaldson et al. (1966) the only data used for testing the different correlations.

Donaldson et al.'s data set stem from gas displacement tests on oil and water. Maini et al. measured three-phase relative permeability at elevated temperatures using the steady- and unsteady-state method in a water-wet system. Oak's data set is of an intermediate-wet system. Oak applied the steady-state method.

Careful considerations were given when selecting the three-phase relative permeability models to test. Pejic and Maini chose models where they had all the necessary data the models required. The chosen models also needed to have showed promising results compared to experimental data applied in previous studies. Pejic and Maini chose the models by Hirasaki (Dietrich and Bondor (1976)), Aziz (1979), Baker (1988), Pope (Delshad and Pope (1989)), Kokal and Maini (1990), Goodyear and Townsley (Balbinski et al. (1999)) and Blunt (1999). As already mentioned, the models of Aziz are modified versions of the Stone models.

Pejic and Maini came up with a model to quantify the accuracy of each model for one particular experimental data set. The sum of squared deviations between experimental and calculated values of three-phase relative permeabilities are expressed as such:

$$\sum DEV = \sum_{i=1}^{n} (k_{ro,exp,i} - k_{ro,calc,i})^2 \qquad (3.10)$$

Where the constant n is the total number of experimental data points for a given experimental data set. This means $\sum DEV$ only should be compared within the same data set. Table 3.1 summarizes the results. None of the models were the better choice for all three data sets. There are however some models that stick out and perform better

Table 3.1: Values of $\sum DEV$ of the oil relative permeability models, (Pejic and Maini, 2003)

		Experimental Data Set		
		Donaldson & Dean 1966	Maini et al. 1990	Oak 1991
Model	Hirasaki 1976	0.09344	0.45020	0.09574
	Aziz & Settari-1 1979	0.05305	0.04196	0.08359
	Aziz & Settari-2 1979	0.09168	0.46770	0.09816
	Baker 1988	0.03864	0.40546	0.06198
	Pope 1989	0.03536	0.67184	0.06503
	Kokal & Maini 1989	0.03820	0.02773	0.09491
	Goodyear & Townsley 1999	1.05187	0.39000	0.06179
	Blunt 1999	0.07519	0.43240	0.02080

than others. By highlighting the three best models within each data set, three different models are one of the top three in two of the data sets. Baker's model for Donaldson et. al. and for Oak. Kokal and Maini for Donaldson et. al. and Oak. And Goodyear and Townsley for Maini et al. and Oak. Models performing poorly were Hirasaki's and Aziz' second model. Pejic and Maini do however express how Hirasaki's and Aziz' models might work well on other data sets. Pejic and Maini conclude that models that works well on water-wet systems perform poorly in intermediate-wet systems.

A modified version of Stone model 1 is the one implemented in this study. Because of this, a closer examination of the results of Aziz' results are provided.

Pejic and Maini presented the results of the different models with the experimental data. One can clearly see a strong tendency of oil isoperms in a water-wet system being concave towards the oil apex (S_o = 1.0). This can also be observed in other literature such as Manjnath and Honarpour (1984). Anyway, Baker's method with linear oil isoperms prove to be a better estimate for two of the data sets (one of them being

intermediate-wet). In Bakers's own study, the experimental data sets shows linear oil isoperms (Baker, 1988). Baker found having more straight oil isoperms proved a better fit and is the basis for developing his own models: saturation-weighted interpolation and true-linear interpolation, both of which are highly appreciated for their simplicity. Baker (1988) also compared three-phase relative permeability models with his own proposed methods. Similarly to Pejic and Maini (2003), he concluded linear oil isoperms are better than the models proposed by Stone. However, if one studies the results of Stone model 1 in Pejic and Maini (2003)'s paper, one can observe how the model fits quite well at lower oil saturations (actually being the second best model for Maini et al.'s dataset). The deviations are greater at higher oil isoperms, where the model produces oil isoperms with greater concavity compared to the experimental data. Figure 3.3 shows the fit of Stone model 1 (Aziz (1979)) with Maini et al.'s data set. Even though linear oil isoperms might have greater deviations locally as may be seen in a ternary diagram, it has the benefit of neither grossly over- or underestimating oil recovery. Although Baker's models might not estimate relative permeability accurately according to physics, they may prove to be a better choice because deviations from experimental relative permeabilities are smaller in total and will have less of an erroneous effect on simulated recovery data.
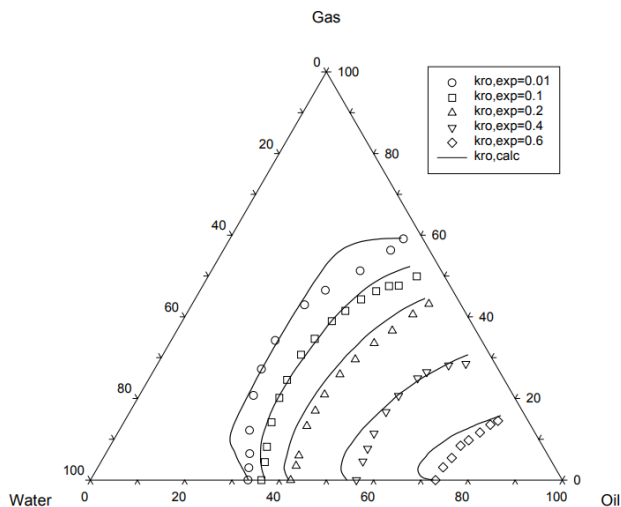
Figure 3.3: Stone model 1 for Maini et. al. data set, (Pejic and Maini, 2003).

The benefit of Baker's linear models are more clearly shown in his own study, (Baker, 1988). When comparing different models to the provided data set, the Stone models are far off. Figure 3.4 illustrates the deviations between calculated and experimental data.
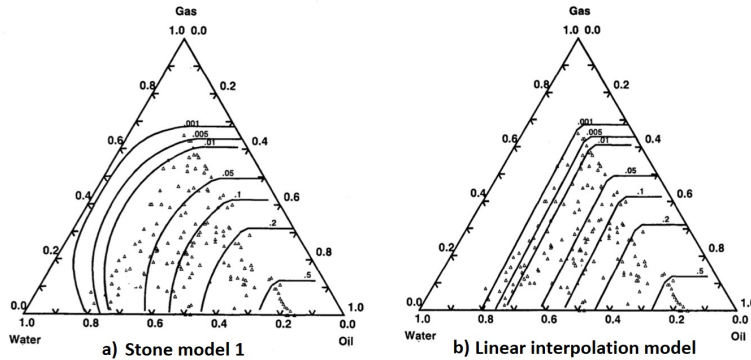
Figure 3.4: Comparison of Stone model 1 and Linear Interpolation model, (Baker, 1988).

Another person who considered Baker's straight oil isoperms was Martin J Blunt. When Ren et al. (2005) simulated their tertiary gas injection experiments as mentioned in Chapter 2, they wanted to use a three-phase relative permeability model proposed by Blunt in 2000. However, Blunt's model was not available in their simulation tool and they had to settle for the Stone and Baker models. Blunt (2000) developed an empirical three-phase relative permeability model that allows for different saturation paths, changes in hydrocarbon composition and trapping of oil, water and gas. Blunt defined the relative permeabilities as unique functions of a flowing saturation, making the model fit for predicting the behavior of any saturation change sequence (Blunt, 2000).

Blunt listed three main limitations among the available models and studies to date. First, most of the models were developed for a water-wet medium. As can be seen in the study by Pejic and Maini (2003), the different models were never suitable for both water- and intermediate-wet datasets. Blunt also claimed many models did not account for trapping of oil and gas phases for any displacement sequence. Lastly Blunt

commented how models tended to model relative permeability at low oil saturations badly. This is especially bad considering enhanced oil recovery methods happen at lower oil saturations.

Blunt developed a model to overcome the mentioned limitations. His model is based on saturation-weighted averages of two-phase relative permeability data, which was first proposed by Baker (1988). To allow for oil and gas trapping, Blunt included the work of Land (1968) and Carlson (1981). To accurately model three-phase relative permeability at a low oil saturation, Blunt applies a model for oil layer drainage that allows for extrapolation to low saturations. The model is extended to ensure smooth changes in relative permeability with changing oil and gas composition.

Blunt tested his model on water-wet Berea cores and showed how including oil trapping and layer drainage improved the predictions of three-phase relative permeability. Blunt was able to predict three-phase relative permeability for any saturation path, reservoir wettability and hydrocarbon composition using two-phase data (Blunt, 2000). Blunt's model was also tested in Pejic and Maini's study. If one studies the results of their investigation in Table 3.1, one can see how Blunt's model (initally published in 1999) performed best on Oak's dataset.

Determining which three-phase relative permeability model to use seems like a question of trial and error. One model can be efficient for one data set while creating substantial errors in another. The Stone models are still widely used today even though it is said to produce erroneous oil recoveries. Hustad and Holt's modified version of Stone model 1 considered Baker's recommendation on straight oil isoperms. This version will be explained i Chapter 5. After a comprehensive study on three-phase relative permeability models, one observation is clear. The most promising models are the ones considering the saturation weighted average model proposed by Baker (1988).

3.2.2   Capillary Pressure

Capillary pressure is the pressure difference between two immiscible phases. The pressure difference arises at the interface between the phases due to capillary forces caused by surface tension existing at the boundaries of the phases. Capillary forces, together with gravity, control the fluid distribution in a porous medium, which again have an effect on production of the present fluids. Capillary pressure is an opposing force for fluid transport, meaning it can have both a positive and negative effect on fluid recovery (PERM Inc, b). Capillary pressure, P_c is related to wettability and is defined according to the next equation:

$$P_c = P^{nw} - P^w$$

Where nw and n stands for non-wetting and wetting, respectively. There are three main methods of measuring capillary pressure and they are all deemed reliable yielding representative data. The methods are: Mercury Injection, Centrifuge Method and Porous Plate Method.

Before capillary pressure curves are implemented in a simulation model, the curves need to be scaled to correct conditions if they were measured at different conditions. However, capillary pressure between fluids is often neglected by a reservoir engineer and is set to 0 in simulation models. On a full reservoir field scale, it is common to believe capillary pressures have very little effect on recovery.

Capillary End Effect

An important aspect and potential issue in coreflooding experiments is capillary end effects. Capillary end effects influence calculation of relative permeability and residual saturations (?). The outlet of a core is often set to zero capillary pressure and this can lead to trapping of the wetting phase close to the outlet. This means that in a water-wet system, capillary end effects occur because of a discontinuity in capillarity of the water seen as an accumulation of water close to the outlet. With this "falsely" high water saturation near the outlet, the corresponding measured relative permeability will be not

be representative value.

Capillary end effects will be particularly visible in smaller cores because a bigger percentage of the core will be affected by the phenomenon.

3.2.3 Hysteresis

Hysteresis occurs when a property, like capillary pressure, depend on the direction of change of an independent variable, like saturation (PERM Inc, c). Hysteresis means that capillary pressure and relative permeability are affected by the saturation change history of a porous medium.

In a two-phase system, there is only one independent phase saturation. As a consequence, there are only two directions of saturation change, i.e. decreasing or increasing (Alizadeh and Piri, 2014). In a three-phase system, saturation history is more complicated as there are two independent phase saturations. This leads to several combinations of saturation paths and would yield multiple capillary pressure- and relative permeability curves if it is accounted for and applied in a simulation model.

Alizadeh and Piri (2014) did research on saturation history on both two- and three-phase systems in water-wet sandstones. He concluded that, in a three-phase system, it is only the three-phase gas relative permeability that is significantly influenced by saturation change history. Alizadeh and Piri observed that three-phase oil relative permeability is independent of saturation change while saturation change only has a minor effect on water relative permeability. This is however in contrast to what Hustad and Holt (1992) found when they measured three-phase oil isoperms with two different initial phase saturations. They concluded the oil isoperms were process dependent.

3.3 Fluid Properties and Phase Behavior

Fluid properties are related to the phase behavior of the reservoir. Phase behavior is the behavior of vapor, liquid and solids as a function of pressure, temperature and compo-

sition (volume) (Whitson and Brule, 2000). For a reservoir engineer, pressure, volume and temperature (PVT) relation is of great importance when calculating oil and gas reserves, evaluating enhanced oil recovery methods and production estimation (goals of reservoir simulation).

In systems of gas injection, a black-oil model might be insufficient to capture the process properly if there is mass transfer between the phases. If vaporization effects are present, a compositional model is necessary to describe the phase behavior accurately. Defining phase behavior involves defining number of phases, phase amounts, phase compositions, phase properties and interfacial tension between phases.

If the black-oil model can describe the system, interpolation of PVT data as a function of pressure will suffice. However, if a compositional approach is necessary, a more complex relation between PVT data is needed, often described by something called equations of state (EOS).

In modern reservoir engineering, with the access of super computers, cubic equations of states handle the PVT data. These equations describe the volumetric- and phase behavior of a system requiring critical properties and the acentric factor of each component. Equation of state is however not a new concept. Van der Waals was the first to propose an EOS with an equation relating pressure, temperature and molar volume in 1873 (Rowlinson, 1988). Later, more complicated EOS' have arrived, improving the accuracy of EOS predictions. Equations of state try to describe the behavior of the fluid, and they can be made for both reservoir and surface conditions. Equations of state and its associated input data (critical properties and acentric factor) must be tuned and calibrated against PVT until actual PVT data agree.

There are many established equations of state found in the literature. The most applied cubic EOS' in reservoir simulation today are the ones from Peng and Robinson (1976) (PR) and Soave (1972) (SRK). Because this simulation study implements the SRK, this EOS is described in further detail in Chapter 5.

To understand how the SRK works, it is necessary to go through the EOS developments from van der Waals ((Rowlinson, 1988)) and Redlich and Kwong (1949).

As mentioned, van der Waals came up with the first cubic equation of state in 1873 when he proposed an equation offering a relation between pressure, temperature and molar volume:

$$p = \frac{RT}{v - b} - \frac{a}{v^2} \tag{3.11}$$

Where R is the universal gas constant, a is an attraction parameter, b is a repulsion parameter, v is molar volume and p is pressure. As one can see, equation 3.11 is quite similar to the ideal gas law, $P = \frac{RT}{v}$, however it contains some improvements. The b parameter arises a limiting value to the volume at high pressures. The first term in van der Waals' equation controls the liquid behavior of the substance and represents the repulsive component of pressure, all on a molecular scale. Van der Waals' equation also holds the advantage of describing non-ideal gas behavior. The last term in the equation reduces the pressure of the system and is interpreted as the attractive component of pressure. The EOS constants a and b are determined from the derivatives of pressure with respect to volume:

$$\left(\frac{\partial p}{\partial v}\right)_{p_c, T_c, v_c} = \left(\frac{\partial^2 p}{\partial v^2}\right)_{p_c, T_c, v_c} = 0$$

From this relationship, a and b become:

$$a = \frac{27}{64} \frac{R^2 T_c^2}{P_c} \tag{3.12}$$

$$b = \frac{1}{8} \frac{RT_c}{P_c} \tag{3.13}$$

Van Der Waals' equation is not applied in reservoir simulation today. However, his

equation laid the outline for later established EOS' which are highly used today.

In 1949, Otto Redlich and Joseph Nen Shun Kwong were the first to come up with a suc-
cessful modification to the original van der Waal equation of state (Redlich and Kwong,
1949). They made the *a* factor from equation 3.12 dependent on temperature which
improved the EOS greatly. The Redlich-Kwong EOS is expressed as follows:

$$p = \frac{RT}{v - b} - \frac{a}{v(v + b)}$$

Where *a* and *b* have been modified from van Der Waals:

$$a = \Omega_a^0 \frac{R^2 T_c^2}{P_c} \alpha(T_r), \qquad\qquad \Omega_a^0 = 0.42748 \qquad\qquad (3.14)$$

$$b = \Omega_b^0 \frac{RT_c}{P_c}, \qquad\qquad \Omega_b^0 = 0.08664 \qquad\qquad (3.15)$$

With: $\alpha(T_r) = T_r^{-0.5}$

The RK EOS became a popular equation of state and it has been tried modified and im-
proved many times. One of the successful versions is the Soave-Redlich-Kwong equa-
tion of state, and this EOS will be explained in detail in Section 5.2.

3.4 History Matching

As mentioned in an earlier section, when a simulation model is constructed, it is fi-
nalized by tuning it using the concept of history matching. History matching involves
running several simulations to observe and adjust for uncertain parameters analyzing
the sensitivity of the parameters. The goal of history matching is to improve the match
between experimental/field data to simulated data. This is a time consuming effort as
there are many different parameters involved in a reservoir simulation process. History
matching can be conducted manually by the reservoir engineer or automatically by the

computer instructed by the simulation model itself.

After tuning the simulation model to match observed data, a reservoir engineer can alter operating parameters such as well placement and injection rates to optimize production of the field. When the process of history matching is finished, the prediction stage begins.

Chapter 4

The Experiments

This study simulates two experiments previously conducted by Odd Steve Hustad and Torleif Holt (Hustad and Holt, 1992). This chapter will describe the experiments in detail and provide the recommendations Hustad presented after their work. Measured data will also be presented and discussed.

4.1   Preparation of Experiments

Experiment 1 and 2 are tertiary gas injection processes. The displacement experiments are conducted on Bentheimer sandstone cores. Because water and oil are present in the core when gas is injected in both experiments, the systems become three-phase. The cores are water-wet.

The cores are vertically mounted and initiated with 100% water saturation. Reservoir oil is then injected from the top to establish the irreducible water saturation, S_{wir}, followed by a water injection from below. This way the core is at water residual oil saturation, S_{orw}, when gas injection starts from the top.

The displacement experiments are performed with live oil from a North Sea reservoir. The oil is recombined from known separator production rates. An equilibrium system is established by adding separator gas to the recombined oil until a two-phase system

with specified phase volumes occurs at 91.9°C and 313.5 bar. Then the two phases are separated into two different cells. The molecular weight distribution is estimated.

Artificial water is used as the water phase. The most important ions found in the North Sea reservoir are represented in the solution. The water has a formation volume factor of 1.02187 cm^3/Scm^3 at 92°C and 314 bar and 1.0255 cm^3/Scm^3 at 99°C and 315 bar.

Both experiments are conducted under reservoir conditions. The fluid recoveries are reported at standard conditions which is at 1 bar and 15°C.

4.2   Execution of Experiment 1

The purpose of Experiment 1 is to analyze how oil is produced due to convective flow without compositional effects caused by mass transfer. To avoid compositional effects, the equilibrium gas to oil at reservoir conditions is injected into the core from the top. As already stated, the core is at residual oil saturation after water has been flooded from the bottom of the core. The rate of gas injection is kept at a certain value to ensure a gravity stable mode, which is a measure to keep high sweep efficiency.

Experiment 1 is conducted under a pressure of 314 bar and a temperature of 92°C. The experiment was conducted on a 122.6 cm long Bentheimer core with a porosity of 22.7%.

Figure 4.1 presents the experimental recoveries from Experiment 1. Water production starts immediately after gas injection. When oil and eventually gas break through, a reduction in water production rate is observed. Water continues to be produced as long as gas is injected. The oil rate also decreases when gas break through. Hustad and Holt's results showed an establishment of an oil bank, however it takes time for the oil bank to be produced because of the large volume of water present in the pores.
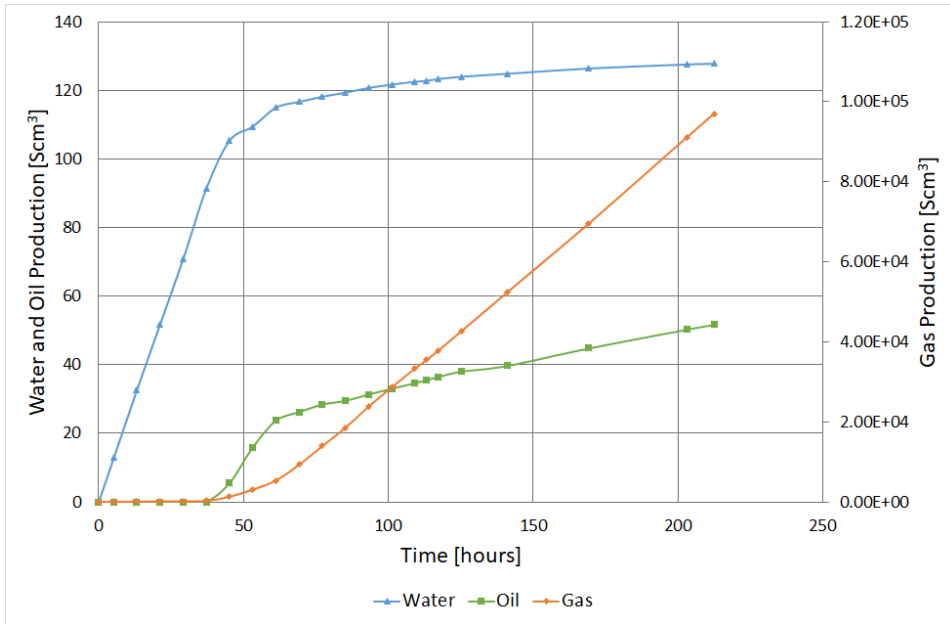
Figure 4.1: Experiment 1: Production data, (Hustad and Holt, 1992)

The oil production in Experiment 1 comes from production of equilibrium oil by convective flow and condensate production of the equilibrium gas.

4.3 Execution of Experiment 2

The purpose of Experiment 2 is to observe the effects of vaporization of oil. The experiment is conducted under almost similar conditions as Experiment 1, however a dry/lean gas, separator gas, is injected instead of equilibrium gas. A lean gas injected into an oil reservoir can result in vaporizing gas drive where light and intermediate hydrocarbons from the oil transform into the gas phase. Such a process can lead to miscibility, however full miscibility is not reached in this experiment.

Experiment 2 is conducted under a pressure of 315 bar and a temperature of 99°C. The experiment was conducted on a 122.1 cm long Bentheimer core with a porosity of 23.3%.

Figure 4.2 illustrates the experimental fluid recoveries from Experiment 2. Until gas breakthrough, Experiment 2 shows the same tendencies in water production as Experiment 1. Unlike Experiment 1, there is an increase in water production rate around 120 hours while there is a simultaneous decrease in oil production rate. The gas production is unaffected by this extra water production. Hustad and Holt (1992) suggest the extra water production comes from new available pore space allowing immobile water to flow after oil is vaporized. The oil production in Experiment 2 is higher than in Experiment 1. This illustrates how vaporization of oil is an important mechanism for further oil production during gravity stable tertiary displacement of oil by gas. Some caution needs to be given to the reported experimental data in Figure 4.2 as the values are read off from a graph displayed in the report by Hustad and Holt (1992). This is because experimental data was unavailable.
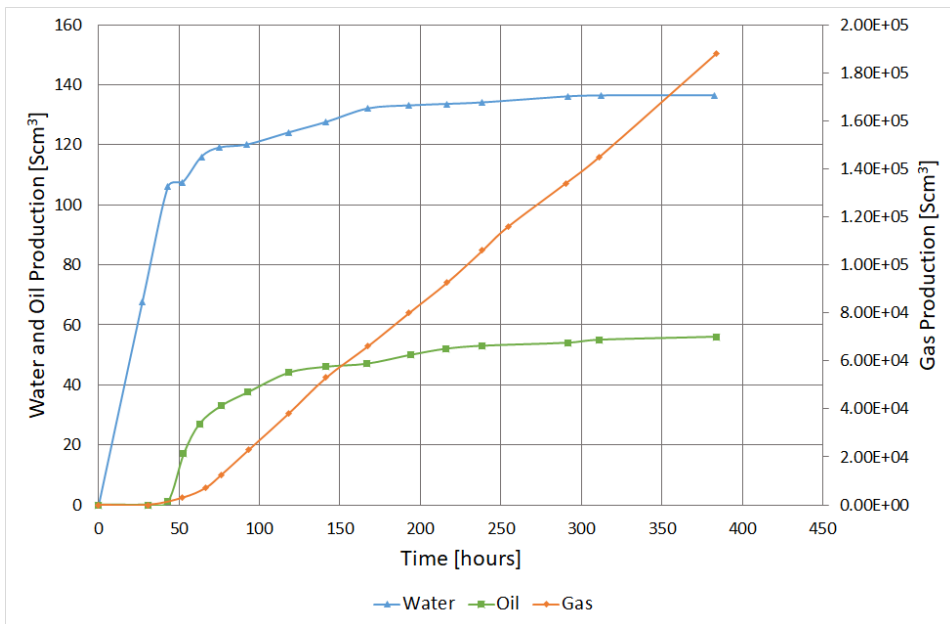
Figure 4.2: Experiment 2: Production data, (Hustad and Holt, 1992)

4.4   Flow Mechanisms

The formation of an oil bank through convective flow was important for oil recovery in both experiments. In addition to convective flow, vaporization contributed to fur-

ther recovery in Experiment 2. Conductivity (relative permeability), capillary forces and mass exchange are flow mechanisms observed in either or both experiments.

4.4.1 Conductivity

Relative permeability controls the conductivity. Relative permeability is important for flow estimation because it says to which degree a certain phase will preferentially flow in the presence of other phases. Relative permeability is discussed further in Chapter 3.

4.4.2 Capillary Forces

Capillary forces are controlled by capillary pressure. Capillary pressure can restrict a phase from flowing if the capillary pressure is too high. Capillary pressure will also be discussed in further detail in Chapter 3.

4.4.3 Mass Exchange

Mass exchange only occurs in Experiment 2 because the separator gas is dry. In Experiment 2, some components changes its phase, and this can lead to additional recovery if originally trapped oil transform to gas for then to be produced.

4.5 Measurements

Several measurements were conducted prior to the simulation study of Hustad and Holt (1992). Measurements on core characteristics, relative permeability, capillary pressure, residual phase saturations, interfacial tension and fluid properties (flash data) will be presented in this section.

4.5.1 Core Characteristics

The cores used for the displacements experiments and the relative permeability measurements are all from the same Bentheimer sandstone. Table 4.1 lists the different properties of the cores. The cores were treated similarly to achieve the same wetting characteristics (saturation history).

Table 4.1: Characteristics of core material, (Hustad and Holt, 1992).

Length	Diameter	Pore vol.	Porosity	Permeability	Use
(cm)	(cm)	(cm^3)	(%)	(μm^2)	
122.6	3.78	312.8	22.7	2.566	Exp. 1
122.1	3.77	317.2	23.3	2.645	Exp. 2
61.9	3.77	156.9	22.7	2.467	Rel.perm.

4.5.2   Relative Permeability

Figures 4.3 to 4.6 show the measured and extrapolated drainage data Hustad and Holt (1992) applied in their simulations. Relative permeability data was measured using the steady-state method with small cores coming from the same Bentheimer sandstone used in the displacement experiments. Further details on the measurements can be found in the report by Hustad and Holt (1992).

Figures 4.3 to 4.6 show oil-water and gas-oil relative permeabilities and they are valid for drainage processes where water decreases and gas increases.

Hustad and Holt (1992) observed that the irreducible water saturation, S_{wir}, was always reduced when gas was injected during the measurements of gas-oil relative permeability and lowest at residual oil saturation, S_{org}, (Hustad and Holt, 1992). They found out from repeated measurements that the water reduced from 17.7% to an average saturation of 14.5%.

Hustad and Holt (1992) also measured zero oil isoperms (lines of equal relative permeabilities) in a three-phase system with two different initial phase saturations. The initial saturation were water residual oil saturation, S_{orw}, and initial water saturation, S_{wir}. Hustad and Holt observed how the points of no oil flow were process dependent.
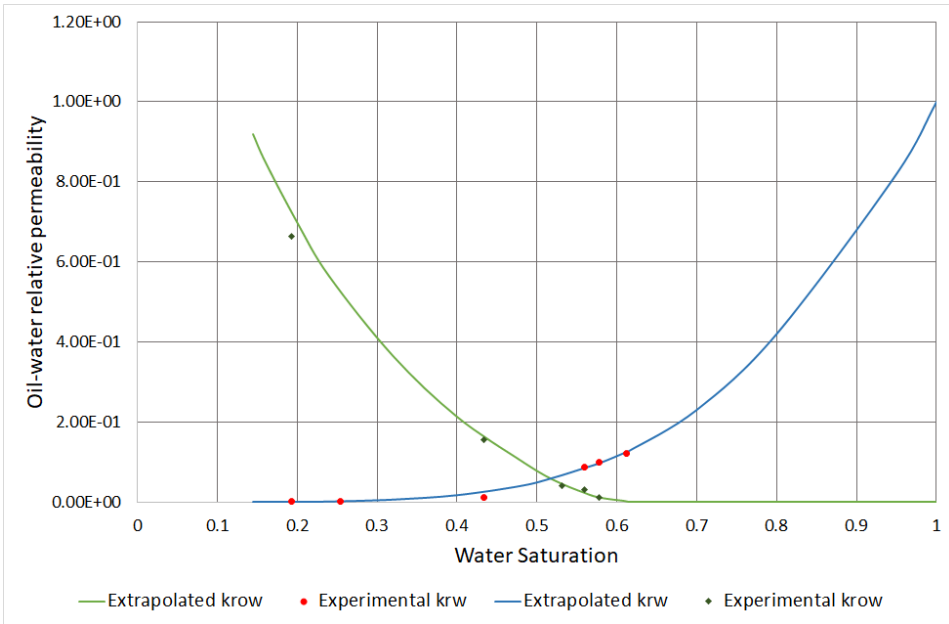
Figure 4.3: Oil-water relative permeability: Experimental data and Hustad's extrapolations. Linear scale.
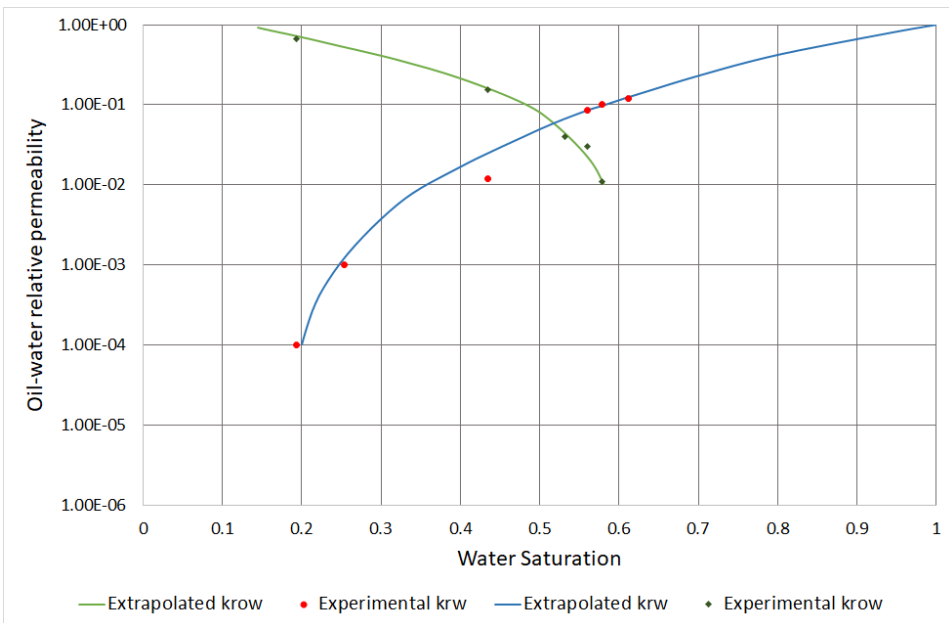
Figure 4.4: Oil-water relative permeability: Experimental data and Hustad's extrapolations. Logarithmic scale.
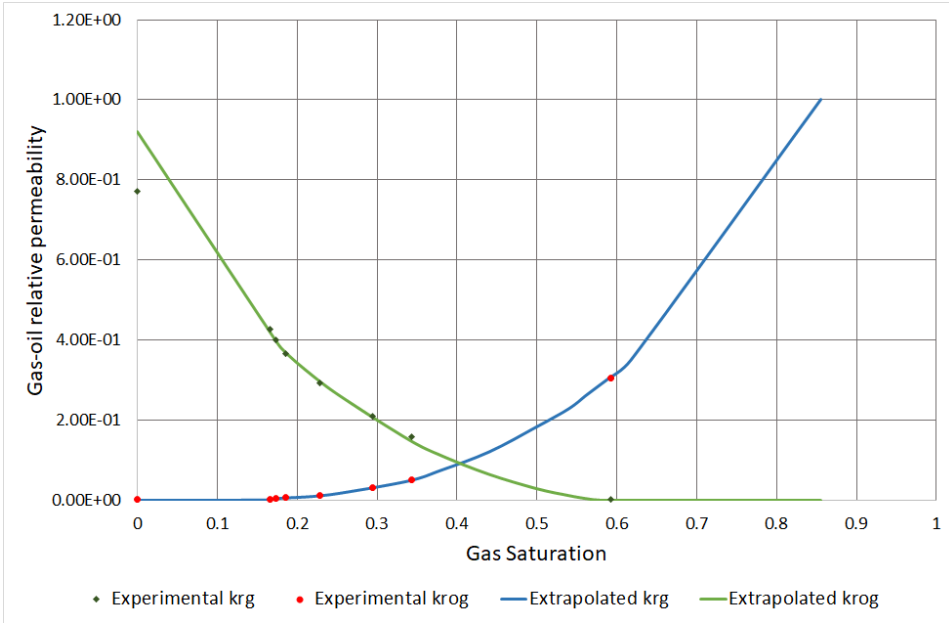
Figure 4.5: Gas-oil relative permeability: Experimental data and Hustad's extrapolations. Linear scale.
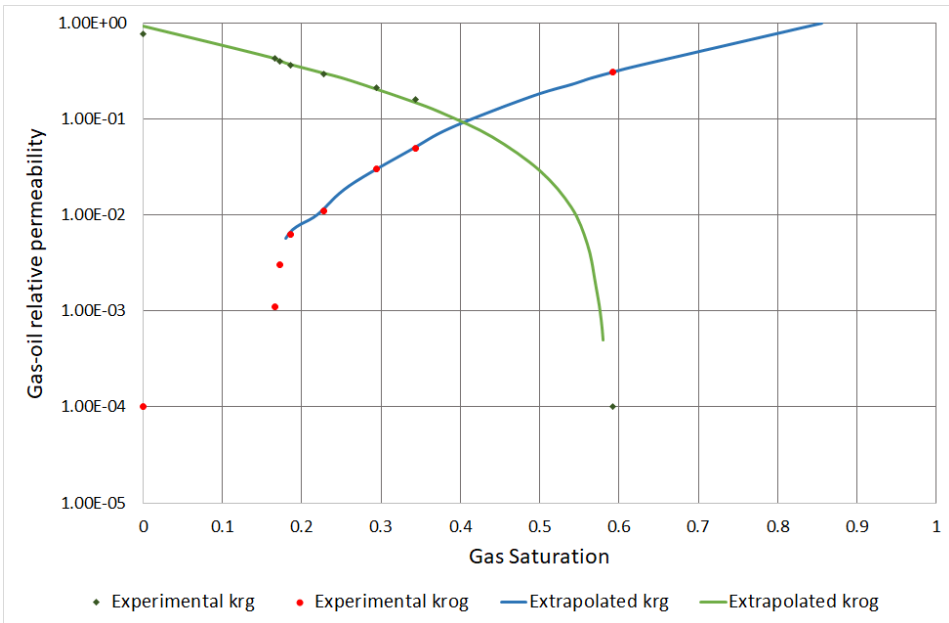
Figure 4.6: Gas-oil relative permeability: Experimental data and Hustad's extrapolations. Logarithmic scale.

4.5.3   Capillary Pressure

Capillary pressure was measured using the centrifuge method. Four sets of data were measured at different interfacial tensions (IFT), (Hustad and Holt, 1992):

1. Draining decane (oil) by air (gas) to $S_{or} = 5.3\%$ at IFT=23.4mN/m

2. Draining water by decane to $S_{wir} = 13.2\%$ at IFT=37.1mN/m

3. Draining water by decane to $S_{wir} = 16.5\%$ and thereafter drained by air to $S_{wir} = 0.5\%$ and $S_{org} = 4.5\%$

4. Draining water by air to $S_{wir} = 4.5\%$ at IFT=72mN/m

The same conclusion can be drawn from this data as from relative permeability data, namely that when gas is injected, liquid residual saturations are reduced. Figure 4.7 presents the different experimentally obtained capillary pressure curves and the simulation capillary pressure curves used by Hustad and Holt (1992).
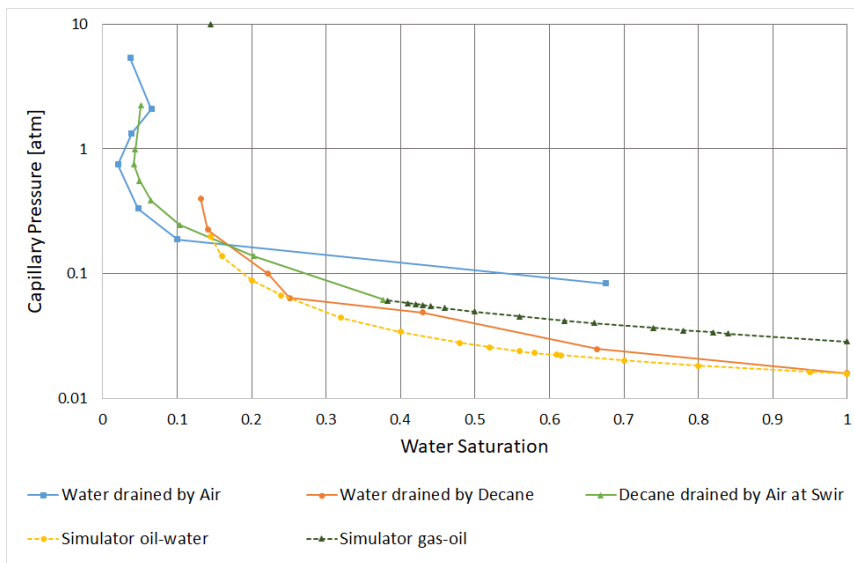
Figure 4.7: Capillary pressure from centrifuge experiments, (Hustad and Holt, 1992)

4.5.4   Residual Phase Saturations

Different residual phase saturations have been obtained during measurements of different parameters. Although residual saturations already are stated in other sections,

this section will sum up the different data.

Figure 4.8 presents experimental measurements only visually provided in the report by
Hustad and Holt (1992). It can be observed that Experiment 2 drains to lower water
saturations than Experiment 1 for the entire core. Hustad and Holt's simulations are
also included, showing some deviations from experimental data. For the upper blocks,
where the water is the most drained, it can be seen that Experiment 2 drains to a water
saturation less than $S_w = 10.0\%$ while Experiment 1 drains to right above $S_w = 10.0\%$.
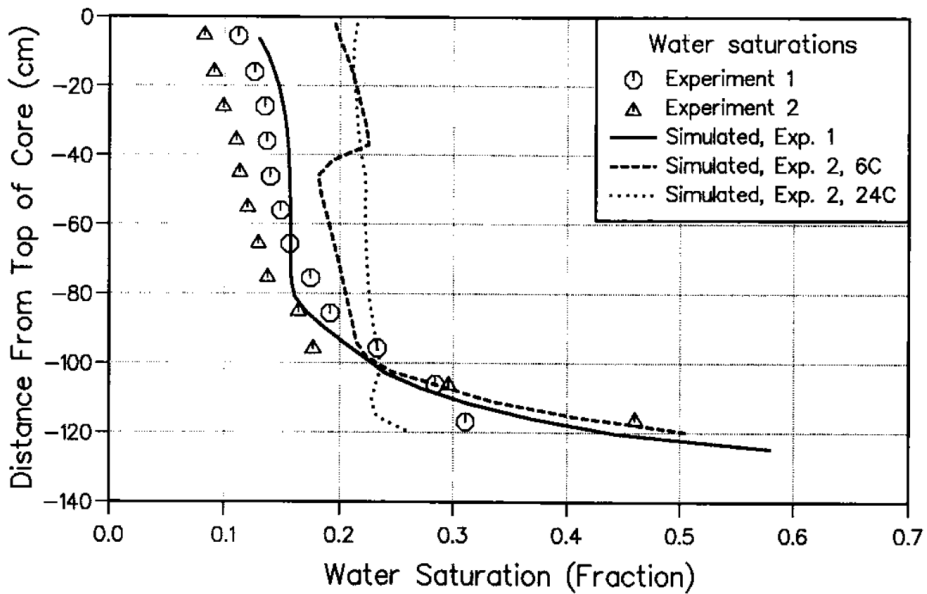
Figure 4.8: Simulated and experimental final water saturations of Experiments 1 and 2,
(Hustad and Holt, 1992)

As mentioned, the relative permeability measurements concluded an average irreducible
water saturations of $S_w = 14.5\%$, with one of the saturations being measured down
to $S_w = 13.2\%$. The measured residual oil saturations were $S_{orw} = 38.4\%$ and $S_{org} = 27.7\%$.

The capillary pressure recordings measured lower water saturations. Water drained by

decane led to a water saturation of $S_w = 4.5\%$. and even $S_w = 0.5\%$ when the draining was followed by air injection.

4.5.5 Interfacial Tension

Interfacial tension (IFT) was measured using the pendant drop technique in a high pressure cell. The measurements were between equilibrium gas and oil and between equilibrium oil and water. The IFT's were as follows:

1. IFT between eq. gas and oil = 1.2mN/m at 313 bar

2. IFT between eq. oil and water = 21.6mN/m at 313 bar

4.5.6 Fluid Properties (Flash Data)

The hydrocarbon compositions and properties were characterized by gas chromatography. The molecular weights were estimated and assumed equal molecular weight in the stock tank oil and condensate. Tables 4.2 and 4.3 provide the fluid properties. Associated equations of state parameters are not included in this section, but can be found in the report by Hustad and Holt (1992).

Table 4.2: Experimental flash data from recombined hydrocarbon fluids , (Hustad and Holt, 1992).

	Experiment 1				Experiment 2	
	Equilibrium Oil		Equilibrium Gas		Oil	Inj. Gas
MW ($g/mole$)	-	226	-	159	-	205
Density (g/cm^3)	9.922E-4	0.8485	9.111E-4	0.8033	1.013E-4	0.845
Formation Volume Factor (cm^3/Scm^3)	1.62		18.0		1.61	
Gas/Oil Ratio (Scm^3/Scm^3)	200.9		4341.63		204.1	
Saturation Temperature ($°C$)	91.9		91.9		98.4	
Saturation Pressure (bar)	313.5		313.5		275.1	
Saturation Density (g/cm^3)	0.6468		0.2644		0.6532	
Viscosity (cp)	0.43		-		-	
Interfacial Tension (mN/m)	1.2					

Table 4.3: Experimental flash data from recombined hydrocarbon fluids 2, (Hustad and Holt, 1992).

Comp.	Molecular Weight	Experiment 1				Experiment 2		
		Equilibrium Oil		Equilibrium Gas		Oil		Inj. Gas
		Gas Mole %	Oil (STO) Weight %	Gas Mole %	Condensate Weight %	Gas Mole %	Oil (STO) Weight %	Gas Mole %
N2	28.02	1.202	0.00	1.7	0.00	1.467	0.00	1.762
C1	16.04	72.350	0.00	79.471	0.00	71.461	0.00	80.218
CO2	44.01	0.737	0.00	0.651	0.00	0.693	0.00	0.714
C2	30.07	11.359	0.00	8.582	0.00	10.793	0.03	9.053
C3	44.09	7.873	0.03	4.971	0.03	8.244	0.21	4.945
iC4	58.12	1.014	0.03	0.611	0.04	1.129	0.12	0.544
nC4	58.12	2.848	0.18	1.655	0.19	3.203	0.53	1.406
iC5	72.15	0.693	0.22	0.444	0.25	0.793	0.45	0.309
nC5	72.15	0.880	0.43	0.605	0.52	1.016	0.81	0.396
C6	86.17	0.590	1.23	0.573	2.05	0.711	1.90	0.294
C7	91.62	0.418	2.96	0.598	6.09	0.446	4.04	0.359
C8	104.53	0.0357	4.54	0.139	11.41	0.04351	5.05	
C9	118.84		4.26		12.26		4.94	
C10	134		3.76		11.14		4.54	
C11	147		3.42		8.86		3.83	
C12	161		3.18		7.46		3.45	
C13	175		3.35		6.94		3.67	
C14	190		3.25		5.82		3.37	
C15	206		3.67		5.62		3.41	
C16	222		3.16		4.14		3.20	
C17	237		2.55		3.27		2.96	
C18	251		3.07		3.18		3.23	
C19	263		2.83		2.82		2.99	
C20	275		2.50		2.06		2.44	
C21	291		2.14		1.78		2.50	
C22	300		2.14		1.53		2.05	
C23	312		1.66		0.49		1.42	
C24	324		1.55		0.39		1.33	
C25	337		1.50		0.30		1.28	
C26	349		1.46		0.24		1.25	
C27	360		1.28		0.16		1.09	
C28	372		1.42		0.15		1.21	
C29	382		1.47		0.14		1.26	
C30	394		1.52		0.11		1.30	
C31	404		1.25		0.079		1.07	
C32	415		1.05		0.052		0.90	
C33	426		1.07		0.039		0.92	
C34	437		0.98		0.036		0.84	
C35	445		1.00		0.043		0.86	
C36	456		0.88		0.049		0.75	
C37	464		0.90		0.079		0.77	
C38	475		0.72		0.059		0.62	
C39	484		0.68		0.022		0.58	
C40	495		0.61		0.016		0.52	
C41	502		0.54		0.020		0.46	
C42	512		0.50		0.020		0.43	
C43	521		0.41		0.013		0.35	
C44	531		0.35		0.007		0.30	
C45	539		0.29		0.003		0.25	
C46	548		0.24		0.002		0.21	
C47	557		0.19		0.001		0.16	
C48	791.5		23.58		0.010		20.15	

4.6   Simulation of Experiments

Hustad and Holt used an IMPES type compositional simulator to reproduce the core-flooding experiments. They reproduced the hydrocarbons to fit a 6 and 24 components model. They initially simulated Experiments 1 and 2 applying two different three-phase relative permeability models proposed by Stone for estimating three-phase oil relative permeability. Stone model 1 and 2 proved inapplicable for the experiments with great deviations from experimental results. Figure 4.9 illustrates the erroneous simulations of Experiment 1 applying Stone model 1 and 2. Stone model 1 overestimates oil production, while Stone model 2 underestimates it. Both models underestimate water after gas breakthrough.
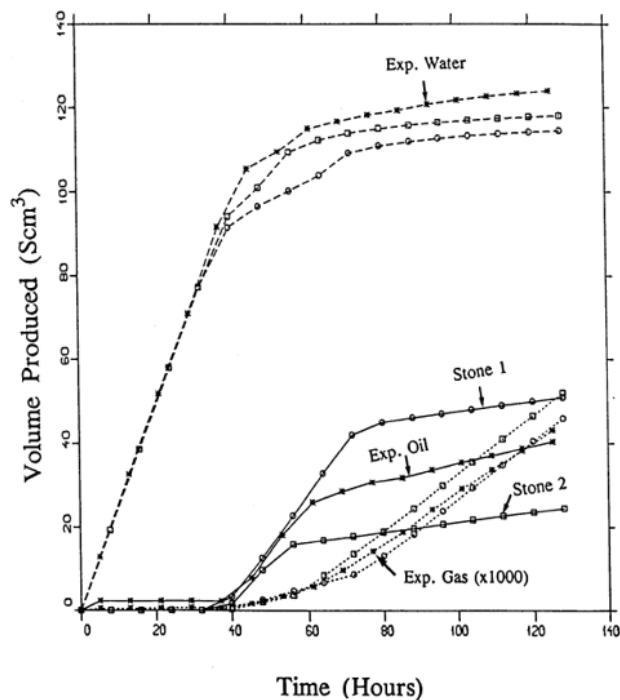
Figure 4.9: Simulation of Experiment 1 applying Stone model 1 and 2, (Hustad, 2007).

Hustad saw the need for an improved relative permeability model. He developed a modified version of Stone model 1, called Extended Stone model 1. This modified version will be explained in further detail in Section 5.1. Anyway, with the new modified

model, Hustad and Holt were able to achieve a perfect match with Experiment 1. How-
ever, as already mentioned in Chapter 1, Extended Stone model 1 did not capture the
additional water recovery in Experiment 2, and a match was not achieved. Figure 4.10
shows simulation results of Experiment 1 and 2 applying Extended Stone model 1.
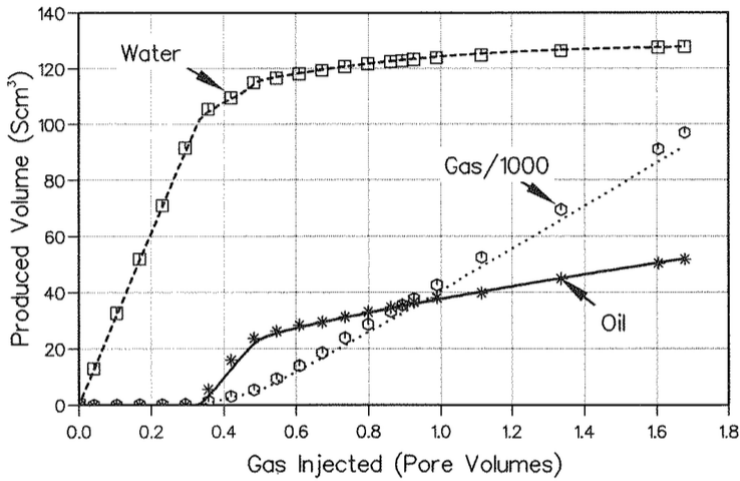
(a) Experiment 1
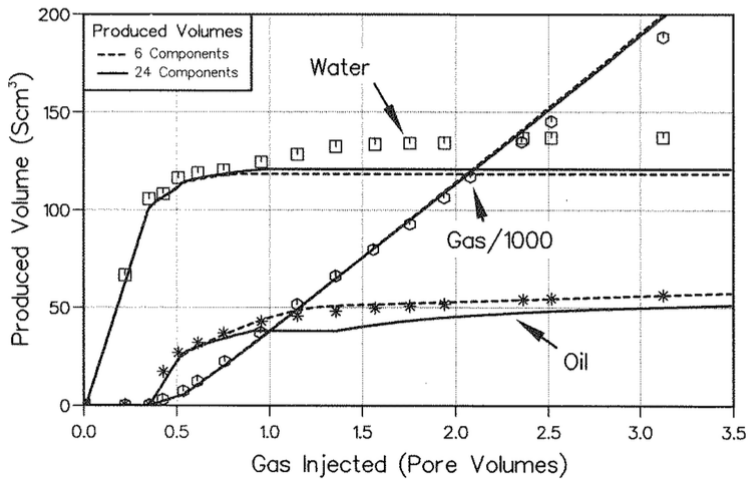
(b) Experiment 2

Figure 4.10: Simulation results applying Extended Stone model 1, (Hustad and Holt,
1992)

4.7 Hustad's Recommendations for Further Work

What can be done to match the water recovery in Experiment 2? What is happening when there is a sudden increase in water production around 120 hours?

The simulation model Hustad and Holt used to simulate both experiments, do not apply gas-water data. Hustad suspects because vaporization effects are present in Experiment 2, the oil-water data applied in Experiment 1 is insufficient for capturing the additional water recovery in Experiment 2. This is believed to be an effect of new forces between the gas and the water. While the oil phase is believed to always separate the gas from the oil in Experiment 1, another scenario is considered in Experiment 2.

The scenario suggests that the increasing pressure from water and gas will eventually lead to a snap-off of the oil phase, introducing a contact between gas and water. Figure 4.11 illustrates the oil phase rupture very simply. The capillary pressure between gas and water are lower than for oil-water at lower water saturations. This requires a new capillary pressure curve for Experiment 2 and leads to Hustad's suggestion: joining of oil-water and gas-water capillary pressure curve at the water saturation where vaporization effects affect the displacement. By manually inserting gas-water capillary pressure data in the simulation model, one force the system to change to a gas-water system, thus making it possible for the simulation model to capture the additional water recovery. This is the essence of this study: study the effects of applying gas-water capillary pressure data while applying Extended Stone model 1.
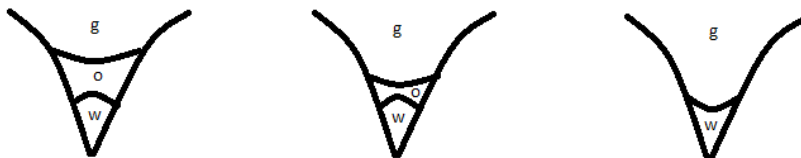
Figure 4.11: Rupture of oil phase

Chapter 5

Theory

This chapter will explain the applied three-phase relative permeability model Extended Stone model 1, the Soave-Redlich-Kwong equation of state in detail and scaling of capillary pressure.

5.1   Extended Stone Model 1

Extended Stone model 1 is a modification of Stone model 1. It is however, when specified in reservoir simulation tools such as Eclipse, with the basis of Aziz' improvements which was discussed in Sections 3.2.1.2 and 3.2.1.3. This means from now on, when Stone models are mentioned, the models that are actually discussed are the ones proposed by Aziz (1979).

Extended Stone model 1 is proposed by Hustad and Holt (1992) with the purpose of altering the oil isoperms in a three-phase system which can be visually displayed in a ternary diagram. Hustad and Holt (1992) saw that both Stone models over- and underestimates the oil recovery of Experiment 1, so they introduced an exponent term, n, to the normalized saturations to overcome this issue:

$$k_{ro} = \frac{k_{row}(S_w)k_{rog}(S_g)}{k_{rocw}}\beta^n \tag{5.1}$$

Where the equations of β and normalized saturations in equations 3.1, 3.2, 3.3, 3.4 and 3.5 are redefined as:

$$\beta = \frac{S_o^*}{(1 - S_w^*)(1 - S_g^*)} \tag{5.2}$$

$$S_o^* = \frac{S_o - S_{om}}{1 - S_{wir} - S_{om} - S_{gc}}$$

$$S_g^* = \frac{S_g - S_{gc}}{1 - S_{wir} - S_{om} - S_{gc}}$$

$$S_w^* = \frac{S_w - S_{wir}}{1 - S_{wir} - S_{om} - S_{gc}}$$

With this definition, β is a variable going from 0 at low oil saturations to 1 for high oil saturations. With a value of n equal to 1, Extended Stone model 1 is identical to Stone model 1 (Aziz' version). n above 1 results in more spread oil isoperms at low values. n below 1 causes the opposite effect. Figure 5.1 illustrates the difference in oil isoperms with different n-values. What is also interesting is that n above 1 results in more linear oil isoperms in the low-value region, a suggestion discussed and investigated by Baker (1988). Different values of n has an impact on fluid distribution. Above 1, the n causes the gas to bypass the oil resulting in lower oil production. Values less than 1 keeps the oil between water and gas and keeps oil production at a lower level.
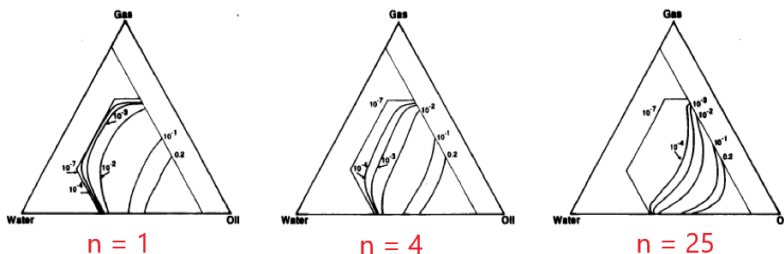
Figure 5.1: Different n-values for Extended Stone 1, (Hustad, 2007).

5.2 Soave-Redlich-Kwong Equation of State

The Soave-Redlich-Kwong (SRK) equation of state (EOS) is the most applied modification to that of Redlich and Kwong (RK).

What differ the SRK from the original RK EOS is the α correction factor used in equation 3.14. The rest of the equations are similar to the Redlich-Kwong equation of state. In the SRK, the correction term is component-dependent and it is expressed as a function of acentric factor. Acentric factor is a concept introduced by Pitzer in 1995 and is a measure of the non-sphericity of a molecule (Pitzer et al., 1955). The correction factor, α, now becomes:

$$\alpha = \left[1 + m(1 - T_r^{0.5})\right]^2 \tag{5.3}$$

Where: $m = 0.480 + 1.574\omega - 0.176\omega^2$

The acentric factor, ω, is a function of reduced saturation vapor pressure and it determines, in practical sense, the steepness of the vapor-pressure curve at reduced temperatures, T_r, from 0.7 to 1. The definition of acentric factor is:

$$\omega = -\log\left(\frac{p_v^*}{p_c}\right) - 1 \tag{5.4}$$

Where p_v^* is vapor pressure at temperature $T = 0.7T_c$, meaning $T_r = 0.7$. T_r is 0.7 at saturation pressure. In equations of state, reduced properties like reduced pressure and temperature are used instead of actual temperature and pressure to follow the corresponding-states theory (Whitson and Brule, 2000). This theory says that all fluids have the same compressibility factor and deviate from the ideal gas behavior at the same degree when at the same reduced pressure and temperature (Rowlinson, 1988). Practically speaking, the acentric factor is the difference between a compound and the vapor-pressure line for a noble gas. This implies a noble gas has an acentric factor of 0.

The SRK is said to underestimate liquid densities while overestimating liquid volumes of petroleum mixtures (Whitson and Brule, 2000). However, it is considered yielding accurate predictions of vapor/liquid equilibrium (VLE) and vapor properties.

5.3   Scaling of Capillary Pressure

Capillary pressures measured at other conditions than the ones specified in a simulation model need to be scaled to the correct conditions to be applicable. Whether the capillary pressures are scaled manually before they are implemented as inputs or by the simulation model itself depends on what kind of three-phase relative permeability model that is applied. For Extended Stone model 1, the capillary pressures need to be scale beforehand.

Scaling of capillary pressures are done according to the method mentioned in the report by Hustad and Browning (2010). Capillary pressure is scaled by the ratio of two interfacial tension values (IFT), reservoir condition IFT and reference IFT. Reference IFT is the interfacial tension measured during measurements of capillary pressure. The capillary pressure scaling factor is:

$$f_{ij}^{Pc} = (\frac{\sigma_{ij}}{\sigma_{ij}^r})^{l_{ij}}$$ (5.5)

Where l_{ij} is a user-specified constant, σ_{ij} is the experimental IFT and σ_{ij}^r is the reference IFT. The constant is changed until a satisfactory match is obtained. The capillary pressures measured at reference IFT are then multiplied with the scaling factor, f_{ij}^{Pc} to obtain applicable capillary pressure curves.

$$\hat{P}_{cij} = f_{ij}^{Pc} \cdot \tilde{P}_{cij}$$ (5.6)

Where $\tilde{P}_{cij}$ are the unscaled capillary pressures. i and j represent two different fluids, i.e. gas, oil or water. Equation 5.6 results in either reduced or increased capillary pressure curves dependent on the value of the IFT ratio and the user-specified constant.

Chapter 6

Method

As explained in Chapter 4, this study is based on a simulation study performed by Hustad and Holt (1992) where they simulated two different coreflooding experiments (Experiment 1 and 2) conducted by the authors themselves. The same experiments are simulated in this study to achieve a fluid recovery match which Hustad and Holt did not accomplish for Experiment 2. The process of obtaining a satisfactory match in this study is based on Hustad's hypothesis concerning applying gas-water capillary pressure data in the simulation model. Other adjustments to the original simulation models came along the way during this study.

Hustad and Holt simulated the experiments with both 6 and 24 components. This study only simulates with 6 components using Eclipse Rservoir Simulator.

The goal of the simulations is to capture the extra water recovery occurring around 120 hours in Experiment 2 applying Extended Stone model 1 (while also history matching oil and gas recovery). To achieve this, a match of Experiment 1 is obtained to get the correct scaling levels of capillary pressure and relative permeabilities before simulations of Experiment 2 can begin. When a match for Experiments 2 is achieved, the same input properties need to be simulated for Experiment 1 to observe whether they still give a match for Experiment 1. This is because the joining of capillary gas-water capillary pressure data should occur at a water saturation not reached in Experiment 1, and con-

sequently not affect the match of this experiment. The procedure of achieving a match for both Experiment 1 and 2 can be summarized in a flow chart:
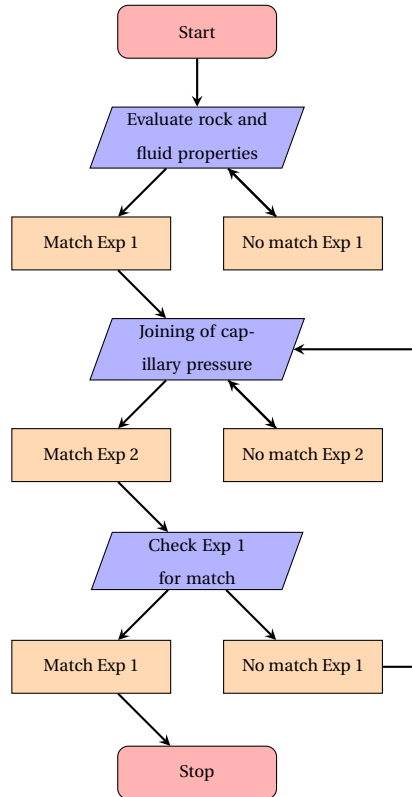
Figure 6.1: Flow Chart of Simulation Process

6.1   Phase Behavior

This study implements data obtained by Hustad and Holt (1992). However, caution needs to be taken to some of the parameters as Hustad and Holt used another simulation tool than Eclipse. Because different simulation tools not necessarily treat input parameters similarly, it is important to make sure the input properties used in the simulation model in this study is read correctly by Eclipse. As a consequence, fluid- and critical properties reported by Hustad and Holt (1992) were checked and changed (if necessary) to fit Eclipse.

As mentioned in Section 3.3, equations of state (EOS) are simple equations describing phase behavior at a certain state. If the EOS at reservoir conditions is not sufficient for modeling the phase behavior at another condition (surface), it is necessary to construct an equation of state at surface, a surface equation of state. It was clear during early simulations of both Experiment 1 and 2 that an establishment of a surface equation of state was beneficial for a satisfactory oil recovery match. The equation of state has little or no effect on water recovery.

Hustad and Holt (1992) reported critical properties at reservoir conditions. To obtain a corresponding surface equation of state, a regression tool can extend data to other pressures, temperatures, densities and gas-oil ratios (GOR). This was done for both Experiment 1 and 2. Because the oil and injection gas in Experiment 1 and 2 are different, the surface equations of state are also different.

6.1.1 Experiment 1

6.1.1.1 Oil Composition

The oil composition used in this simulation study is recombined from the properties listed in Table 4.3. These values are also listed in Table 4 in the original report by Hustad and Holt (1992). Table 6.1 lists the oil composition.

Table 6.1: Experiment 1: Oil composition

	Z_i
HC1	5.16E-01
HC2	1.41E-01
HC5	6.12E-02
HC9	1.69E-01
HC21	6.85E-02
HC40	4.41E-02

6.1.1.2   Injection Gas Composition

In Experiment 1 it is the equilibrium gas to the reservoir oil that is injected into the core. Because of this, it is very important that the input gas composition in the simulation model is read as the equilibrium gas by Eclipse. To make sure the gas composition is treated as the equilibrium gas, a simple simulation of oil with a pressure decrease of 0.4 bar is run in Eclipse where the gas composition can be retrieved from the output files. This is done to compare it with the recombined compositions coming from Table 3 in the original report written by (Hustad and Holt, 1992). It is observed when the pressure drop simulation is run that the output gas composition is slightly different to that of Hustad and Holt (1992). The output gas composition is chosen for further use in simulations. Table 6.2 gives the new and old equilibrium gas composition.

Table 6.2: Experiment 1: New and old gas injection composition

	Old Zi	New Zi	Deviation
HC1	7.79E-01	7.79E-01	-0.01 %
HC2	1.33E-01	1.33E-01	0.04 %
HC5	3.73E-02	3.73E-02	0.06 %
HC9	4.76E-02	4.76E-02	0.07 %
HC21	2.62E-03	2.62E-03	0.00 %
HC40	5.02E-05	5.01E-05	-0.18 %

6.1.1.3   Surface Critical Properties and Acentric Factor

When the correct gas composition is set, a regression tool can provide critical properties and acentric factors at surface conditions to establish a surface equation of state. The Soave-Redlich-Kwong EOS is also chosen for surface conditions. The regression tool take in the different hydrocarbons with its associated molecular weight, critical properties and acentric factor at reservoir conditions. Molecular weights do not change according to different pressure- and temperature regimes, thus these values stay constant during regression. Pressure and temperature at reservoir conditions are specified as the first regime, followed by the pressure and temperature at surface conditions. This way the regression tool knows which conditions the data should extend to. Oil- and gas

densities and gas/oil ratio (GOR) are also specified. To obtain representative values for critical properties and acentric factor, densities and GOR should not vary from the input values.

It proved difficult to obtain the mentioned parameters while staying within an accepted error of density and GOR. The regression tool had difficulties obtaining values while keeping oil and gas properties as they should. It was then decided to only focus on the oil. This will naturally yield erroneous gas results, but this could be accounted for when analyzing simulated recovery results. Table 6.3 gives the new critical properties and acentric factor at surface conditions for Experiment 1. Critical volumes were not changed and thus not included.

Table 6.3: Experiment 1: Reservoir and surface critical properties and acentric factor

	Reservoir Pc [atm]	Surface Pc [atm]	Dev	Reservoir Tc [K]	Surface Tc [K]	Dev	Reservoir AF	Surface AF	Dev
HC1	45.40	46.44	2.30 %	190.17	182.31	-4.13 %	0.01	0.01	-0.38 %
HC2	45.67	46.73	2.30 %	334.46	320.64	-4.13 %	0.13	0.13	-0.38 %
HC5	33.56	34.33	2.30 %	455.12	436.32	-4.13 %	0.24	0.24	-0.38 %
HC9	25.23	25.48	0.99 %	565.87	571.30	0.96 %	0.59	0.59	0.06 %
HC21	15.04	15.19	0.99 %	766.60	773.96	0.96 %	1.01	1.01	0.06 %
HC40	13.02	13.15	0.99 %	982.43	991.86	0.96 %	1.28	1.28	0.06 %

6.1.1.4 Inaccurate Simulation of Condensate Production

It was discovered during simulations of Experiment 1 an erroneous overestimation of oil production. This was found out to be a cause of incorrect simulation of condensate production by Eclipse. As a consequence, no matter how you treat the properties related to oil, the simulated and experimental oil production will never match.

To compensate for this effect, the experimental oil production data is adjusted for the extra condensate production. This is possible because the properties of the injection gas is known and reported in the study by Hustad and Holt (1992). The overestimation of condensate production can be calculated using the gas-oil ratio (GOR). By comparing

the GOR one retrieves from the simulations and what it actually should be, one can calculate the difference in condensate production. This difference is then added to experimental oil production data, and this new curve, modified experimental oil production, will be used as the new experimental oil production curve. Calculation of condensate contribution is done according to the next equation:

$$V_{\bar{o}g} = \frac{V_{\bar{o}}GOR_o - V_{\bar{g}}}{GOR_o - GOR_g} \tag{6.1}$$

Where $V_{\bar{o}g}$ is surface volume of oil coming from gas, $V_{\bar{o}}$ is total surface volume of oil, $V_{\bar{g}}$ is total surface volume of gas, GOR_o is equilibrium oil gas/oil ratio and GOR_g is injection gas gas/oil ratio. In Table 3 from the report by Hustad and Holt (1992), a GOR_g of 4341.63 Scm^3/Scm^3 is recorded. The simulations yield a GOR_g of 2620 Scm^3/Scm^3. GOR_o is always 200.9 Scm^3/Scm^3. With these three GOR's one can determine the condensate contributions from both simulated and experimental oil production, calculate the difference and add that difference to experimental oil production data. Because of this modification, simulated and experimental oil recovery values are "falsely" high and should not be compared value wise, only match wise.

The erroneous condensate production is not an issue in simulations of Experiment 2.

6.1.2   Experiment 2

6.1.2.1   Oil and Injection Gas Composition

The oil and injection gas composition are recombined from the properties listed in Table 4.3. Since it is not important for Eclipse to handle the injection gas as an equilibrium gas in Experiment 2, the injection gas composition is not changed as it is for Experiment 1. Table 6.4 lists the oil and injection gas composition.

Table 6.4: Experiment 2: Oil and injection gas composition

	Oil Zi	Inj. Gas Zi
HC1	4.88E-01	8.20E-01
HC2	1.36E-01	1.47E-01
HC5	8.04E-02	2.95E-02
HC9	1.88E-01	3.59E-03
HC21	7.10E-02	0.00E+00
HC40	3.68E-02	0.00E+00

6.1.2.2   Surface Critical Properties and Acentric Factor

The fluid properties needed to be evaluated separately for Experiment 2. This is because another type of gas is injected into the core, namely a dry gas. As may be seen in Table 3 from the report by Hustad and Holt (1992), the oil composition is slightly different between Experiment 1 and 2 as well. Because of this, regressions of critical properties and acentric factors were conducted for Experiment 2 similarly (but separately) as for Experiment 1. Table 6.5 lists the new critical properties and acentric factors.

Table 6.5: Experiment 2: Reservoir and surface critical properties and acentric factor

	Reservoir Pc [atm]	Surface Pc [atm]	Dev	Reservoir Tc [K]	Surface Tc [K]	Dev	Reservoir AF	Surface AF	Dev
HC1	45.40	45.60	0.44 %	190.17	175.86	-7.52 %	0.01	0.01	7.69 %
HC2	45.67	45.88	0.44 %	334.46	309.30	-7.52 %	0.13	0.15	7.69 %
HC5	33.56	33.70	0.44 %	455.12	420.88	-7.52 %	0.24	0.26	7.69 %
HC9	25.23	23.98	-4.94 %	565.87	527.71	-6.74 %	0.59	0.64	7.59 %
HC21	15.04	14.30	-4.94 %	766.60	714.91	-6.74 %	1.01	1.09	7.59 %
HC40	13.02	12.37	-4.94 %	982.43	916.18	-6.74 %	1.28	1.38	7.59 %

6.2   Construction of Simulation Model

The simulation models for Experiment 1 and 2 can be found in the appendix. They are quite similar, however there are some differences concerning handling of fluid prop-

erties. The keywords will be listed following the chronological order in the respective
models and further discussed according to descriptions presented in the Eclipse Man-
ual by Schlumberger (2016a). Keywords related to ouput/report files and well place-
ments are not included.

An Eclipse data file is divided into different sections, which are defined by a keyword.
The other keywords are entered in one of these sections. Table 6.6 lists the different
sections. The descriptions are taken from the Eclipse Reference Manual (Schlumberger,
2016a).

Table 6.6: Eclipse Section Description, (Schlumberger, 2016a)

Section Name	Description
RUNSPEC	Title, problem dimensions, switches, phases present and components for example.
GRID	Specification of geometry of computational grid (location of grid block corners), and of rock properties (porosity and absolute permeability for example) in each grid block.
PROPS	Tables of properties of reservoir rock and fluids as functions of fluid pressures, saturations and compositions (including density, viscosity, relative permeability and capillary pressure). Contains the equation of state description in compositional runs.
REGIONS	Splits computational grid into regions for calculation of: - PVT properties (fluid densities and viscosities) - Saturation properties (relative permeabilities and capillary pressures) - Initial conditions (equilibrium pressures and saturations) - Fluids in place (fluid-in-place and inter-region flows) - EoS regions (for compositional runs). If this section is omitted, all grid blocks are put in region 1.
SOLUTION	Specification of initial conditions in reservoir. May be: - Calculated using specified fluid contact depths to give potential equilibrium - Read from a restart file set up by an earlier run - User-specified for every grid block (not recommended for general use)
SCHEDULE	Specifies the operations to be simulated (production and injection controls and constraints) and the times at which output reports are required. Vertical flow performance curves and simulator tuning parameters may also be specified in the SCHEDULE,section.

RUNSPEC

<u>LAB</u>
LAB indicates lab units are to be used.

<u>OIL/WATER/GAS</u>
OIL, WATER and GAS are specified to introduce a three-phase system with three different phases.

<u>COMPS</u>
COMPS specify a compositional mode. The associated number decides the number of components. This study has 6 components. COMPS imply a much more complicated simulation model because it requires data for each specific hydrocarbon and an equation of state which will treat these parameters. COMPS is necessary when mass transfer exist, which is the case for Experiment 2.

Associated data: 6

<u>DIMENS</u>
DIMENS defines the size of the grid in x, y and z-direction. 1 1 74 are decided to represent the core, where blocks 2-73 represent the actual core while block 1 and 74 represent dead end volumes.

Associated data: 1   1   74

<u>TABDIMS</u>
TABDIMS describe the sizes of saturation and PVT tables and number of fluid-in-place-regions. The data consists of:

- NTSFUN   The number of saturation tables.

- NTPVT   The number of PVT tables.

- NSSFUN   The maximum number of saturation nodes.

- NPPVT The maximum number of pressure nodes. Default: 50.

- NTFIP   The maximum number of FIP (fluid in place) regions.

Associated data: 2   1   50   1*   2

EQLDIMS

EQLDIMS specify the dimensions of the equilibrium tables. This keyword is different for Experiment 1 and 2. The data consists of:

- NTEQUL   The number of equilibration regions entered using EQLNNUM.

- NTPVT   The number of depth nodes.

Associated data:

Experiment 1:   1   200
Experiment 2:   2   200

Experiment 2 defines two different equilibration regions, one for the top dead end volume block (block 1) and one for the rest (blocks 2-74). Different equilibration regions are used to initialize different parts of the reservoir (core) that are not in mutual hydrostatic equilibrium.

CPR

CPR is a linear solver and can often reduce simulation times and improve performance when linear equations fail to converge.

FULLIMP

FULLIMP selects the Fully Implicit Solution option. The fully implicit solution is often not recommended for compositional runs if there are too many components. However, since the simulation models only consist of 6 components, the fully implicit solution is considered a good option.

GRID

<u>DX/DY/DZ</u>

DX, DY, and DZ specify the size of the gridblocks in x-, y- and z-direction respectively. DX and DY are equal for every block. DZ varies throughout the core, and have bigger blocks in the middle. The blocks closer to the ends are smaller to observe end effects more easily. Associated data can be found in the appendix.

<u>TOPS</u>

TOPS set the depths of each gridblock. Associated data can be found in the appendix.

<u>PERMX/PERMY/PERMZ</u>

PERMi specify the permeability in i-direction where i=X,Y,Z for each gridblock. Associated data can be found in the appendix.

<u>PORO</u>

PORO sets the porosity for each gridblock. Associated data can be found in the appendix.

PROPS

<u>ZI</u>

ZI specify the composition for each reservoir region. Because there are 6 components, there will be 6 different Z_i's for one region. Associated data can be found in the appendix.

<u>EOS</u>

EOS should be followed by the chosen equation of state. SRK (Soave-Redlich-Kwong) is chosen for these simulations. EOSS is the corresponding keyword at surface conditions.

<u>RTEMP</u>

RTEMP sets the reservoir temperature.

MW

MW associates a mean molecular weight with each component. MWS is the corresponding keyword at surface conditions.

PCRIT

PCRIT associates critical pressure with each component. PCRITS is the corresponding keyword at surface conditions.

VCRIT

PCRIT associates critical volume with each component. VCRITS is the corresponding keyword at surface conditions.

TCRIT

PCRIT associates critical temperature with each component. TCRITS is the corresponding keyword at surface conditions.

ACF

ACF associates an acentric factor with each component. ACFS is the corresponding keyword at surface conditions.

BIC

BIC specify the binary interaction coefficients between the components. BICS is the corresponding keyword at surface conditions.

LBCCOEF

LBCCOEF enable the possibility to enter non-default (not Lorentz-Bray-Clark viscosity correlation) values. The default values are 0.1023, 0.023364, 0.058533, -0.040758, 0.0093324.

STCOND

Sets temperature and pressure at standard conditions.

DENSITY

DENSITY sets the density of oil, water and gas at surface conditions respectively. Default: oil= $600 kg/m^3$, water= $999.014 kg/m^3$ and gas= $1 kg/m^3$.

PVTW

PVTW specify the water formation volume factor, the water compressibility, water viscosity and water "viscobility". The first and third item are at reference pressure which is the first input. Associated data can be found in the appendix.

ROCK

ROCK specify reference pressure and rock compressibility.

SWOF

SWOF treats the relative permeability and capillary pressure as one-dimensional properties as they are only dependent on water saturation ($S_o = 1 - S_w$). Two regions are specified, one for the core and one for the dead end volumes. There is zero capillary pressure in the dead end volumes.

Table 6.7 shows an example of table data in the SWOF keyword. The first column is the water saturation, the parameter the other functions are dependent on. The water saturations are in ascending order. The second column is the water relative permeability, the third column is the oil relative permeability in water and the last column is the oil-water capillary pressure, P_{cow}. In this table there are three saturations of special interest:

1. The critical water saturation: The highest saturation for which the water relative permeability is zero. This value must be entered in the table.

2. The minimum water saturation: Keyword, EQUIL, sets this value in gridblocks above water contact. This is the connate water saturation.

3. The maximum water saturation: EQUIL sets this value as the water saturation in gridblocks below the water transition zone.

Table 6.7: Typical SWOF data

Sw	Krw	Krow	Pcow
0.145	0.00	9.20E-01	1.97E-01
0.20	0.00	7.00E-01	8.88E-02
0.24	0.00	5.65E-01	6.70E-02
0.32	0.00	3.65E-01	4.45E-02
0.40	0.01	2.13E-01	3.42E-02
0.52	0.06	5.54E-02	2.58E-02
0.56	0.09	2.20E-02	2.40E-02
0.58	0.10	1.01E-02	2.33E-02
0.62	0.13	0.00E+00	2.23E-02
0.70	0.23	0.00E+00	2.01E-02
0.95	0.82	0.00E+00	1.64E-02

SGOF

SGOF treats the relative permeability and capillary pressure as one-dimensional properties as they are only dependent on gas saturation ($S_o = 1 - S_g - S_{wc}$). Two regions are specified, one for the core and one for the dead end volumes. There is zero capillary pressure in the dead end volumes.

Table 6.8 shows an example of table data in the SGOF keyword. The first column is the gas saturation. Similarly to the water saturation in SWOF, the gas is the parameter the other functions are dependent on. The gas saturations are in ascending order. The second column is the gas relative permeability, the third column is the oil relative permeability in gas at connate water saturation and the last column is the oil-gas capillary pressure, Pcog. In the SGOF table there are three gas saturations of interest:

1. The critical gas saturation: The highest gas saturation for which the gas relative permeability is zero. This value must be defined and entered in the table.

2. The minimum gas saturation: EQUIL sets the gas saturation to this value in the gridblocks below the gas contact.

3. The maximum gas saturation: EQUIL sets the gas saturation to this value in the gridblocks above the gas transition zone.

Table 6.8: Typical SGOF data

Sg	Krg	Krog	Pcog
0.00	0.00	0.92	2.86E-02
0.16	0.00	0.44	3.33E-02
0.22	0.01	0.31	3.52E-02
0.26	0.02	0.25	3.68E-02
0.34	0.05	0.15	4.02E-02
0.44	0.12	0.07	4.54E-02
0.50	0.18	0.03	4.97E-02
0.54	0.23	0.01	5.32E-02
0.56	0.26	0.01	5.50E-02
0.57	0.28	0.00	5.62E-02
0.62	0.35	0.00	6.11E-02
1.00	1.00	0.00	9.87E+00

STONE1

STONE1 specify that the three-phase oil relative permeability values are to be calculated using the Stone model 1 (Actually the modified version proposed by Aziz (1979)).

STONE1EX

STONE1EX specifies the value of the exponent term which is to be applied to the combination of saturation terms. The associated data consist of a exponent value per saturations table.

REGIONS

PVTNUM

Specify what PVT region a gridblock belongs to.

Associated data: 74*1

FIPNUM

Specify what fluid-in-place region a gridblock belongs to.

Associated data: 2   72*1   2

<u>SATNUM</u>

Specify what saturation function region a gridblock belongs to.

Associated data: 2   72*1   2

SOLUTION

<u>SWAT</u>

Specify the initial water saturation for each gridblock.

Associated data: 0.01   72*0.616   0.999

<u>SOIL</u>

Specify the initial oil saturation for each gridblock.

Associated data: 0.01   72*0.384   0.001

<u>PRESSURE</u>

Specify the initial pressure for each gridblock.

Associated data: 74*309.8939

<u>NEI</u>

NEI generates a non-equilibrium initialization composition. Used to generate consistent oil and gas compositions for each gridblock, by flashing to gridblock pressure. The associated data is not similar for Experiment 1 and 2. Experiment two has two regions and have different compositions (dry injection gas in top gridblock and oil composition in the rest).

Associated data:

Experiment 1:

0.51639   0.14067   0.06116   0.16916   0.06848   0.04414

Experiment 2:

0.8198   0.1471   0.0295   0.0036   0.0   0.0

0.4880   0.1359   0.0804   0.1878   0.0709   0.0367

<u>FIELDSEP</u>

FIELDSEP introduces a field separator. Associated data are the field separators stage index, temperature, pressure, destination of liquid output and vapor output.

Associated data: 1   15.0   0.986923

SCHEDULE

<u>CVCRIT</u>

CVCRIT sets convergence criteria.

<u>TSCRIT</u>

TSCRIT controls timestepping. Timestep is 0.01.

<u>WELLSTRE</u>

WELLSTRE specifies the composition of the injection fluid.

Associated data:

Experiment 1:   0.779171   0.13325   0.037295   0.047617   0.002618   5.01E-05

Experiment 2:   8.20E-01   1.47E-01   2.95E-02   3.59E-03   0.00E+00   0.00E+00

6.3   Capillary Pressure

The experimentally obtained capillary pressure curves are inapplicable in a simulation model because the curves are not one-to-one. Section 4.5.3 presents the experimental centrifuge capillary pressure. One can observe in Figure 4.7 how the gas-water curve curves back around 2.0% water saturation. Eclipse, applying the keywords SWOF and

SGOF, will not be able to read this, and the curve needs to be adjusted and smoothed out. This is done in this study and will be presented in Chapter 7. The oil-water curve shows a "drop" from its trend around $S_w = 25.0\%$ and this should also be adjusted and straightened out. However, the oil-water and gas-oil curve are already adjusted by Hustad and Holt, as can be seen in Figure 4.7 as the simulator-curves.

The capillary pressure curves are also extended to fit an irreducible water saturation of $S_{wir} = 4.5\%$. This will be later showed to be a necessary measure to achieve a match.

6.3.1 Experiment 2

While equation 5.6 will scale the centrifuge oil-water capillary pressure, P_{cow}, for Experiment 1, Experiment 2 will use this equation on both oil-water capillary pressures, P_{cow}, and gas-water capillary pressure, P_{cgw}. Then P_{cow} and P_{cgw} will be joined together at the water saturation where vaporization effects are observed and extended to lower saturations. In this way, the fluid system is changed and additional recovery of the water will be visible. This is because the water will be allowed to flow to lower water saturations. Because even though oil-water capillary pressure is extended down to $S_w = 4.5\%$, the values at lower saturations are too high and will prevent water production. At the same water saturation, the gas-water curve allows for further water production.

Before the water saturation at which the joining of capillary pressure curves should occur is decided, evaluation of the block saturation with corresponding capillary pressure is conducted. The water saturation where the path should change from oil-water to gas-water is user-specified and it is chosen for where the vaporization effects are believed to be present. Practically speaking, it means that in the P_{cow} column in SWOF, the pressures are changed from oil-water to gas-water from the value of the user-specified water saturation, hereby called $S_{w,u}$, and below. This alteration makes the system drain to even lower water saturations if the system reaches $S_{w,u}$, and can then potentially capture the additional water recovery observed in Experiment 2. The user-specified water saturation is decided with trial and error, however a certain interval of potential water saturations is narrowed down at first. By investigating the behavior of block water sat-

uration and capillary pressure at upper, middle and lower blocks, one can spot an area where the capillary pressure prevents further water production.

When $S_{w,u}$ is decided, the gas-water capillary pressure curve is scaled according to equations 5.5 and 5.6 down to a level which creates an intersection at $S_{w,u}$.

6.4   Extension of Relative Permeability Curves

As for the capillary pressure curves, the water relative permeability curve is extended down to $S_w = 4.5\%$. The oil in water relative permeability curve, k_{row}, is also extended to higher water saturations.

Chapter 7

Results

The results of the simulations of Experiment 1 and 2 will be presented in this chapter. The results will be presented in chronological order, following the steps of the flow chart given in Figure 6.1. Furthermore, saturation profiles at different time steps will be provided to observe how the fluids flow through the core. Lastly a sensitivity study is conducted and presented here. Parameters such as gridblocks, time steps and capillary pressures are tested for sensitivity.

7.1 Best Match

As stated, the overall goal of this study is to history match Experiment 2 and thus capture the extra water recovery suspected to be an effect of vaporization effects. But before that is possible, Experiment 1 is matched to determine the correct rock properties such as relative permeability and oil-water and gas-oil capillary pressure. Since the two cores used for Experiment 1 and 2 have similar rock characteristics, this method is useful. This section will take the reader through the steps of a achieving a satisfactory match for Experiment 1 and 2.

7.1.1 Step 0: Evaluate Input Data

Before a match of Experiment 1 is achieved, a simulation of the experiment applying the simulation curves used by Hustad and Holt is conducted. This way one can see what

kind of effects one wants out of changing the input data. This run is called Basecase for
further reference.

In Basecase, the irreducible water saturation, S_{wir}, goes down to 14.5%. This implies a
maximum gas saturation, $S_{g,max}$, of 85.5%. Figures 7.1, 7.2 and 7.3 present the relative
permeabilities and capillary pressures applied in this simulation model. The capillary
pressures are scaled according to equations 5.5 and 5.6 with the user-specified constant
equal to 1. That means the capillary pressures are only scaled with regards to interfacial
tension, not being further scaled by the user-specified constant. The relative perme-
abilities are exactly the same as the ones presented in Section 4.5.2.
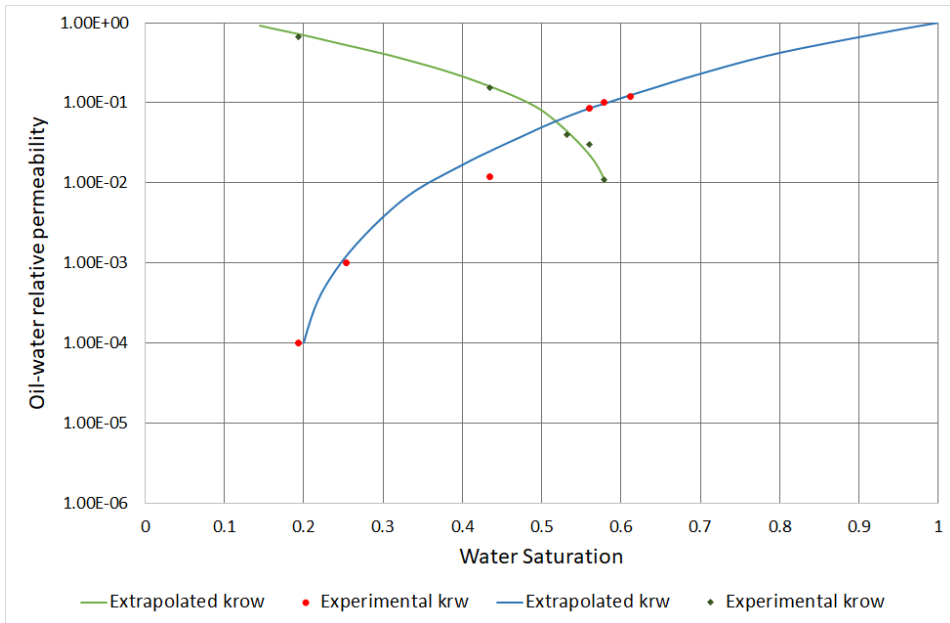
Figure 7.1: Oil-water relative permeability of Basecase
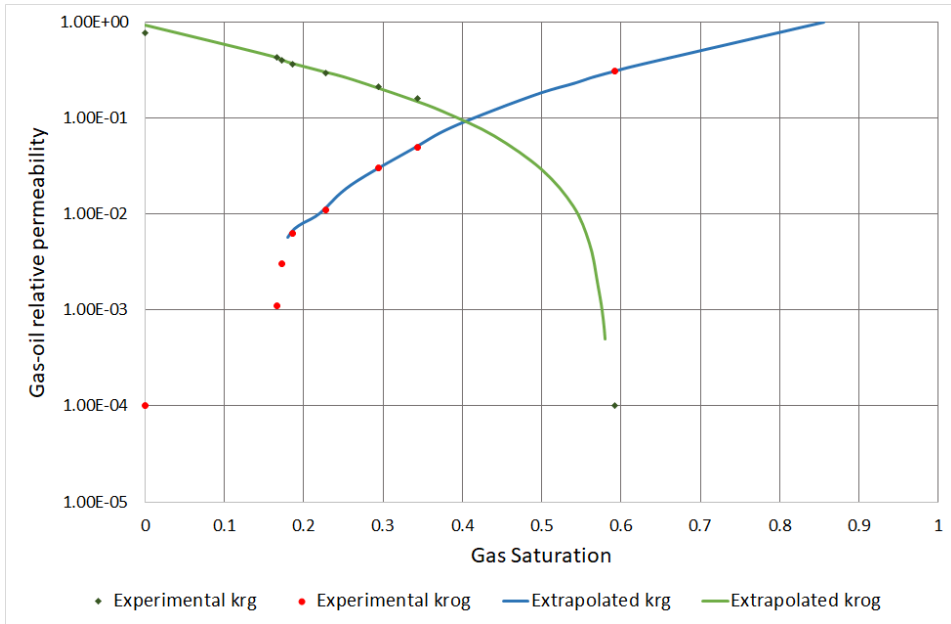
Figure 7.2: Gas-oil relative permeability of Basecase
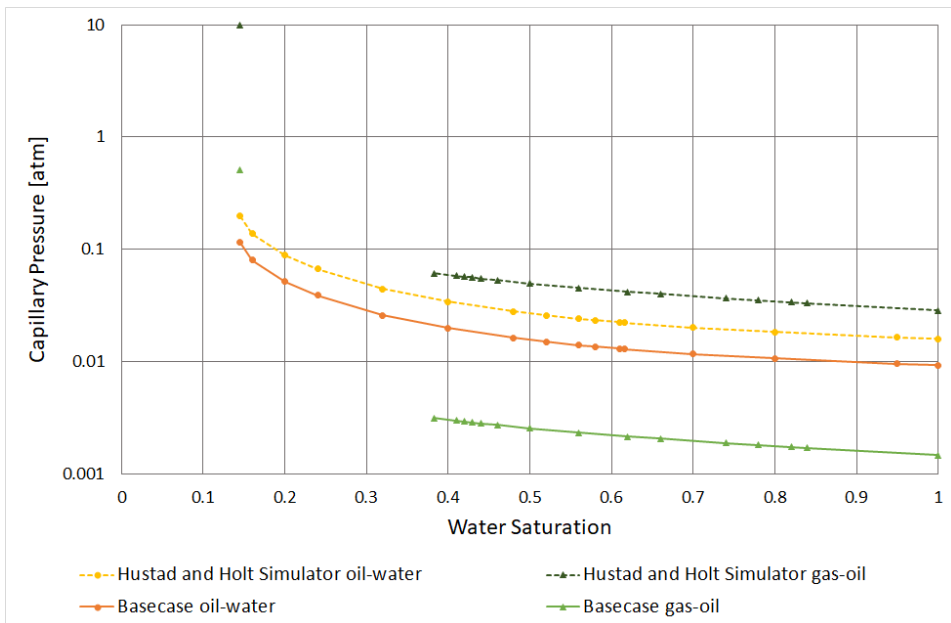
Figure 7.3: Capillary Pressure of Basecase

Basecase lacks a surface equation of state (EOS), only having a reservoir EOS which was

set prior to this study by Hustad. The Soave-Redlich-Kwong is also applied in Basecase. Basecase also has the gas injection that is recombined from the compositions given in Table 3 in the report by Hustad and Holt (1992).

Figure 7.4 shows the different fluid recovery matches of Basecase.
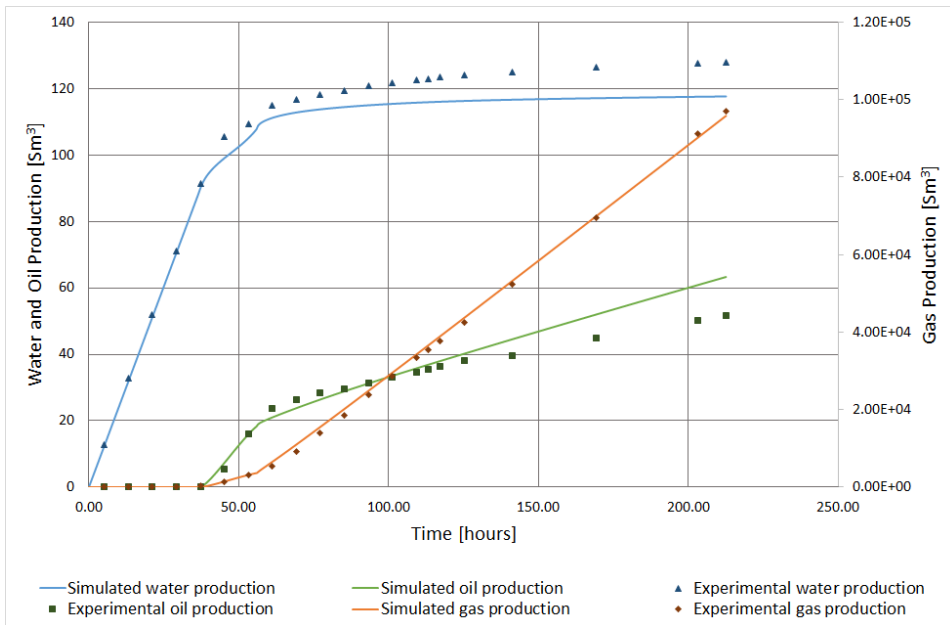
Figure 7.4: Experiment 1: Simulation of Basecase

Simulation of Basecase shows a clear deviation of water and oil production from experimental data. Simulated gas production match well. It is clear that the water production is too low after oil and gas breakthrough. While water production is too low compared to experimental data, oil is too high after 125 hours. At this point in the study, the deviation of oil recovery is not suspected to be an effect of erroneous simulation of condensate production in Eclipse. Table 7.1 presents production data and corresponding deviation at end time.

Table 7.1: Basecase: Production and deviation at end time

	Time	Oil [Sm^3]	Gas [Sm^3]	Water [Sm^3]
Experimental	212.51	51.70	96980.00	127.80
Basecase	212.51	63.29	95822.48	117.64
Deviation	-	22.42 %	-1.19 %	-7.95 %

7.1.2   Step 1: Achieve a Match for Experiment 1

To achieve a match for Experiment 1, several changes to the input parameters are nec-
essary. Even though the gas production match well with experimental data, the gas
injection composition needs to be changed so it is treated as the equilibrium gas to the
oil by Eclipse. Water production needs to be elevated at a higher level, and oil produc-
tion needs to be reduced after 125 hours. Many different variations of changes are tried.
The modifications that ended up being the best are as follows:

1. New gas injection composition.

2. Establishment of a surface equation of state.

3. Extend capillary pressure and water relative permeability data down to Sw =
   4.5%.

4. Extend oil in water relative permeability to higher water saturation.

5. Scale water-oil capillary pressure curve, P_{cow}, further down to increase the water
   production level around oil and gas breakthrough.

The new gas composition and the surface equation of state data are obtained and speci-
fied as written in Section 6.1. Figures 7.5 and 7.6 shows the difference between capillary
pressure and relative permeability in Basecase and the best match for Experiment 1,
hereby called Best Match 1. Table 7.2 lists the scaling factors and user-specified con-
stant used to scale the oil-water and gas-oil curves. The same user-specified constant,
l_{ij}, is chosen for oil-water and gas-oil capillary pressures. The oil-water capillary pres-
sure and water relative permeability are significantly changed. The new P_{cow} follows

the same curvature as the one for Basecase, however it has been lowered to increase wa-
ter production. In addition, it has been extended down to $S_w = 4.5\%$, a crucial change
to achieve high enough water recovery. Water relative permeability changes its path
around $S_w = 24.0\%$ and extends down to $S_w = 4.5\%$ with a less steep drop in values at
lower water saturations compared to Basecase. The oil in water relative permeability
curve, k_{row}, is on the other hand extended to higher water saturations. This alteration
is crucial to obtain high enough oil production values, however it is questionable as it
means the initial oil saturation set in SOIL is not the residual oil saturation. Neverthe-
less, it is necessary to achieve an oil match. Figure 7.7 shows the extension of k_{row} to
higher water saturations. No changes are done to gas relative permeability, k_{rg}, or the
oil relative permeability in gas, k_{rog}.

Table 7.2: Experiment 1: Scaling parameters

Parameter	P_{cow}	P_{cog}
l_{ij}	1.681	1.681
f_{ij}^{Pc}	0.403	0.007
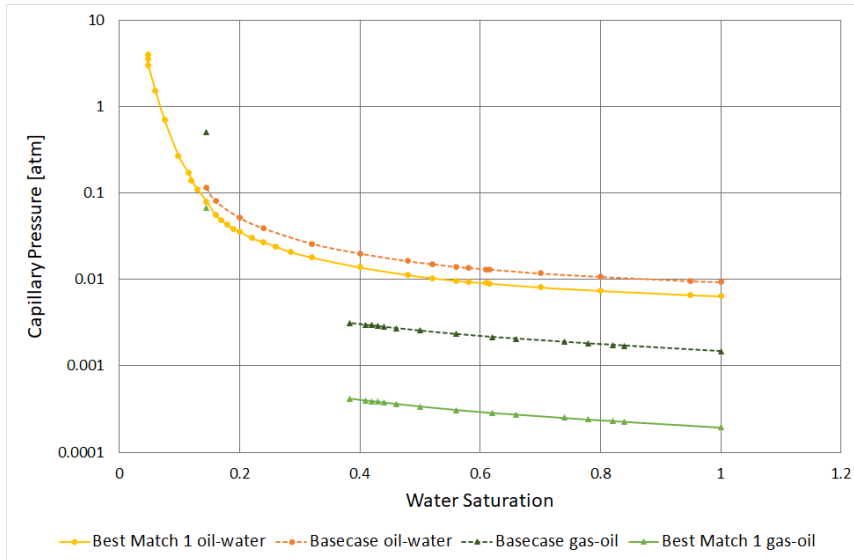
Figure 7.5: Oil-water capillary pressure of Basecase and Best Match 1
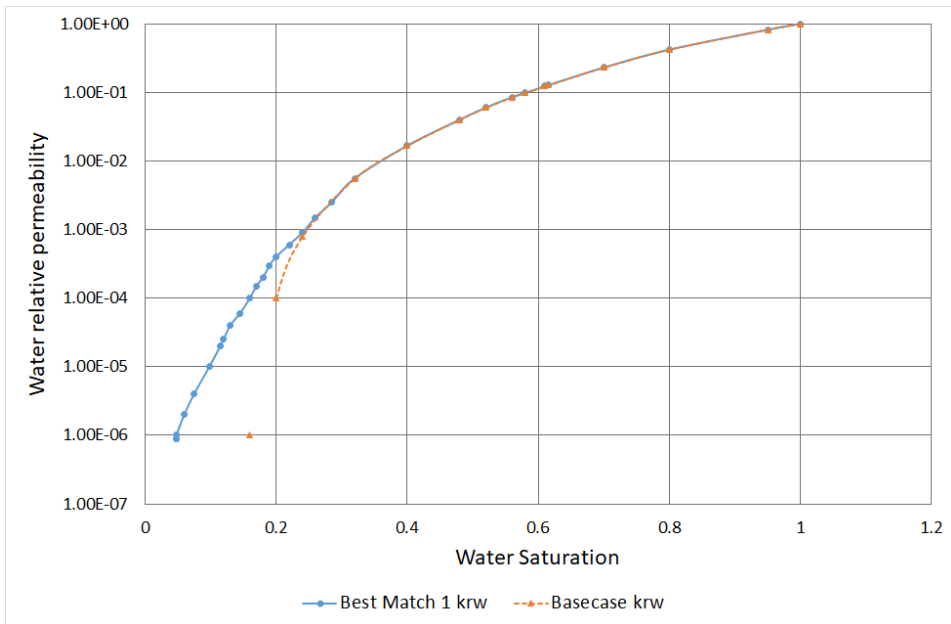
Figure 7.6: Water relative permeability of Basecase and Best Match 1
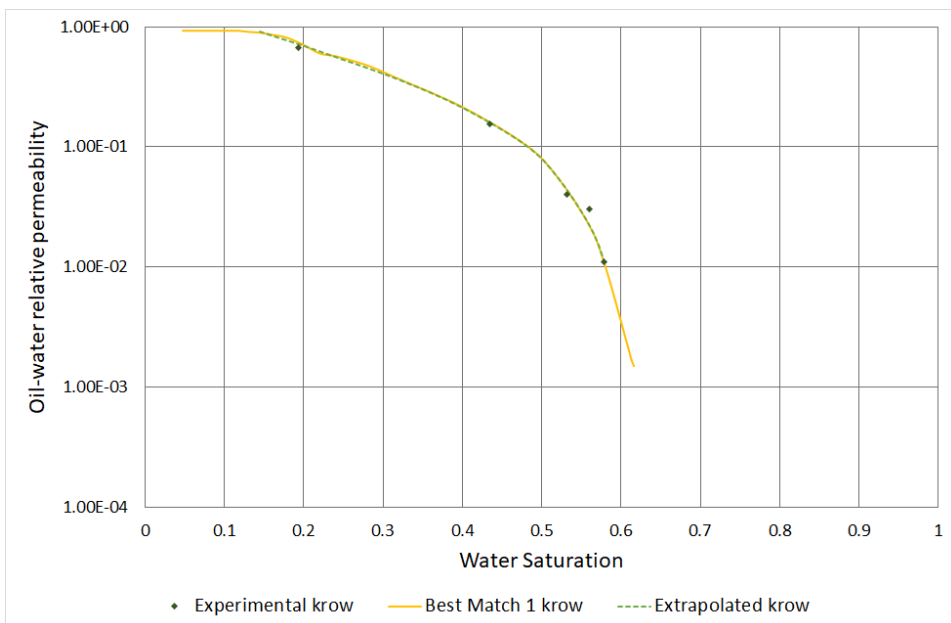
Figure 7.7: Oil in water relative permeability for Best Match 1

Figure 7.8 presents the best match of Experiment 1. It is evident how the changes have

improved the match between simulated and experimental data. Keep in mind that the experimental oil production curve in figure 7.4 is not modified due to incorrect condensate production, but the oil production in figure 7.8 is, making the match look even more improved than it is. Figure 7.9 shows the difference between Basecase and Best match.
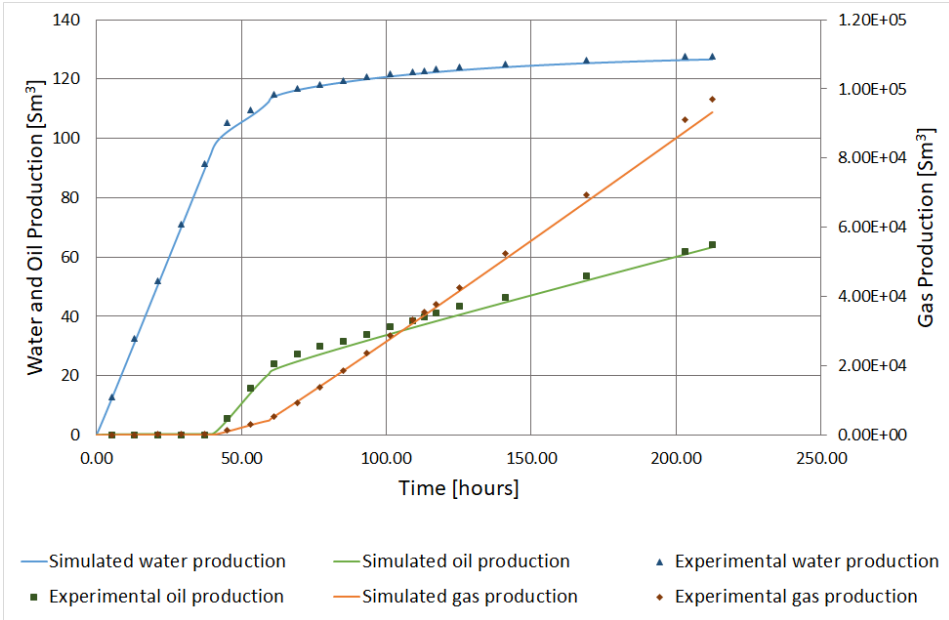
Figure 7.8: Best match of Experiment 1
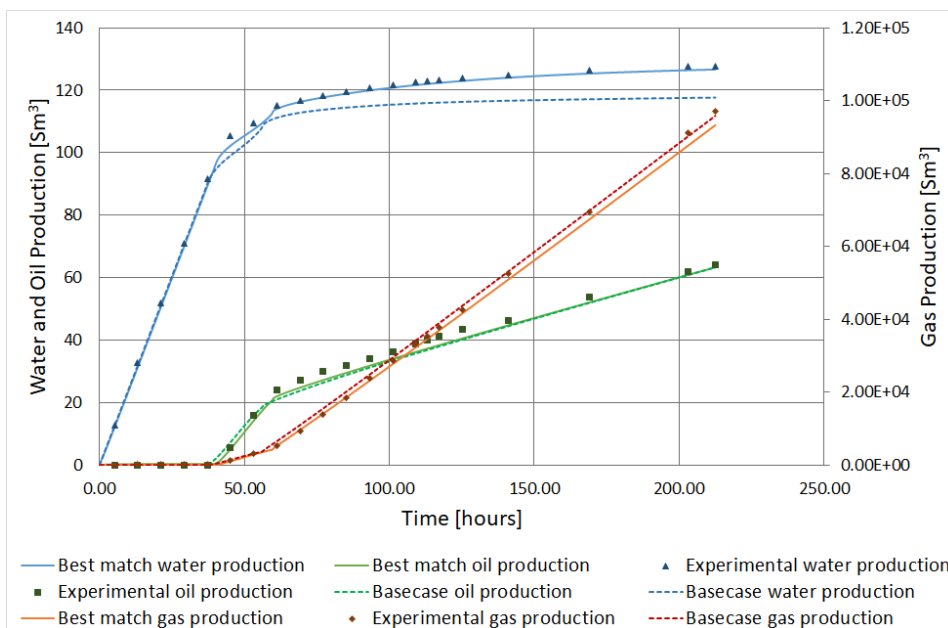
Figure 7.9: Comparison of Best Match 1 and Basecase

It might not seem like the surface equation of state offer much difference to the oil production, but closer examination shows that Best Match 1 delays oil breakthrough and also increases the oil production level around 60 hours. Best Match 1 gas production is actually worse at end time, but the gas production matches better than Basecase up until 100 hours with a later gas breakthrough around 60 hours. Table 7.3 presents production and corresponding deviation at end time. Keep in mind that the experimental oil production is adjusted for extra condensate recovery.

Table 7.3: Best match 1: Production and deviation at end time

	Time	Oil $[Sm^3]$	Gas $[Sm^3]$	Water $[Sm^3]$
Experimental adjusted	212.51	63.71	96980.00	127.80
Best Match 1	212.51	63.31	93256.75	126.64
Deviation	-	-0.64%	-3.84%	-0.91%

7.1.3 Step 2: Achieve a Match for Experiment 2

After a match of Experiment 1 is achieved, Experiment 2 is simulated with the same dynamic rock properties (capillary pressure and relative permeability) to observe the difference between the experiments. However, before the simulation is run, a new surface equation of state is established because of the different type of injection gas. Also, the core is now split in two different equilibration regions to separate the the oil and the new dry injection gas. Figure 7.10 shows simulated production results of Experiment 2 with saturation function rock properties from Experiment 1.
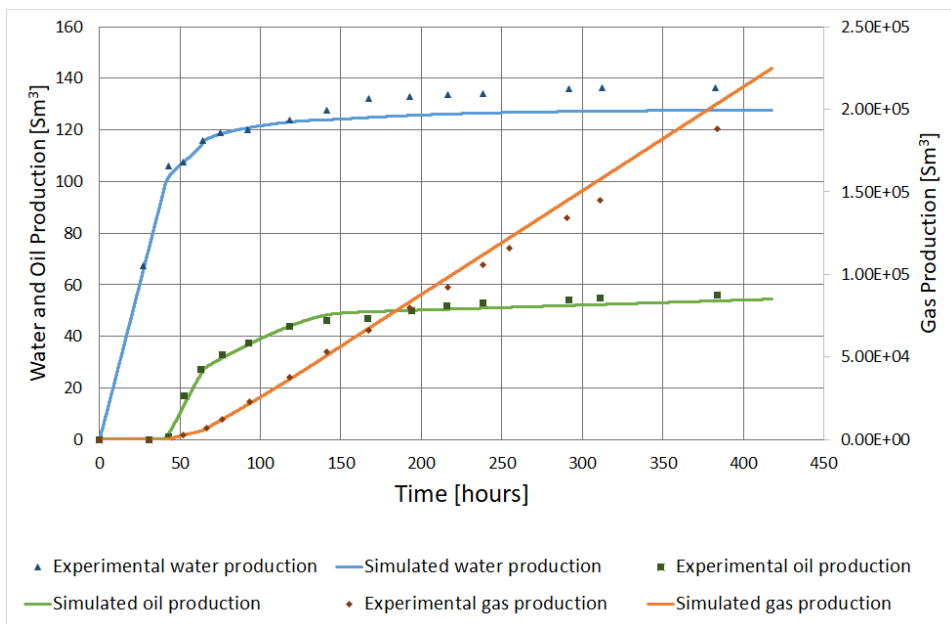
Figure 7.10: Simulation of Experiment 2 with Experiment 1 cap. pressure and rel. perm.

While oil and gas production match well, water recovery is poorly matched. The simulation results are very similar to what Hustad and Holt (1992) achieved when they simulated Experiment 1 and 2 with Extended Stone model 1. This led to the suggestion offered by Hustad concerning joining of capillary pressure curves. The extra water recovery after 120 hours is tried captured with joining the oil-water capillary pressure curve, P_{cow}, and the gas-water curve, P_{cgw} at a water saturation ideally only reached by Experiment 2 and not Experiment 1. Figure 7.11 shows the new modified capillary curve which is a combination of oil-water and gas-water capillary pressures. The joining oc-

curs at $S_w = 22.0\%$ and forces the simulation model to follow lower capillary pressure values from that point on. P_{cgw} is made one-to-one.
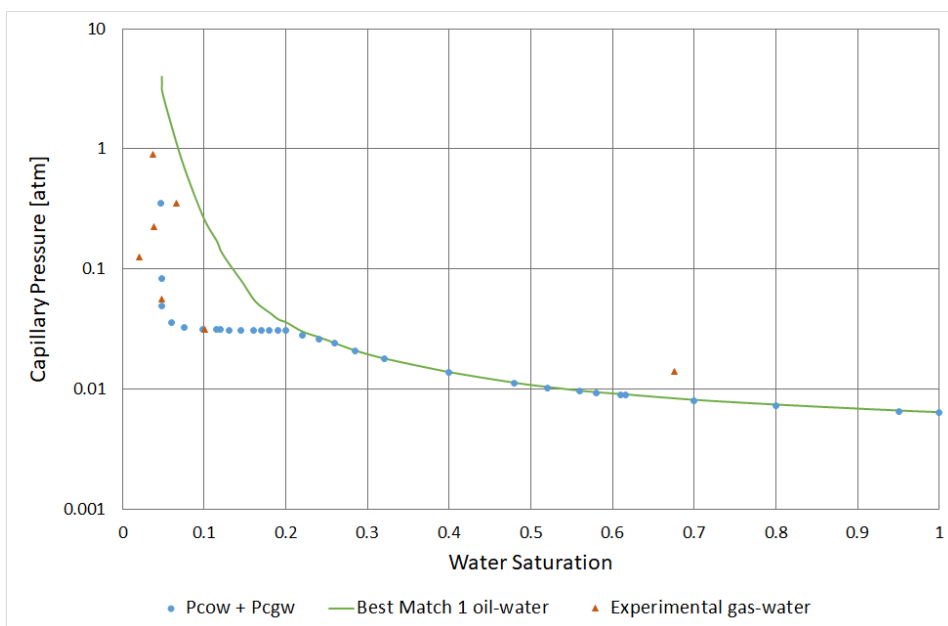
Figure 7.11: Joining of Pcow and Pcgw

Figure 7.12 presents the best match of Experiment 2 with joining of capillary pressure curves, hereby called Best Match 2. It is obvious that the new capillary pressure path down to gas-water values have great effects on water production. With this new curve, the water level is high enough to create a match and the new match increase the water production at end time with 7.0%. However, the match is not perfect. As one can see from the plot, the experimental values show an abrupt increase in water recovery around 120 hours. The simulation model have great difficulties capturing this abrupt change in water production rate. Instead it displays a steady increase eventually leading up to correct water production values. The simulated oil recovery is considered good. The gas recovery displays a deviation towards end time, a similar effect Hustad and Holt (1992) observed in their studies. Table 7.4 presents production data and corresponding deviation at end time.
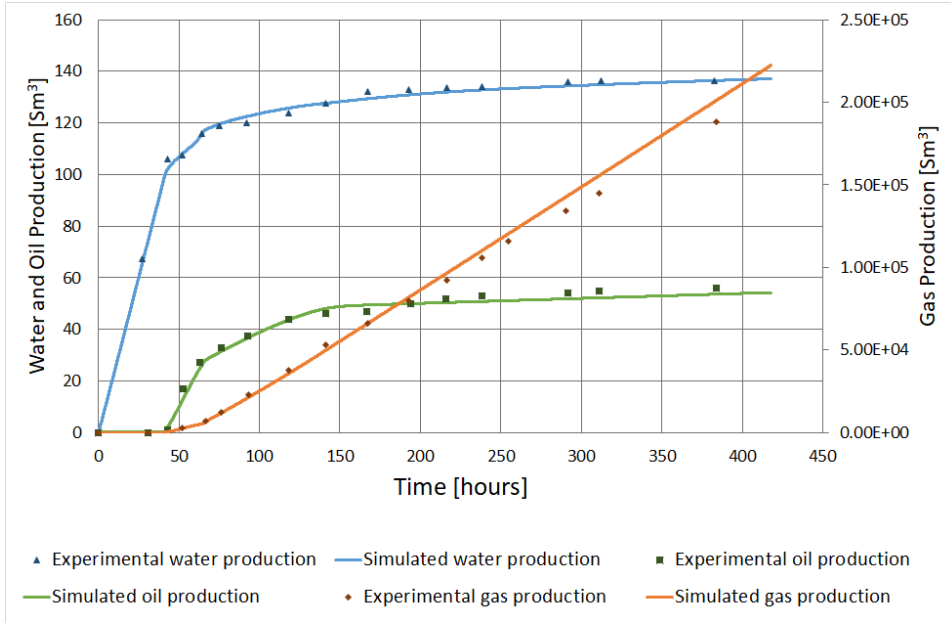
Figure 7.12: Best match of Experiment 2

Table 7.4: Best Match 2: Production and deviation at end time

	Time	Oil [Sm^3]	Gas [Sm^3]	Water [Sm^3]
Experimental	418	56.00	188000.00	136.40
Best Match 2	418	54.28	222614.05	136.77
Deviation	-	-3.07%	18.41%	0.27%

Figure 7.13 shows the applied capillary pressure curve at 418 hours. It is evident how the system applies the gas-water capillary pressures when the system drains to water saturations less than $S_w = 22.0\%$. At this stage, the calculated three-phase relative permeability to oil, k_{ro}, is zero. In fact, k_{ro} is zero from around 120 hours. This indicates that the remaining oil production from that point on is oil coming from gas.
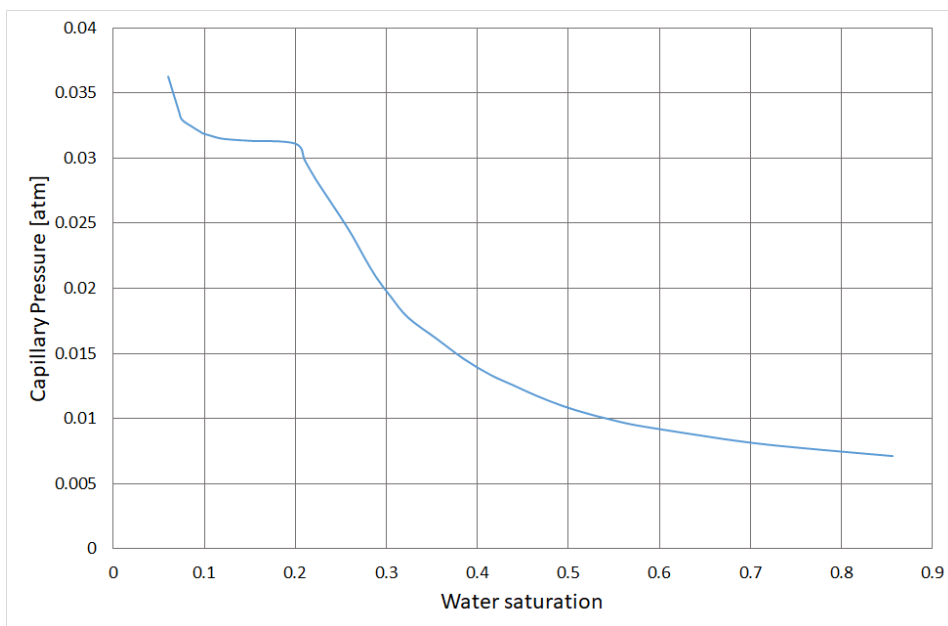
Figure 7.13: Experiment 2: Capillary pressure applied at 418 hours

Calculating backwards with the same user-specified constant, l_{ij}, equal to 1.681, the gas-water interfacial tension at reservoir pressure becomes 24.86mN/m. The gas-water interfacial tension at reference pressure is 72mN/m. This was measured during displacement of water by air as stated in Chapter 4.

7.1.4 Step 3: Check Match for Experiment 1

Ideally the joining of capillary pressure curves will not affect the match of Experiment 1. This needs to be checked where Experiment 1 is run with the joining of capillary pressure curves. Figure 7.14 shows simulated results of Experiment 1 applying the joining of the oil-water and gas-water capillary pressure curves. The water production towards the end of simulation is a bit too high, however it is considered acceptable with a deviation of 2.09% at end time. The oil and gas recoveries are less affected by the new capillary pressure curve and are still considered very good matches. Table 7.5 presents production data and corresponding deviation at end time.
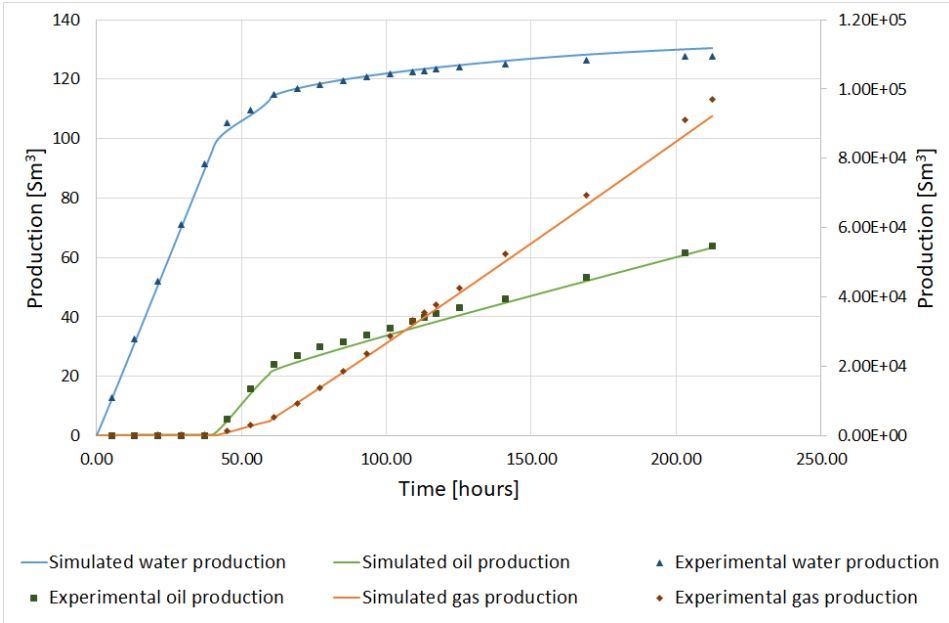
Figure 7.14: Match of Experiment 1 with Experiment 2 cap. pressure and rel. perm.

Table 7.5: New Best Match 1: Production and deviation at end time

	Time	Oil [Sm^3]	Gas [Sm^3]	Water [Sm^3]
Experimental adjusted	212.51	63.71	96980.00	127.80
New Best Match 1	212.51	62.94	92253.23	130.47
Deviation	-	-1.21%	-4.87%	2.09%

Figure 7.15 shows the applied capillary pressures at end time. As already mentioned, the joining should not be visible in the plot because Experiment 1 should not drain down to the saturation where the joining occurs. However, the joining occurs at $S_w = 22.0\%$ and Experiment 1 is therefore affected by it.
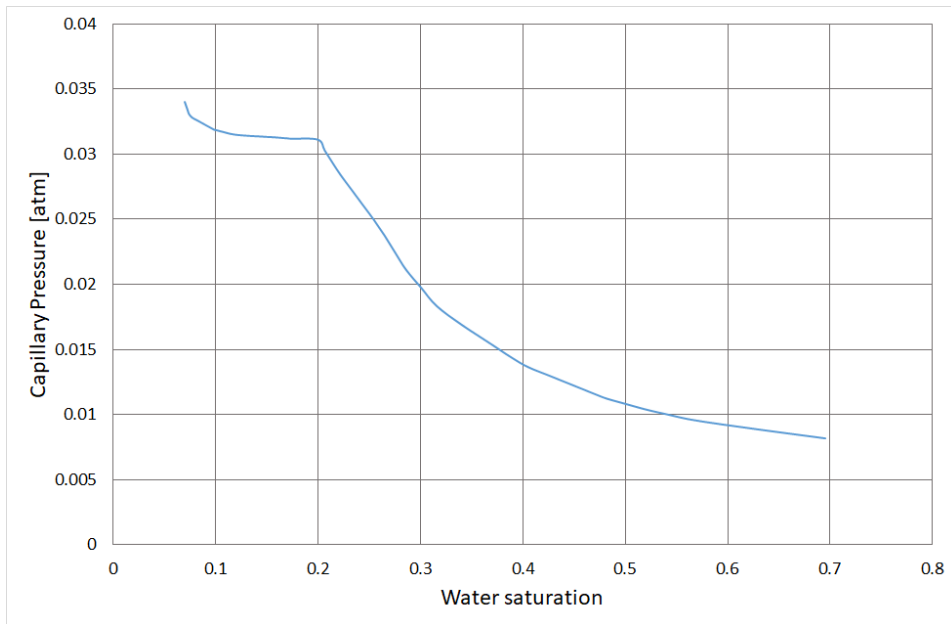
Figure 7.15: Experiment 1: Capillary pressure applied at 212 hours

7.2 Saturation Profile

This section will provide and discuss the observed saturation profiles at different times during simulation. The specific times are chosen because they represent a certain part of the production life, i.e before or after gas breakthrough etc. The saturation profiles are great for explaining the different productions trends observed.

7.2.1 Experiment 1

Figures 7.16, 7.17, 7.18 and 7.19 show the different saturation profiles at equal times between the simulation runs of Experiment 1 with and without joining of capillary pressure. They display quite similar saturation profiles, however some observations are worth mentioning. First of all, because the joining of capillary pressure occurs at $S_w = 22.0\%$, observed water saturation will be less for blocks of lower water saturation. This is typical for upper blocks because gas is injected from the top and will displace the water more efficiently in this area. One can clearly see this tendency in the upper blocks in Figures 7.16 through 7.19. This difference seem great, however because the

upper blocks are smaller than middle blocks and since the water volume is quite low already, it has little effect on water recovery before the end towards 212 hours.

Another interesting observation is that gas breakthrough occurs later in the case of joining of capillary pressure. Figure 7.18 shows how the case without joining reaches gas breakthrough around 59 hours, but the case with joining does not. This is connected to the increased gas displacement efficiency. Because the gas pushes more water out of the core, the gas is delayed and will break through at a later time. Another observation concerns gas breakthrough as well. From the production profiles in Figures 7.8 and 7.14, gas production starts between 37 and 45 hours. However one can see from the saturation profiles in Figure 7.17 how gas does not reach the lowest blocks. This is because the observed gas production is vaporized gas coming from the oil, not injection gas. Gas breakthrough is later, and is shown in production results as an increase in gas rate around 60 hours.

Figure 7.19 displays the saturation profile at end time. For the lower blocks, the water saturation is similar, with the same tendency of increasing towards the end block. This increase in water saturation is caused by capillary end effects, which is explained in Section 3.2.2. Around block 47, water saturation is less for the case with joining of capillary pressure. This is an indication of the extent of the capillary pressure joining and how it affect a large part of the core.

It needs to be stressed that these saturation profiles are not actual phase distributions within one block. The profiles only show the different amounts of phases in one block, and can only be used for discussing difference between the blocks, not within one.
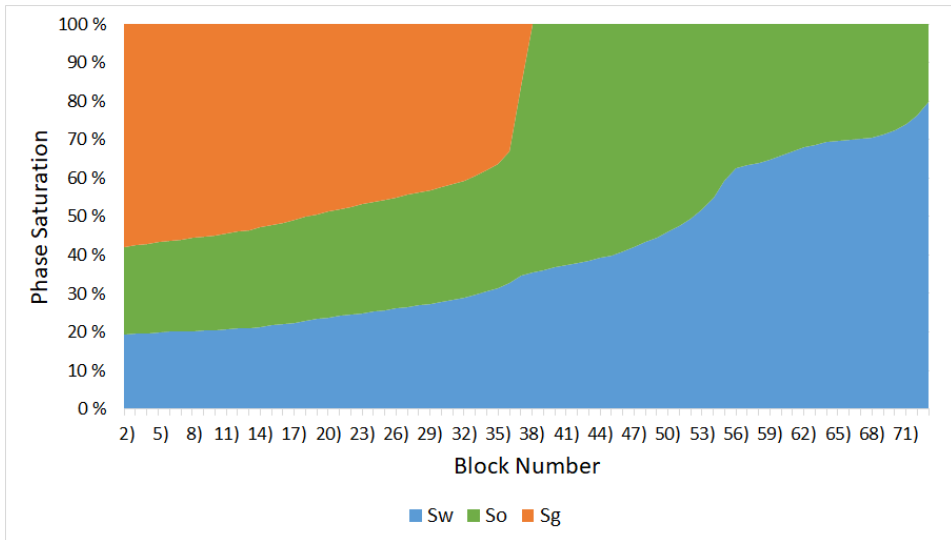
(a) Without joining of capillary pressure
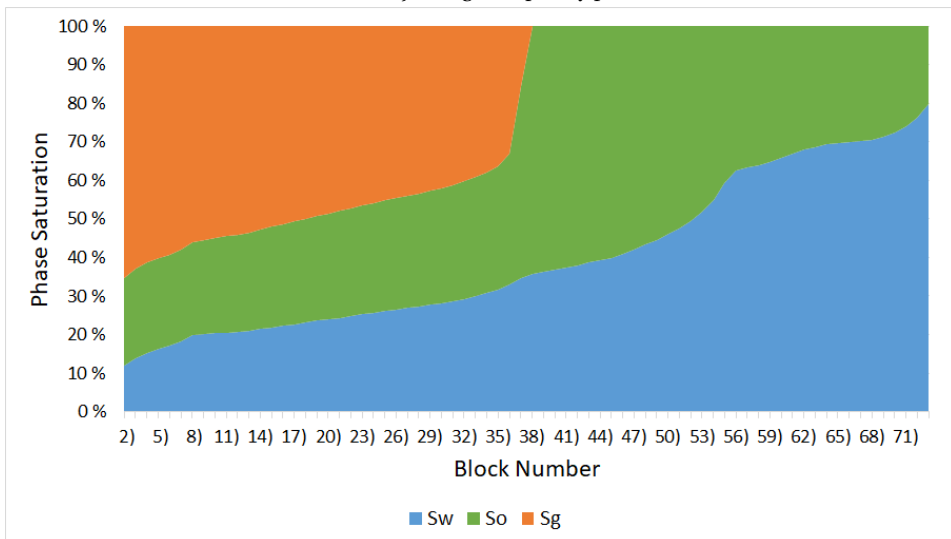
(b) With joining of capillary pressure

Figure 7.16: Experiment 1: Saturation Profiles at 29 hours
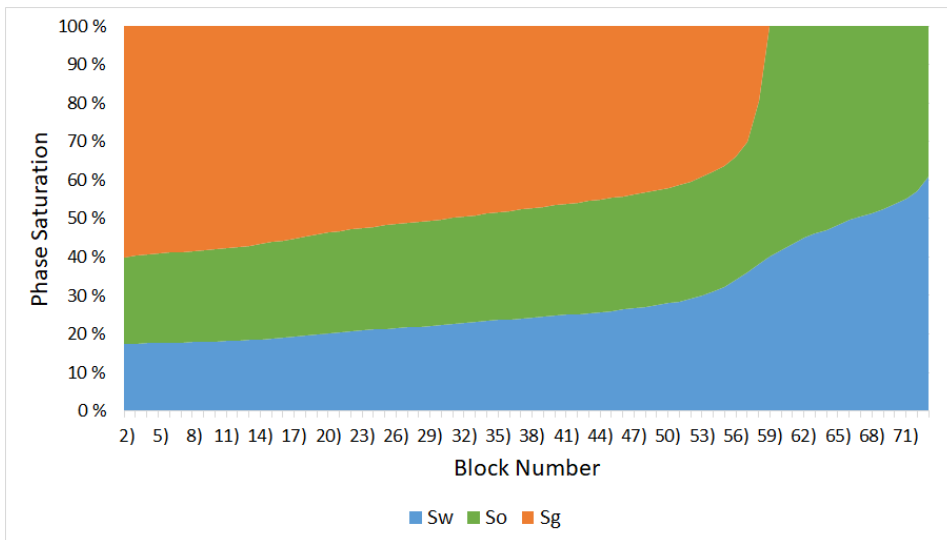
(a) Without joining of capillary pressure
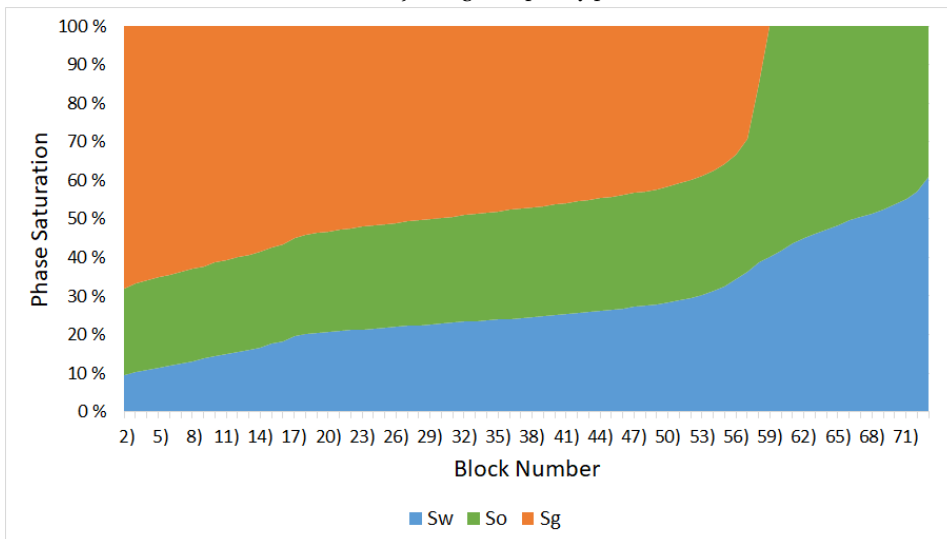
(b) With joining of capillary pressure

Figure 7.17: Experiment 1: Saturation Profiles at 53 hours
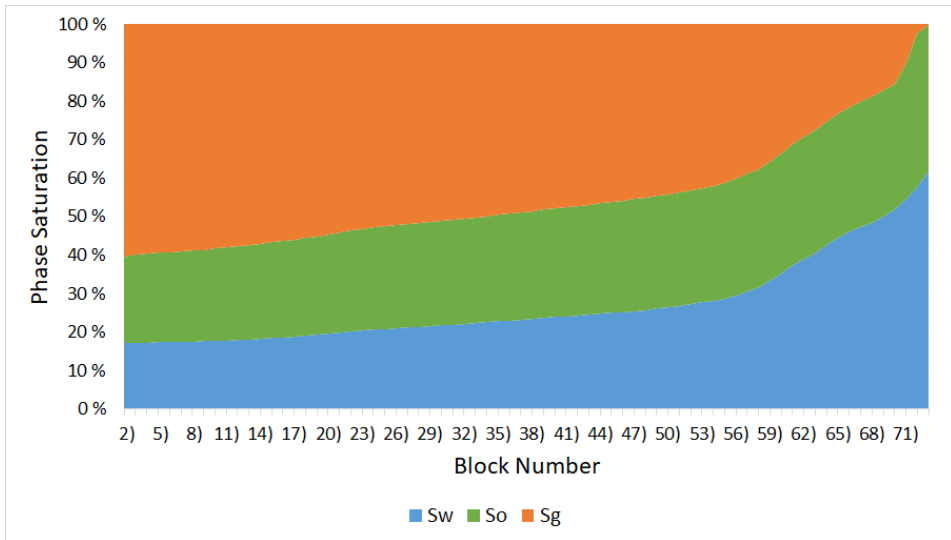
(a) Without joining of capillary pressure
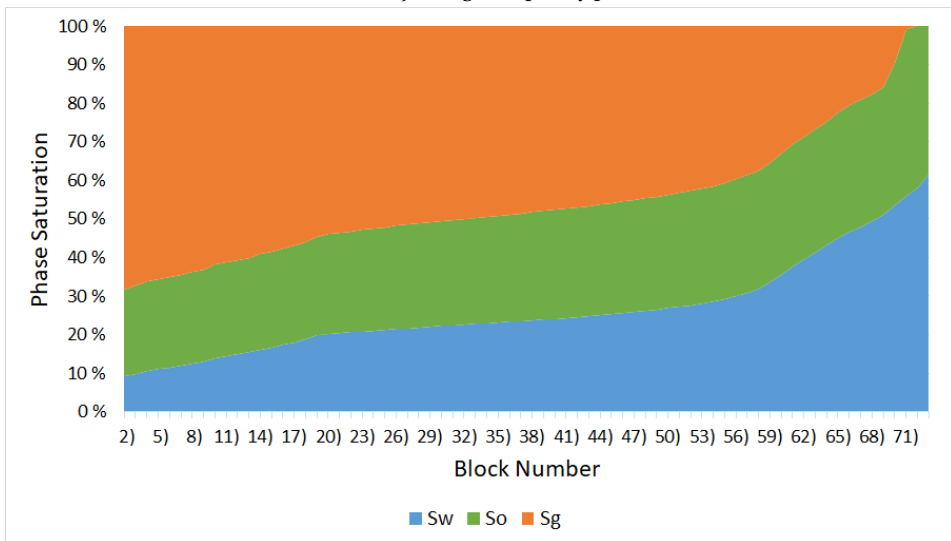
(b) With joining of capillary pressure

Figure 7.18: Experiment 1: Saturation Profiles at 59 hours
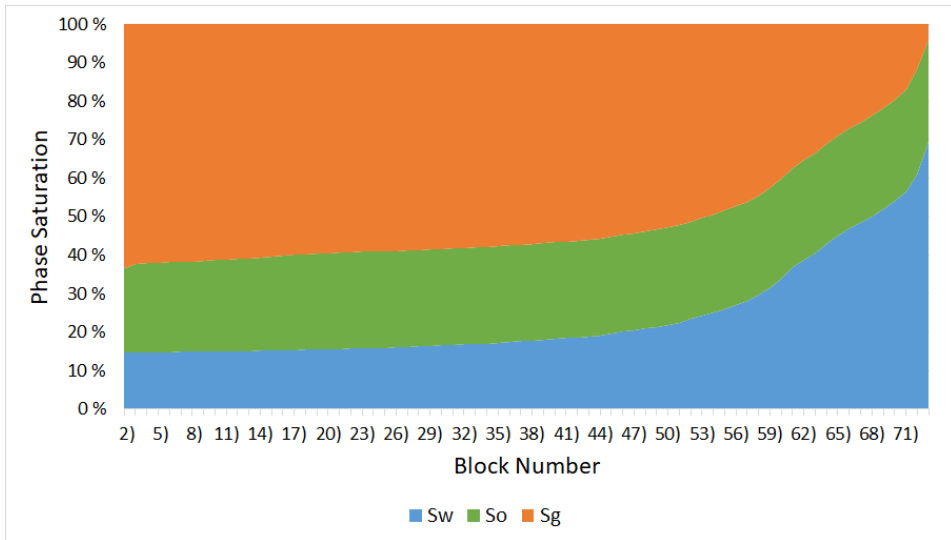
(a) Without joining of capillary pressure
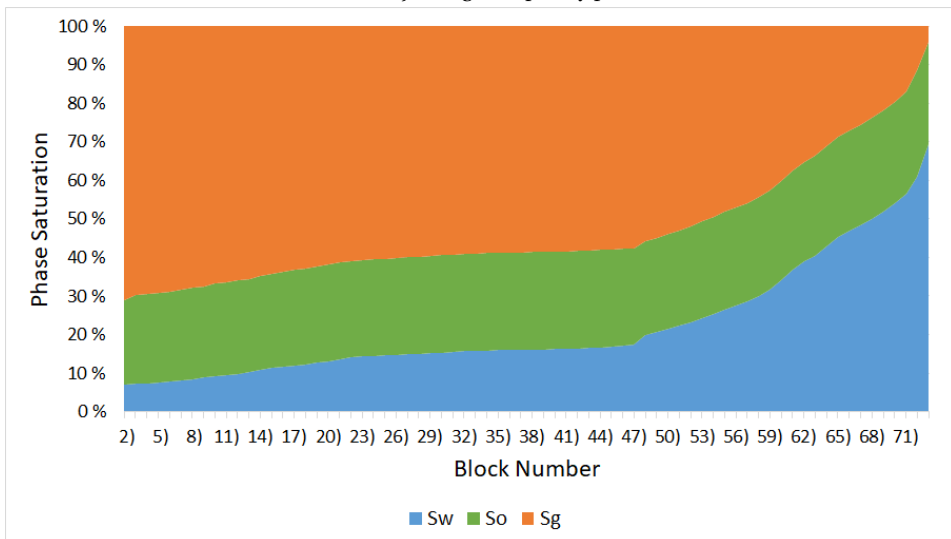
(b) With joining of capillary pressure

Figure 7.19: Experiment 1: Saturation Profiles at 212 hours

7.2.2 Experiment 2

This section will compare saturation profiles of Experiment 2 and Experiment 1 simulated with joining of capillary pressures. Figures 7.20, 7.21, 7.22, 7.24 and 7.25 present saturation profiles throughout the production life of Experiment 1 and 2.

The water saturation profiles show a similar trend between Experiment 1 and 2 in the early stages of production. However, in Figure 7.23, one can observe a higher water saturation level in the lower blocks for Experiment 2. At this time, the vaporization effects in Experiment 2 are believed to be present as indicated in the production results with the abrupt water recovery increase. The increase in water saturation in the lower blocks are caused by capillary end effects and will be discussed further in Chapter 8.

The oil saturation is distributed quite differently between Experiment 1 and 2. Already before gas breakthrough, there is much less oil in the upper blocks in Experiment 2 than in Experiment 1, a trend which extends throughout the core during further production. Gas breakthrough occurs later in Experiment 2 than in Experiment 1. Experiment 2 displaces the oil much more efficiently than Experiment 1, leaving a smaller residual oil saturation in the upper blocks (and later in the middle blocks). The difference in oil distribution is observed from the beginning of the simulations.

Figure 7.25 compares the end time profiles between Experiment 1 and 2 at 212 and 418 hours respectively. Oil saturations clearly pose the biggest differences between the experiments, but it is important to remember that Experiment 2 runs for over 200 hours longer than Experiment 1. This will lead to seemingly bigger differences between the saturation profiles. But then again, Figure 7.24 compares the profiles at both 212 hours, and the saturation distributions are very different at similar times.
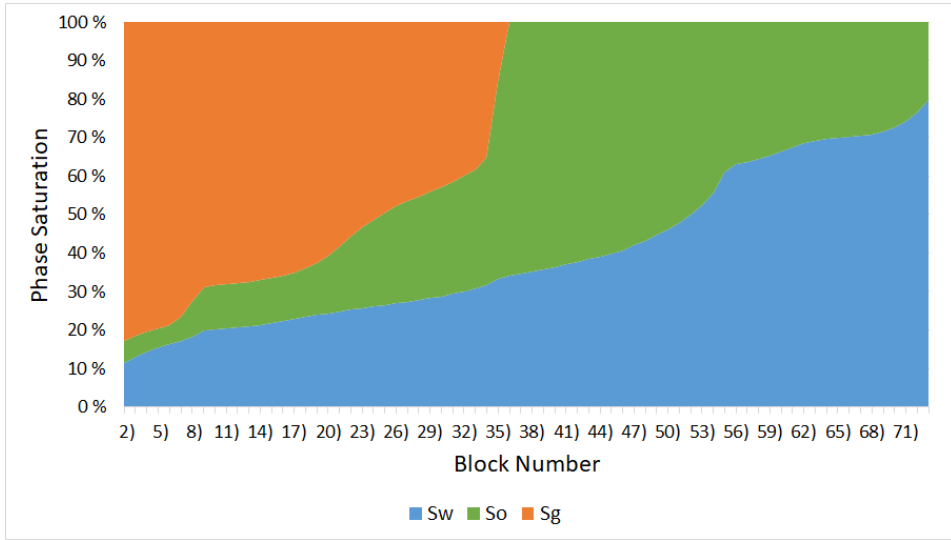
(a) Experiment 2
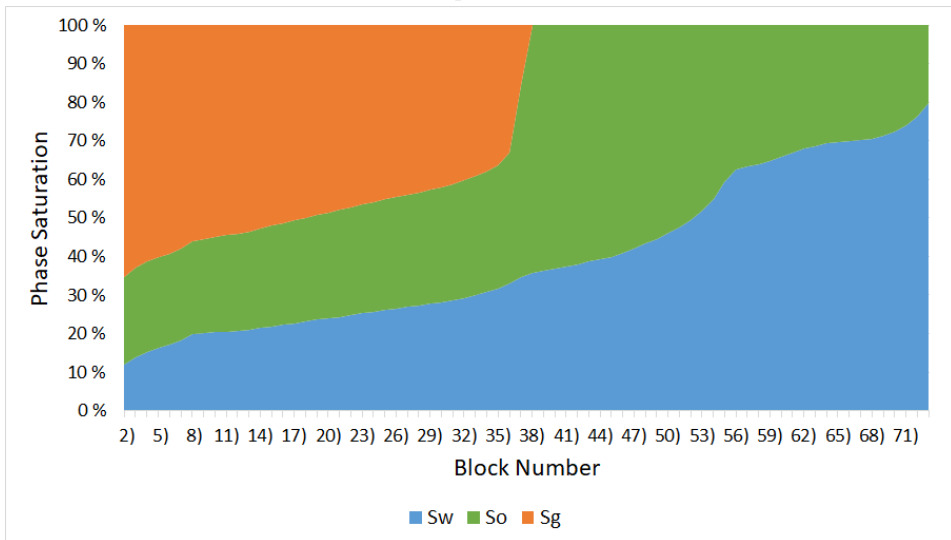
(b) Experiment 1

Figure 7.20: Saturation Profiles at 29 hours
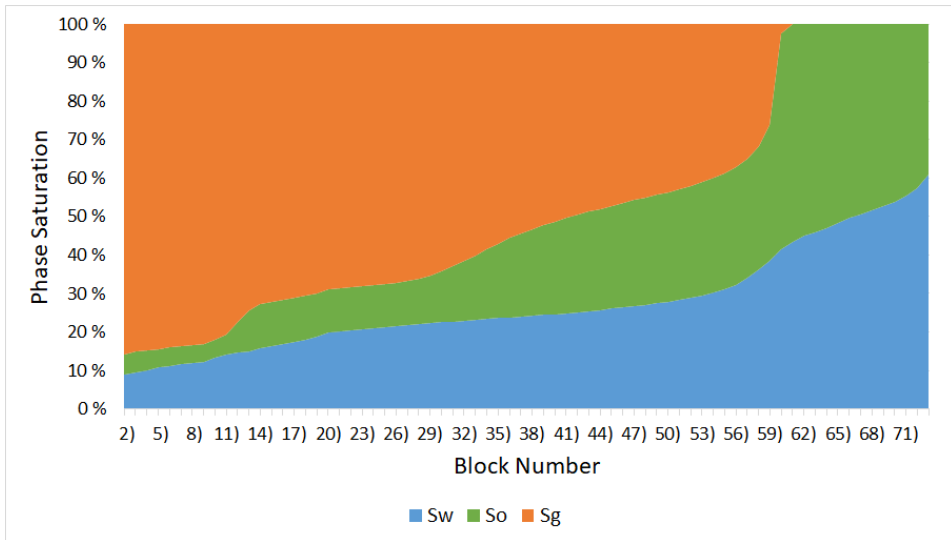
(a) Experiment 2
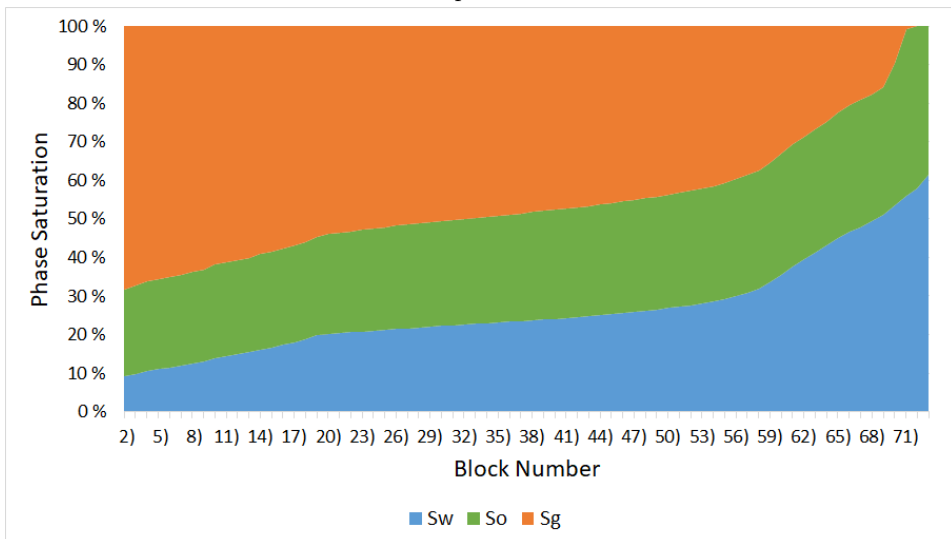
(b) Experiment 1

Figure 7.21: Saturation Profiles at 59 hours
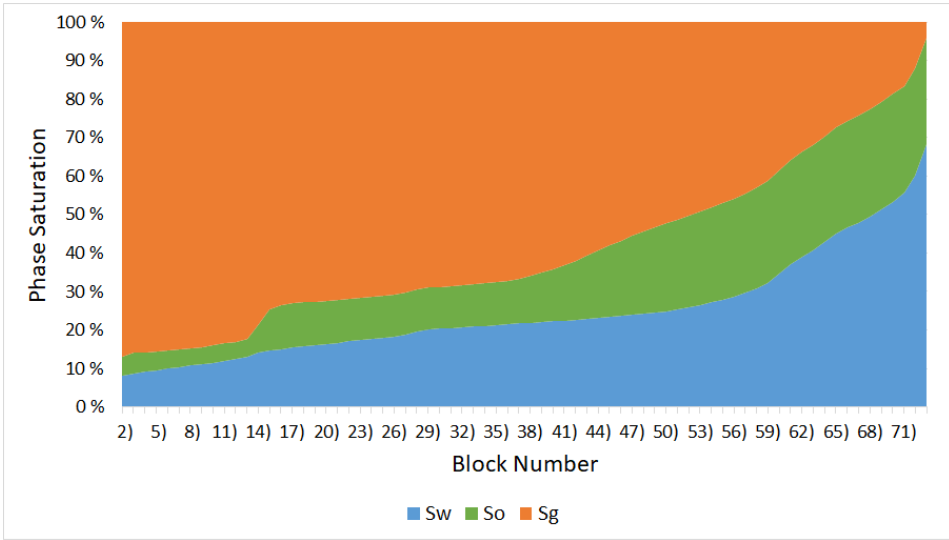
(a) Experiment 2
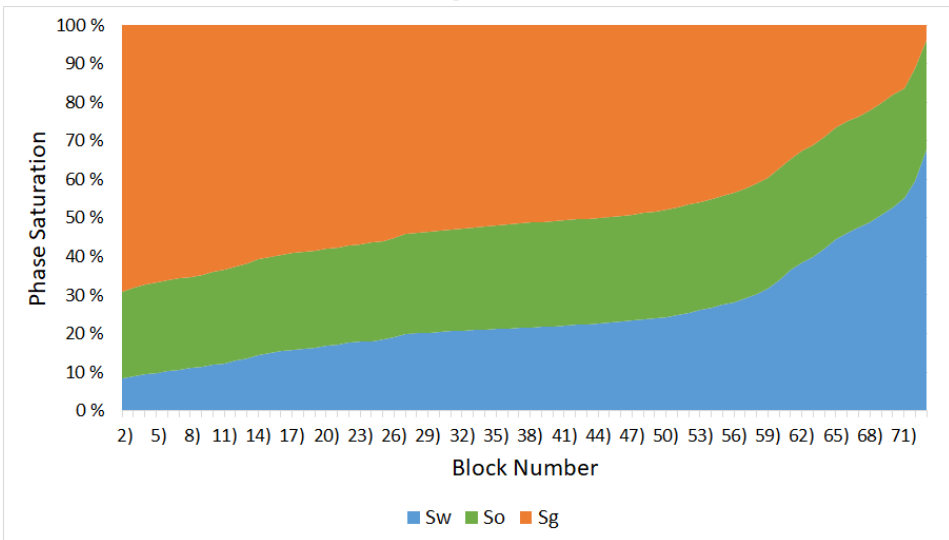
(b) Experiment 1

Figure 7.22: Saturation Profiles at 85 hours
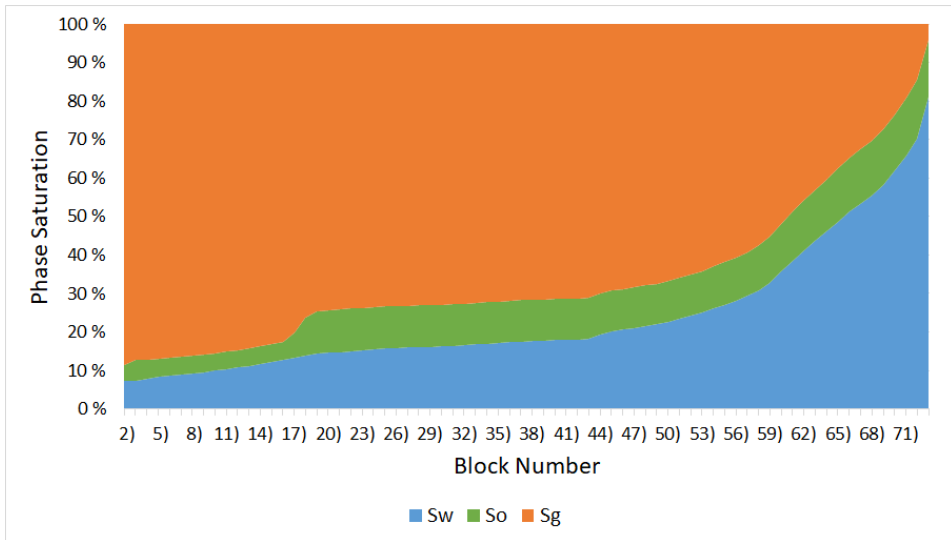
(a) Experiment 2
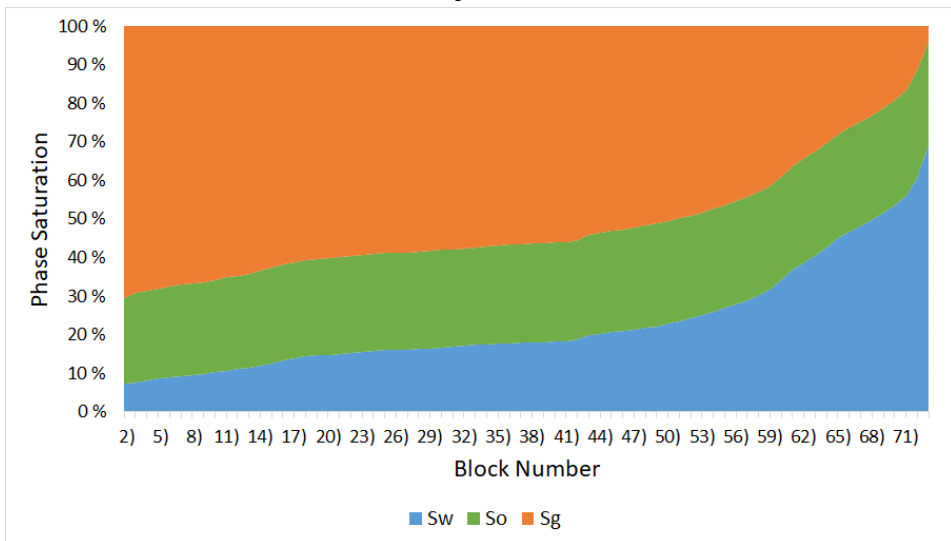
(b) Experiment 1

Figure 7.23: Saturation Profiles at 141 hours
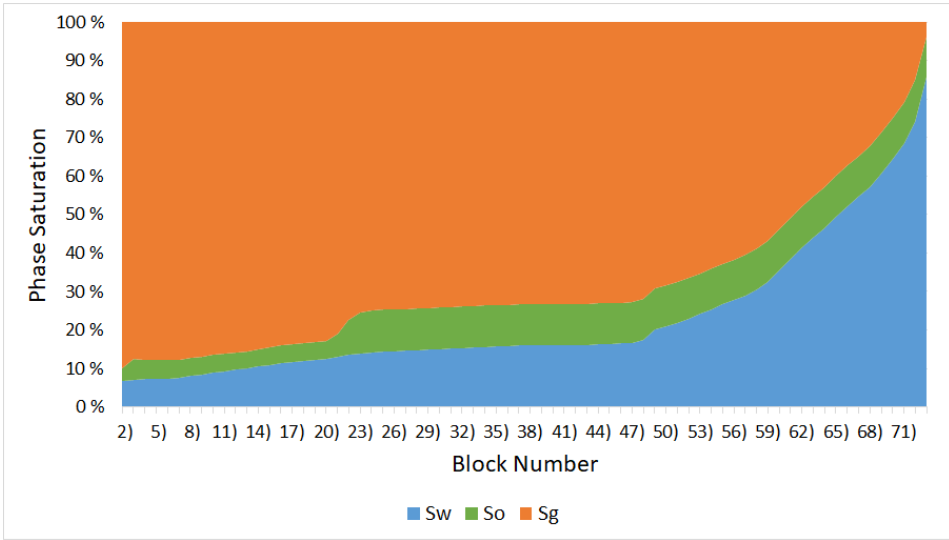
(a) Experiment 2
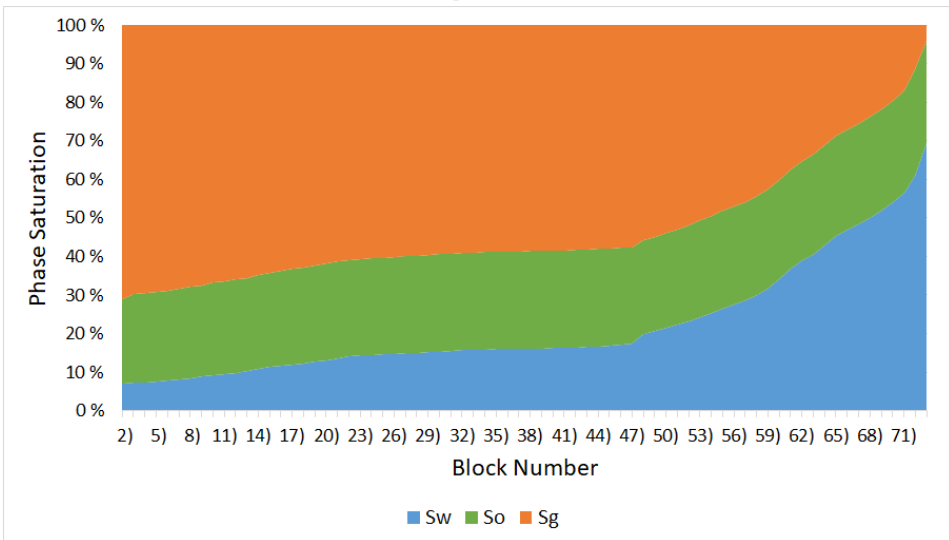
(b) Experiment 1

Figure 7.24: Saturation Profiles at 212 hours
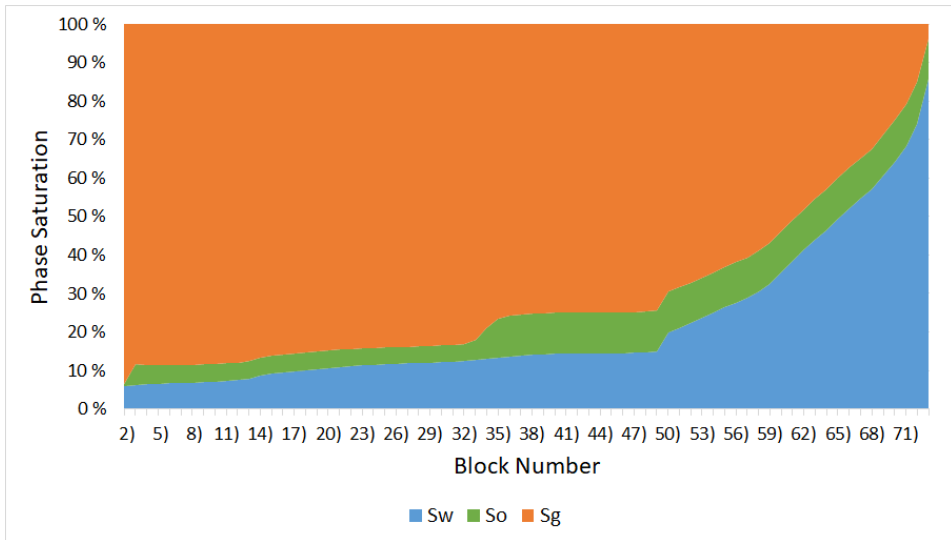
(a) Experiment 2, 418 hours
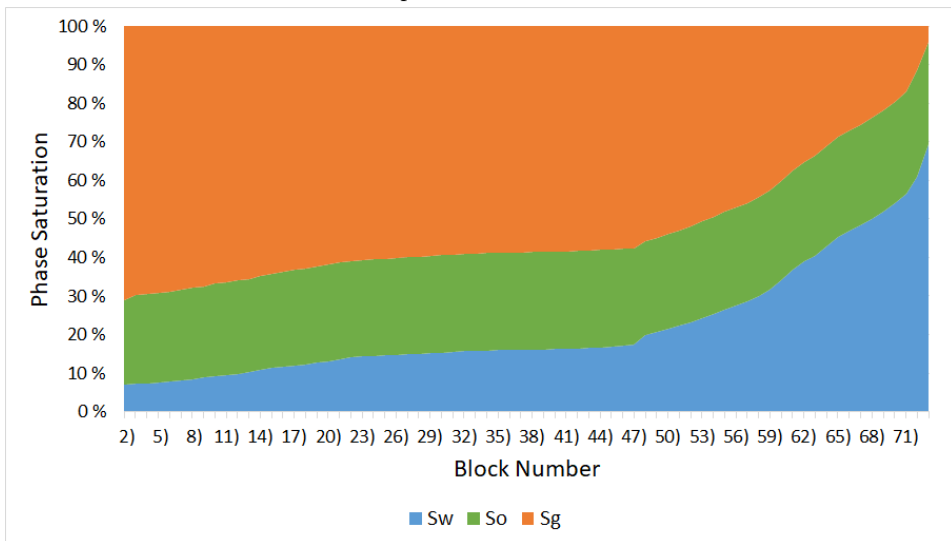
(b) Experiment 1, 212 hours

Figure 7.25: Saturation Profiles at end time

7.3 Sensitivity Study

This section will present results of a sensitivity study conducted on both Experiment 1 and 2. The experiments will be tested for gridblock-, capillary pressure- and time step-sensitivity.

7.3.1 Time step

Experiment 1

7.26 and 7.27 illustrates the sensitivity of time steps. The solid lines represent the best match (original) with a time step of 0.01. The dashed and dashed/dotted lines are run with time steps of 0.001 and 0.1, respectively. The model run with a time step of 0.1 exhibit a great deviation from the best match with deviations from 6.42% to 14.32%. The model run with a time step of 0.001 resulted in deviations of around 1.00%. Table 7.6 summarizes the findings.

The changed time steps only affect the simulation results after gas breakthrough. The oil deviates the most, followed by gas and then water.

Table 7.6: Experiment 1: Sensitivity of time step

Production at end time $[Sm^3]$	Water	Oil	Gas	Deviation Water	Oil	Gas
Time step: 0.1	138.62	71.99	102529.85	6.42 %	14.32 %	11.08 %
Time step: 0.01	130.26	62.97	92303.79	-	-	-
Time step: 0.001	128.92	61.94	91309.02	-1.03 %	-1.63 %	-1.08 %
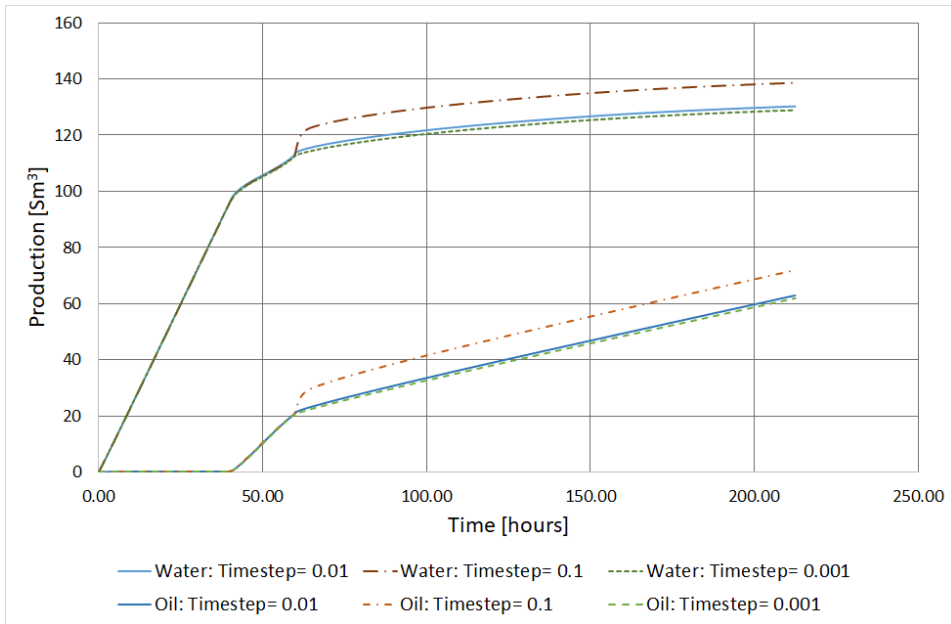
Figure 7.26: Experiment 1: Sensitivity of time steps on oil and water
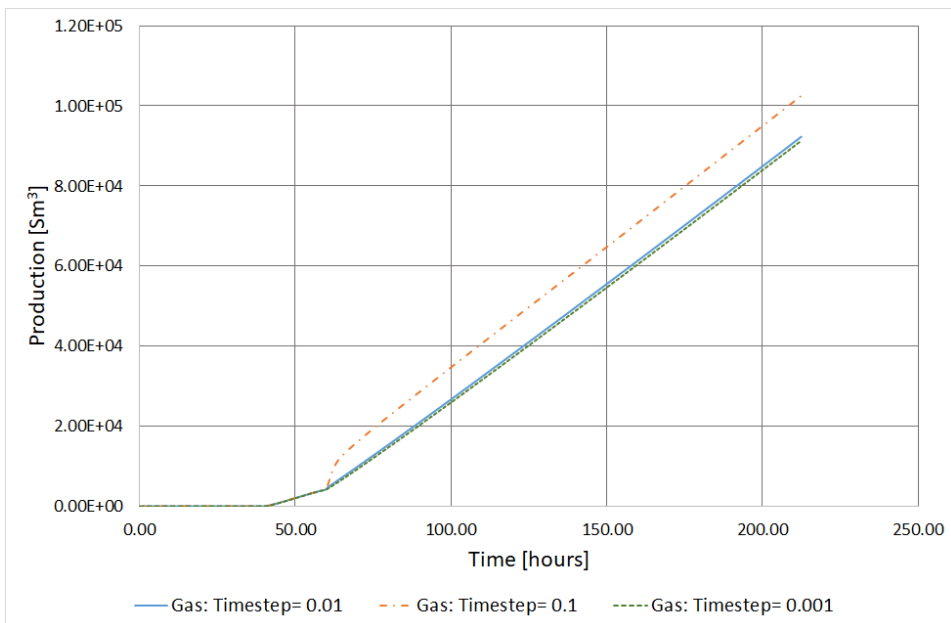
Figure 7.27: Experiment 1: Sensitivity of time steps on gas

Experiment 2

The same cases are run for Experiment 2. The original case is run with a time step of 0.01 hours while the other cases are run with 0.1 and 0.001. Figure 7.28 shows the sensitivity of time steps. Bigger time steps result in large deviations from experimental data. Smaller time steps yields small deviations. Table 7.7 summarizes the end time production and corresponding deviations from experimental data.

Table 7.7: Experiment 2: Sensitivity of time step

Production at end time $[Sm^3]$	Water	Oil	Gas	Deviation		
				Water	Oil	Gas
Time step: 0.1	144.49	64.59	240429.98	5.65 %	19.01 %	8.00 %
Time step: 0.01	136.77	54.28	222614.05	-	-	-
Time step: 0.001	135.42	53.11	220866.17	-0.99 %	-2.15 %	-0.79 %
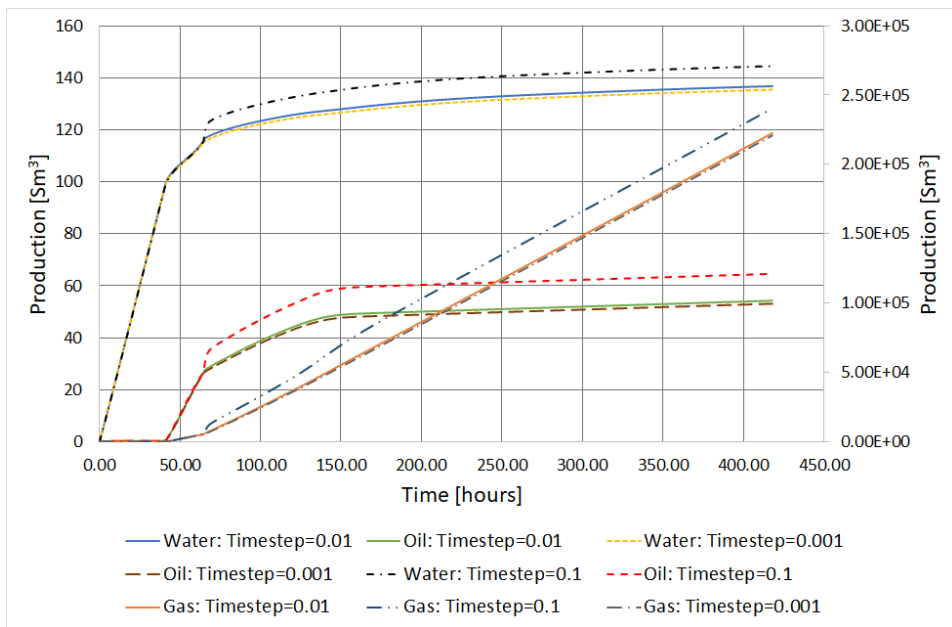
Figure 7.28: Experiment 2: Sensitivity of time steps on oil, gas and water

7.3.2 Gridblock

Experiment 1

The core in Experiment 1 is represented with 74 gridblocks where gridblock 1 and 74 serve as dead end volumes with other characteristics than the rest of the core. The dead end volumes are similar for all the cases in the sensitivity study, it is the core (block 2-73) that are changed.

The original case applies 72 uneven gridblocks to represent the core, where the middle blocks are the largest. This is because the injection and production wells are placed at each end and it is therefore necessary to have smaller blocks to capture the different effects occurring at top and bottom blocks. The next case is 72 even blocks with the original sizes of blocks 1 and 74, the dead end volumes. Third case is 112 (114 total) even blocks. Lastly, the original case is divided in 144 (146 total) uneven blocks, twice as many as in the original case.

The gridblock sensitivity is low, and there is no point displaying the deviation in oil and gas production as the plotted lines are indistinguishable. Figure 7.29 presents the water deviation. The biggest deviation is the model run with 72 (74 total) even blocks. Table 7.8 summarizes the gridblock sensitivity study. Oil deviates the least, followed by gas and then water.

Table 7.8: Experiment 1: Sensitivity of gridblocks

Production at end time [Sm^3]	Water	Oil	Gas	Deviation		
				Water	Oil	Gas
74 uneven	130.26	62.97	92303.79	-	-	-
74 even	128.88	63.07	92625.49	-1.06 %	0.16 %	0.35 %
114 even	129.85	63.03	92388.31	-0.31 %	0.11 %	0.09 %
146 uneven	130.92	62.97	92152.64	0.51 %	0.01 %	-0.16 %
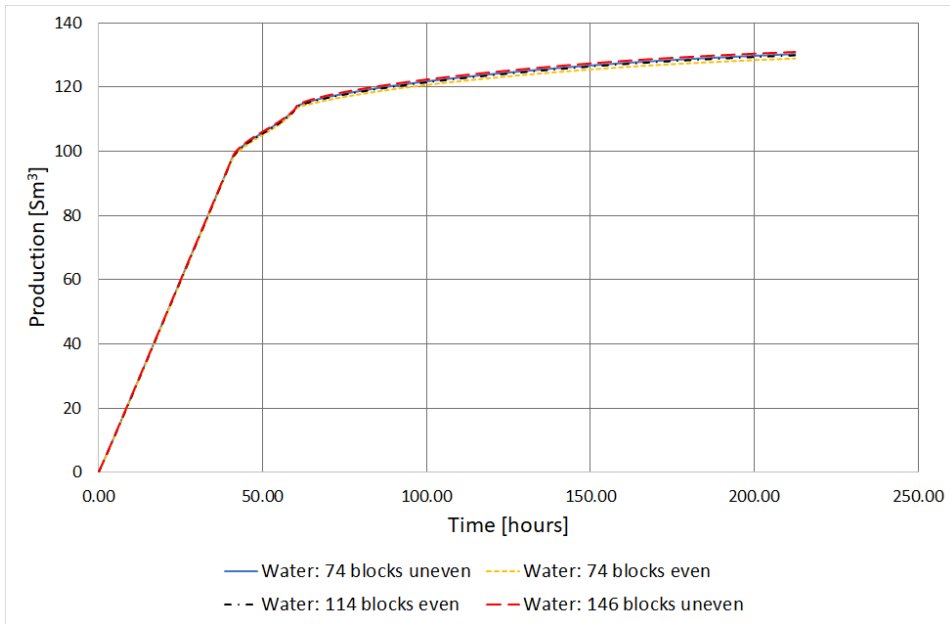
Figure 7.29: Experiment 1: Sensitivity of gridblocks on water

Experiment 2

The same block cases are run for Experiment 2. Similarly to Experiment 1, the sensitivity of number and size of gridblocks is low. Figure 7.30 presents sensitivity results of water and oil production. Only two of the cases are presented in oil production: 74 uneven blocks (original) and 146 uneven blocks. This is because the other cases are somewhere between those two cases and obscure the vision. Gas production is not included because of low deviations.

Table 7.9 summarizes the deviations. Simulation of oil creates the largest deviations while gas creates the smallest.

Table 7.9: Experiment 2: Sensitivity of gridblocks

Production at end time [Sm^3]	Water	Oil	Gas	Deviation		
				Water	Oil	Gas
74 uneven	136.77	54.28	222614.05	-	-	-
74 even	136.17	54.66	223109.16	-0.44 %	0.72 %	0.22 %
114 even	136.87	55.25	222845.98	0.08 %	1.80 %	0.10 %
146 uneven	138.17	55.50	222456.91	1.03 %	2.25 %	-0.07 %
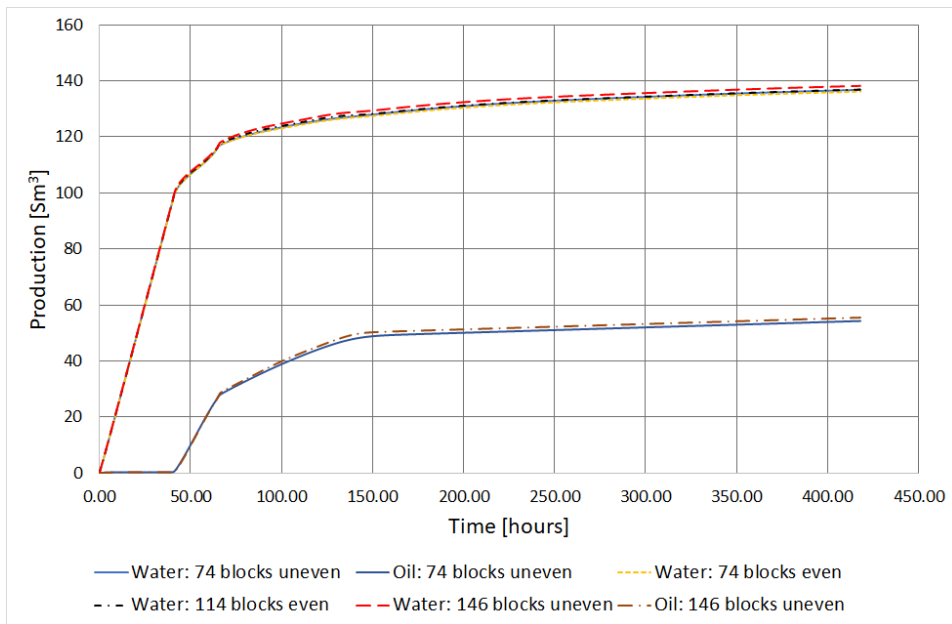
Figure 7.30: Experiment 2: Sensitivity of gridblocks on water and oil

7.3.3 Zero Capillary Pressure

Both experiments are tested for zero capillary pressure. In reservoir engineering it is common to set 0 capillary pressure, so this test is run to show the difference in simulation results.

Experiment 1

Figure 7.31 shows the production results of Best Match 1 (original) and a case with zero capillary pressure. Breakthrough time for both gas and oil are too late. Water recovery is highly overestimated while both gas and oil are underestimated. Table 7.10 summarizes the deviation results.

Table 7.10: Experiment 1: Sensitivity of zero capillary pressure

				Deviation		
Production at end time [Sm^3]	Water	Oil	Gas	Water	Oil	Gas
Zero capillary pressure	144.16	60.74	88781.39	10.67 %	-3.54 %	-3.82 %
Nonzero capillary pressure	130.26	62.97	92303.79	-	-	-
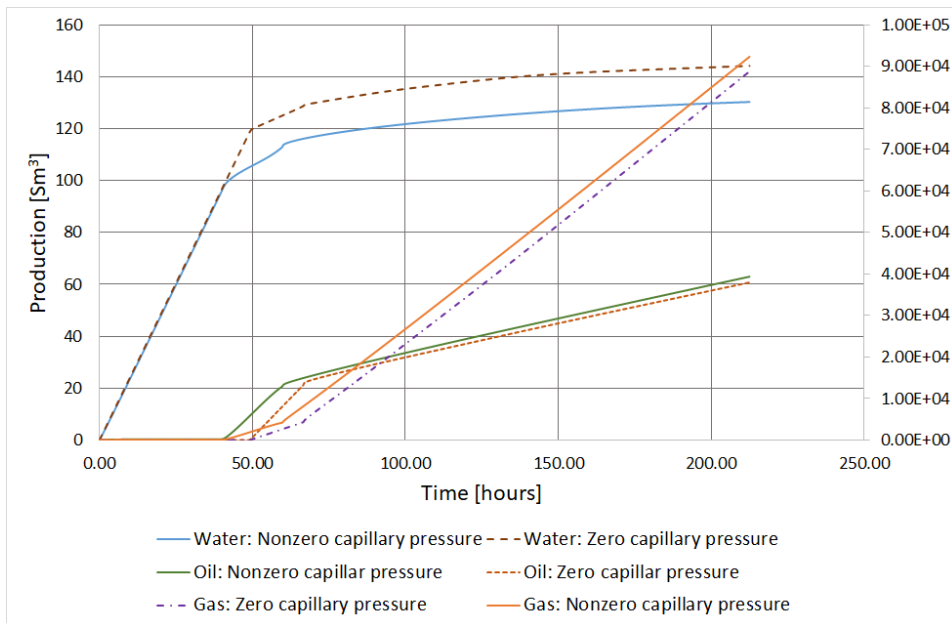
Figure 7.31: Experiment 1: Sensitivity of zero capillary pressure

Experiment 2

Figure 7.31 shows the production results of Best Match 2 (original) and a case with zero capillary pressure. Breakthrough time for gas and oil are either too early or too late. Water recovery is highly overestimated while both gas and oil are underestimated. Table 7.11 summarizes the deviation results.

Table 7.11: Experiment 2: Sensitivity of zero capillary pressure

Production at end time $[Sm^3]$	Water	Oil	Gas	Deviation		
				Water	Oil	Gas
Zero capillary pressure	153.67	53.84	218323.92	12.36 %	-0.81 %	-1.93 %
Nonzero capillary pressure	136.77	54.28	222614.05	-	-	-
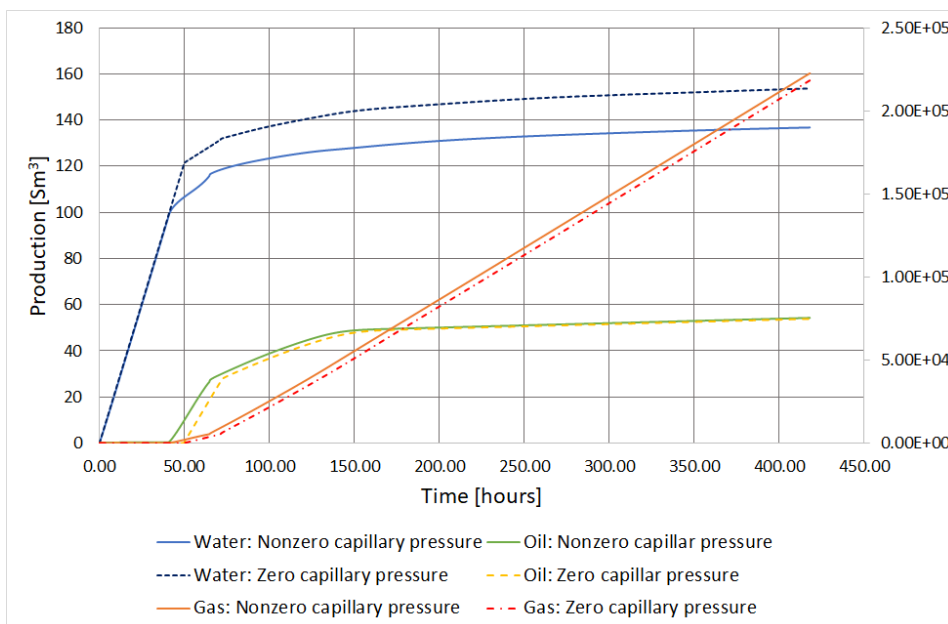
Figure 7.32: Experiment 2: Sensitivity of zero capillary pressure

7.3.4   Oil-Water and Gas-Oil Capillary Pressure

Both experiments are tested for oil-water and gas-oil capillary pressure sensitivity separately. This is to see which capillary pressure influences the system the most. The capillary pressure curves are scaled with the user-specified constant, u_{ij}, changed from the best matches. The best matches have a u_{ij} equal to 1.681.

Experiment 1

Tables 7.12 and 7.13 summarize the deviation results for capillary pressure. It is evident how oil-water capillary pressure has a much bigger impact on the fluid recoveries than gas-oil capillary pressure. Figure 7.33 shows the deviation in oil-water capillary pressure. The sensitivity of oil-gas capillary pressure is not plotted because the sensitivity is too low to exhibit any visible deviations in a graph.

Table 7.12: Experiment 1: Sensitivity of oil-water capillary pressure

Production at end time $[Sm^3]$	Water	Oil	Gas	Deviation		
				Water	Oil	Gas
lij=1.000	118.07	64.35	95383.93	-9.36 %	2.19 %	3.34 %
lij=1.681	130.26	62.97	92303.79	-	-	-
lij=3.000	134.43	62.28	91373.22	3.20 %	-1.10 %	-1.01 %

Table 7.13: Experiment 1: Sensitivity of gas-oil capillary pressure

Production at end time $[Sm^3]$	Water	Oil	Gas	Deviation		
				Water	Oil	Gas
lij=1.000	130.52	62.82	92239.00	0.20 %	-0.24 %	-0.07 %
lij=1.681	130.26	62.97	92303.79	-	-	-
lij=3.000	130.22	62.98	92312.46	-0.03 %	0.02 %	0.01 %
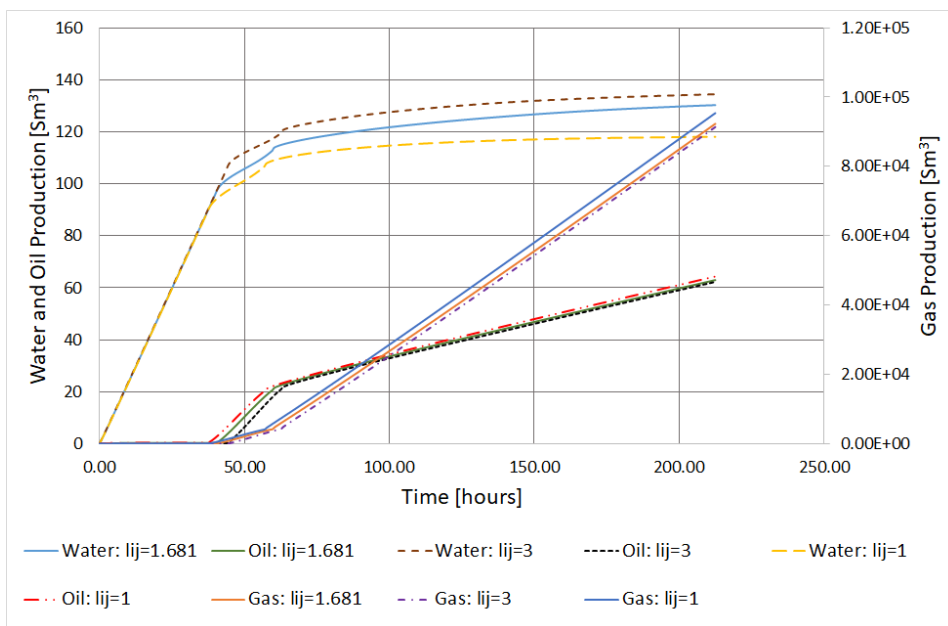
Figure 7.33: Experiment 1: Sensitivity of oil-water capillary pressure

Experiment 2

Tables 7.14 and 7.15 summarize the deviation results for capillary pressure. The results show the same tendency as Experiment 1, namely that oil-water capillary pressure has a much bigger impact on the fluid recoveries than gas-oil capillary pressure. Figure 7.34 shows the deviation in oil-water capillary pressure. For the same reasons as for Experiment 1, gas-oil capillary pressure sensitivity is not plotted.

Table 7.14: Experiment 2: Sensitivity of oil-water capillary pressure

Production at end time $[Sm^3]$	Water	Oil	Gas	Deviation		
				Water	Oil	Gas
lij=1.000	128.97	54.41	224631.52	-5.70 %	0.25 %	0.91 %
lij=1.681	136.77	54.28	222614.05	-	-	-
lij=3.000	145.73	54.06	220365.45	6.56 %	-0.40 %	-1.01 %

Table 7.15: Experiment 2: Sensitivity of gas-oil capillary pressure

Production at end time [Sm^3]	Water	Oil	Gas	Deviation		
				Water	Oil	Gas
lij=1.000	137.25	54.07	222512.58	0.35 %	-0.37 %	-0.05 %
lij=1.681	136.77	54.28	222614.05	-	-	-
lij=3.000	136.67	54.30	222634.86	-0.07 %	0.05 %	0.01 %
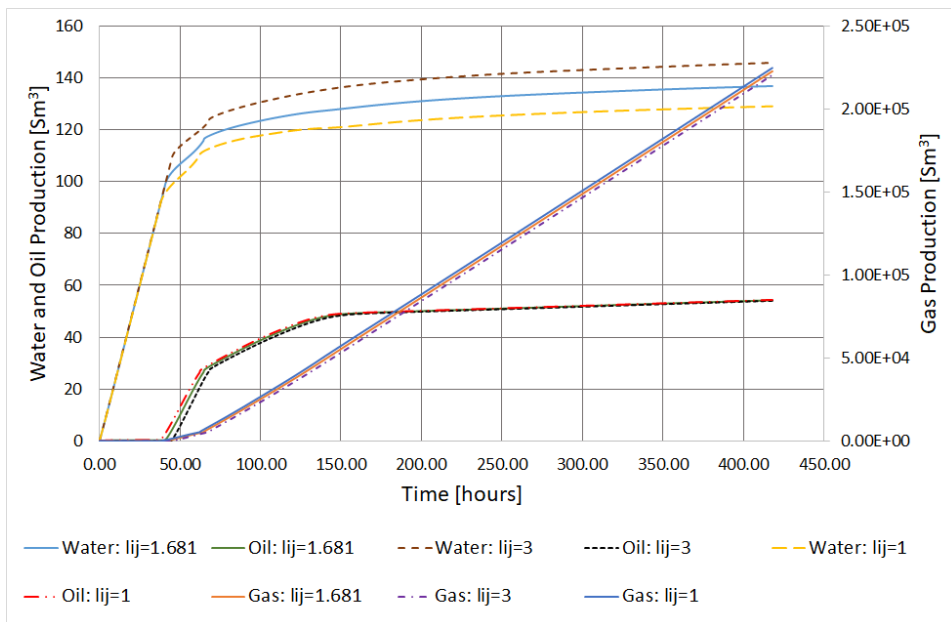
Figure 7.34: Experiment 2: Sensitivity of oil-water capillary pressure

Chapter 8

Discussion

History matching Experiment 1 and 2 is a time consuming effort with many different and complex parameters to control. In addition, unforeseen obstacles such as erroneous condensate production in Experiment 1 delayed the progress of this study. However, a match of both experiments are achieved and the results offer a basis of discussion.

Looking back at the main goals of this thesis, which goals can be ticked off? Certainly the first point: History matching Experiment 1 and 2. Applying the three-phase relative permeability model Extended Stone model 1 (EXS1) on both experiments proves sufficient for achieving a match within acceptable errors. A lot of effort is given to improve the matches by changing input data without overshadowing the physical restrictions of the model. The changes needs to be justified, and cannot be altered simply because it yields a better match.

8.1 Rock Properties

Figure 7.8 shows the best match of Experiment 1 without incorporating the changes made for Experiment 2 (no joining of capillary pressure curves). As mentioned in Chapters 6 and 7, the dynamic rock properties relating water are extended down to $S_w = 4.5\%$ to increase the simulated water production. With the experimentally obtained values

only reaching a water saturation of 14.5%, this seems like a drastic and not a justified change. However, other measurements on the same Bentheimer sandstone conducted by Hustad and Holt (1992), indicate an irreducible water saturation of exactly 4.5%. Because of this, the extension of the curves to this water saturation is considered reasonable.

Looking at the modified water relative permeability curve, k_{rw}, in Figure 7.6, one can also question the increase in values from around $S_w = 25.0\%$, not just the extension. However, the extension is worthless unless the k_{rw} is increased as well. If the same curve is only to be extended, the k_{rw} values would be so low basically yielding a no flow region. Besides, the k_{rw} displayed in Figure 4.4 is only an extrapolated curve made by Hustad and Holt and it is not necessarily correct.

The oil-water capillary pressure curve, P_{cow}, is also extended, but this time it follows the natural curve of the experimentally obtained data. The curve is further scaled according to equations 5.5 and 5.6 and offer less questions of justification.

The change in oil in water relative permeability, k_{row}, contradicts the philosophy of this thesis, however it will be tried justified in this paragraph. As already stated, the natural curve of k_{row} is extended to a higher water saturation, thus indicating lower residual oil saturation, S_{orw}. What this change results in, is an accumulation of water in lower blocks at the beginning of simulation. While the water saturation should be stable, there is a significant increase before water production starts. An assumption of these experiments is that the cores are already at residual oil saturation, so this alteration oppose this condition. However, the change was highly necessary as the simulated oil production is extremely low without this change. One can support this change by questioning the reliability in experimentally obtained data. The cores used in these experiments are short, and can then be too small to obtain correct residual saturation values. There is no way to verify this as the experiments are conducted in a separate study several years before this thesis, so there is no good reason to extrapolate k_{row} other than for creating a match. However, in reservoir simulation and the final stages of history matching, changes like this are common.

Capillary end effects are briefly discussed in Chapter 3. It is mentioned how capillary end effects is observed by an accumulation of the wetting-phase close to the outlet of a core. From the figures presented in Section 7.2, it is obvious how these experiments experience capillary end effects. The cores used for the displacement experiment are approximately 1.2 meters. The cores used for relative permeability measurements are only 62 centimeters, and one can be sure end effects would have influenced the relative permeability and residual saturation data measurements. This weakens the reliability of the experimental data and therefore support the extensive changes of the input parameters just mentioned (Objective 3a). All in all, the changes to the dynamic rock properties in Experiment 1 are considered reasonable. The properties concerning gas (P_{cog}, k_{rog} and k_{rg}) are never changed more than scaling to correct interfacial tensions during this study.

As previously mentioned in this thesis, it is common among reservoir engineers to set capillary pressure equal to zero during reservoir simulation. However, the sensitivity study contradicts this assumption. The simulated fluid recoveries are highly affected by the oil-water capillary pressure. The gas-oil capillary pressure influence the system less, probably because the capillary pressures are already so low. But as one can observe in the sensitivity study, oil-water capillary pressure affect the system significantly and call for a re-evaluation of setting capillary pressure (at least oil-water) to zero.

Another interesting aspect concerning the capillary pressure sensitivity is that the oil recovery is less influenced by oil-water capillary pressure in Experiment 2 than in Experiment 1. This is related to the different flow mechanisms that rule the systems. In Experiment 2, the three-phase oil relative permeability is zero from around 120 hours. From this point on, neither conductivity (relative permeability) nor capillary forces affect the oil production. The production is only oil coming from gas, and this will naturally be observed in the graph as a less sensitivity of capillary pressure.

8.2   Fluid Properties

The fluid properties are treated by the equation of state (EOS). The Soave-Redlich-Kwong EOS is chosen for this study, a popular EOS in reservoir simulation today (Whitson and Brule, 2000). The critical properties and acentric factors extended to surface conditions applying a regression tool are trusted to represent the system. The surface EOS did not produce a large deviation from the simulation without surface EOS, and can thus be concluded to be reliable values. However, the incorrect condensate production is a result of inaccurate vapor-liquid equilibrium predictions. This is contrast to what the SRK EOS is considered to be in the literature (Whitson and Brule, 2000). Because there should be no mass transfer or compositional effects in Experiment 1, a Black Oil model would be sufficient for modeling this experiment, thus removing the need for equations of state. Simulating Experiment 1 with the Black Oil model would be a clever way of comparing the erroneous condensate production, but available data is insufficient for constructing this model.

There is a slight deviation in simulated gas and oil production in Experiment 1. This is observed for both cases with and without joining of capillary pressure curves. The deviation of gas production is suspected to be a result of experimentally obtained data. The molecular weights stated in Table 3 from the report written by Hustad and Holt (1992) are not measured, but assumed by other studies on similar gas. This yields an incorrect gas density and results in wrongly calculated gas volumes. Also, because the regression of the EOS parameters to surface conditions disregarded the gas properties, it will cause a mismatch of gas production. The oil production, compared with modified experimental data, also shows a small deviation, but is considered good with a deviation of only -0.001%. The surface equation of state delays both oil and gas breakthrough and creates a better match.

As already discussed in Chapter 6, the gas composition is changed in Experiment 1 even though the simulated gas production in Basecase (original gas composition) match well with experimental data. There are insecurities with the experimental gas compositions data, so an alternation is considered acceptable. Regardless, it does not matter if the

original gas composition is the correct gas composition, when Eclipse treat it otherwise. To achieve representative simulation results, it is more important that Eclipse "thinks" it has the correct composition, rather than actually using the right one but treat it wrongly. Because Experiment 2 inject dry gas, this is not an issue.

The erroneous condensate production is not a problem in Experiment 2. In Experiment 2, the injection gas is dry, and will not produce condensate as the richer equilibrium gas does in Experiment 1. This means there is no reason to worry about "hidden" condensate production values in the simulation of oil in Experiment 2. Similarly for Experiment 1, Experiment 2 need to establish a new surface equation of state. This is done the same way as for Experiment 2, and the results are considered valid for Experiment 2 just like it is for Experiment 1.

With a new injection gas composition and surface equation of state, a thorough study on the behavior of capillary pressure and saturation behavior on upper, middle and lower blocks is conducted. This leads to the other point on the list of main goals: Prove the effects of capillary pressure on water recovery.

8.3   Joining of Capillary Pressure Curves

There is no doubt that joining the capillary pressure curves increase the water recovery level creating an acceptable match in Experiment 2. However, the simulation tool, Eclipse, does not know that the actual inserted values are the new gas-water capillary pressures. All Eclipse knows is that the capillary pressures are lower for lower water saturations, which of course leads to more water production. The simulation model forces Eclipse to follow a lower capillary pressure curve, there is no advanced physical model behind it. The joining of capillary pressure is based on a scenario where the increasing pressure of gas and water leads to a snap off of the oil phase. However, this phenomenon is not simulated or modelled in the simulation model, it is only assumed. There is nothing in the simulation stating: If the phase pressures exceeds this value, a contact between gas and water exist. Because of this, the model is less predicative as a future scenario is already set. It is dangerous to immediately conclude that joining of

capillary pressures is the right approach only based on new and improved simulation results. However, the simulation results definitely proves the effect of lower capillary pressures on water production.

Applying the gas-water capillary pressures in Experiment 1 yields a small deviation of water recovery towards end time (0.02%). This indicates that the gas-water curve is joined at a too high water saturation. The joining occurs at $S_w = 22.0\%$, but should be lower. However, a joining at a lower water saturation was inadequate for history matching Experiment 2, so $S_w = 22.0\%$ is the best choice.

Because Hustad and Holt (1992) did not consider applying gas-water capillary pressure data in the simulations, interfacial tension between gas and water was not recorded. Because of this, the gas-water capillary pressure curve applied in this study was only scaled to create an intersection with the oil-water curve at the water saturation that gave a water production match in Experiment 2. If this interfacial tension value was known, it could have provided a better indication to where the intersection between the capillary pressure curves should occur.

8.4   Hysteresis

There are only two saturation functions with their respective saturation paths specified in the simulation model: decreasing water saturation and increasing gas saturation. Hysteresis effects are not accounted for, and is a significant simplification of the system. Implementing hysteresis could possibly yield better simulation results, but this is not included in this study as some of the point of this study is to create a simple simulation model with input data easy to handle. Only looking at the core as a whole, it makes sense having a decreasing water saturation path. There is no water injection during the simulation, and one can observe a continuous water production. However, if one look at a block level, the water saturation is not always increasing. Gas displaces water which again displaces oil. While the core as a whole drains itself for water, the lower blocks experience an increase of water saturation as the water from the upper blocks are pushed downwards. In this area, it is not correct to apply dynamic rock properties correspond-

ing to a decreasing water saturation. However, this is done, and considered acceptable. As briefly mentioned in Chapter 3, Alizadeh and Piri (2014) came to the conclusion that water is independent of saturation changes. If this is in fact true, then ignoring hysteresis effects is okay in this study. Alizadeh states gas is much more influenced by change of saturation path, but because gas is injected into the cores, gas is always increasing in every block. This again supports not including hysteresis effects.

8.5 Three-Phase Relative Permeability Model

Lastly, it is important to discuss the chosen three-phase relative permeability model. Extended Stone model 1 is a modification of the widely used Stone Model 1. Hustad developed the new version trying to improve the prediction of three-phase oil isoperms. By introducing a user-specified exponent term to the normalized saturations, the oil isoperms could be more spread and linear. With the exponent term equal to 4, the modified oil isoperms are more similar to what Baker found to be a better approach. It can look as though having linear and more spread oil isoperms is a better choice simply because one avoids either over- or underestimating three-phase oil relative permeability. The question is whether the models actually predict more accurate oil isoperms or if they simply avoid "extreme" values and thus avoid significant simulation errors.

The different studies on three-phase relative permeability described in Chapter 3 are not in agreement. The most common assumption and belief of the authors creating three-phase relative permeability models is that the intermediate phase is the only phase dependent on other phases. The authors only describing experimentally obtained three-phase data seem to be in more disagreement concerning the dependencies on three-phase relative permeabilities. Some authors believe all phases are dependent one every phase, some believe all phases are independent on every phase while some believe only oil is dependant on other phases. The first Stone model, the basis of Extended Stone model 1, is based on the channel flow theory, as stated in Chapter 3. The channel flow theory assumes water- and gas relative permeabilities are the same for a two- and three-phase system, making EXS1 agree with most of the other prediction models.

With all the mentioned aspects in mind, Extended Stone model 1 is a good choice for simulating Experiment 1, the equilibrium gas experiment. However, vaporization effects in Experiment 2 are not properly modelled because vaporization effects influence the capillary forces and that is not dealt with in EXS1. Simulation of maximum gas saturation is a challenge, and a new and improved simulation model is recommended for a dry injection gas experiment.

A weakness of Extended Stone model 1 is that interfacial tension is assumed constant during simulation. This is in relation to how EXS1 lacks the capability of properly modeling changes in capillary forces. In reality, the interfacial tension varies during the displacements. Because the interfacial tension is used to manually scale the capillary pressure curves, the simulation model will not treat interfacial tension as variable.

An advantage of Extended Stone model 1 is how easy it is to use. The model only requires two sets of two-phase data, and this will be sufficient in many cases. However, the model does not incorporate gas-water data, and will be a disadvantage if, like Experiment 2, there is a three-phase system where there exists a gas-water interface. The sensitivity study also supports the model. Neither smaller time steps nor different gridblocks resulted in worrying results. It is reassuring that smaller time steps yield small deviations. This is an indication that he chosen time step is sufficient for simulating the experiments. All in all, the different sensitivity checks proves a rather stable and robust simulation model. Because of all these reasons, EXS1 is considered reliable and objective 3b is reached.

8.6   Simulation results

All the simulation results are considered to yield acceptable matches. However, in Experiment 2, the gas recovery deviates with 18.0% at end time. This trend in deviation is similar to what Hustad and Holt (1992) reported in their report, but it is larger in this study. This is most likely the cause of two reasons: 1. The molecular weight was estimated and not necessarily correct. This is likely because Hustad and Holt saw the same gas recovery trend in their study. 2. The gas properties had to be neglected during re-

gression to surface condition when determining critical properties and acentric factor for the surface equation of state. The gas density had to change, and density will control the gas volume and consequently yield erroneous gas recovery.

Chapter 9

Conclusion

The purpose of this study is to history match two different tertiary gas experiments experiencing three-phase flow. Both experiments are matched with a thorough investigation on capillary pressure, two-phase relative permeability, three-phase relative permeability model and other input data. Joining of oil-water and gas-water capillary pressure curve is essential to achieve a match in Experiment 2 where the injection gas is dry.

The conclusions can be summed up as follows:

1. A match of Experiment 1 and 2 is achieved by altering input data within the physical model, establishing a surface equation of state and most importantly: inserting gas-water capillary pressure in the simulation model.

2. Forcing the simulation model to follow the gas-water capillary pressure curve yields additional water recovery and force the Extended Stone model 1 to simulate to lower water saturation and higher gas saturations.

3. The match in Experiment 2 is not perfect. The simulated additional water recovery caused by joining of the capillary pressure curves lacks the abrupt change seen in experimental data. This suggests that even though Extended Stone model 1 matches experimental data well, it does not handle tertiary gas injection experiments where there are significant vaporization effects by itself.

4. A surface equation of state improved the oil recovery match. While the simulated gas recovery deviates slightly at end time, the match is better around oil- and gas breakthrough.

5. Eclipse erroneously simulates extra condensate production, which will always create a mismatch between simulated and experimental data no matter how much the input data is changed. To compensate for this, a modified experimental oil production curve is created where the extra condensate production is added. This is a measure to observe whether there is an oil match or not (while accounting for wrong condensate production).

Chapter 10

Recommendations for Further Work

Because there are so many insecurities related to experimental data, the same core-flooding experiments should be re-conducted to obtain more reliable data. This time, hysteresis effects should be accounted for in the simulation, so relative permeability and capillary pressure should be measured during different saturation paths. Also, data needed to build a black oil model should also be available so one can construct a comparison study of Experiment 1. Extended Stone model 1 proved applicable, but another model more fitted for changes in capillary forces because of vaporization effects should be used instead.

The simulation study only use 6 components to represent the hydrocarbons. 6 pseudo-components might be insufficient to properly represent the system and can lead to inaccurate modeling of saturation pressure. Modeling with more components could yield a better representation.

As discussed in Chapter 8, the gas-water interfacial tension was not recorded in the study by Hustad and Holt (1992). This data should be measured if mass transfer are present during a displacement experiment where gas-water contact arises.

An issue with the experimental data is the capillary end effects. Because the cores used for relative permeability measurements are so small, a bigger percentage of the core is affected by this phenomenon. A longer core would make measurements much more reliable, and would be a recommendation if the experiments were to be re-conducted.

Nomenclature

Abbreviations

AF   Acentric factor

B   Formation volume factor

EOS   Equation of state

EXS1   Extended Stone Model 1

GOR   Gas/oil ratio

IFT   Interfacial tension

MW   Molecular weight

PR   Peng-Robinson

PVT   Pressure-Volume-Temperature

SCAL   Special Core Analysis Laboratory

SRK   Soave-Redlich-Kwong

Subscripts

        Surface gas

        Surface oil

cij   Capillary

g   Gas

gc   Critical gas

i   Unspecified phase

ir   Residual of i phase

j   Another phase than i

max   Maximum

o   Oil

om   Minimum oil residual

ri   Relative to i phase

rijc   Presence of connate water

u   User-specified

w   Water

wc   Connate water

wir   Irreducible water

Other

Basecase Simulation run using un-altered data from Hustad and Holt

Superscripts

*   Normalized

n   User-specified exponent term

nw   Non-wetting

r   Reference

w   Wetting

Symbols

β Factor that allows for oil blockage, Stone's version

σ Interfacial tension

α Correction factor

$\hat{P}$ Scaled cpaillary pressure

ω Acentric factor

$\tilde{P}$ Unscaled capillary pressure

a Attraction parameter

b Repulsion parameter

ν Molar volume

F   Factor that allows for oil blockage, Aziz' version

f   Scaling factor

k   Permeability

l   User-specified constant

P   Pressure

R   Universal gas constant

S   Saturation

T   Temperature

V   Volume

Units

μm^2 Micro square meter

C Celcius

cm Centimeter

m Meter

Scm^3 Cubic surface centimeter

cp   Centipoise

g   Gram

mN   Milli Newton

References

Alizadeh, A. H. and Piri, M. (2014). The effect of saturation history on three-phase relative permeability: An experimental study. *Water Resources Research*, 50(2):1636–1664.

Aziz, K. (1979). *Petroleum Reservoir Simulation*. Applied Science Publishers.

Baker, L. (1988). Three-phase relative permeability correlations. In *SPE Enhanced Oil Recovery Symposium*. Society of Petroleum Engineers.

Balbinski, E. F., Fishlock, T. P., Goodyear, S. G., and Jones, P. I. R. (1999). Key characteristics of three-phase oil relative permeability formulations for improved oil recovery predictions. *Petroleum Geoscience*, 5(4):339–346.

Blunt, M. (2000). An empirical model for three-phase relative permeability. *SPE Journal*, 5(04):435–445.

Blunt, M. J. (1999). An empirical model for three-phase relative permeability. In *SPE Annual Technical Conference and Exhibition*. Society of Petroleum Engineers.

Carlson, F. M. (1981). Simulation of relative permeability hysteresis to the nonwetting phase. In *SPE Annual Technical Conference and Exhibition*. Society of Petroleum Engineers.

Carlson, L. (1988). Performance of hawkins field unit under gas drive-pressure maintenance operations and development of an enhanced oil recovery project. In *SPE Enhanced Oil Recovery Symposium*. Society of Petroleum Engineers.

Caudle, B., Slobod, R., and Brownscombe, E. (1951). t. *Journal of Petroleum Technology*, 3(05):145–150.

Chen, Z. (2007). *Reservoir Simulation: Mathematical Techniques in Oil Recovery (CBMS-NSF Regional Conference Series in Applied Mathematics)*. Society for Industrial and Applied Mathematics.

Corey, A., Rathjens, C., Henderson, J., and Wyllie, M. (1956). Three-phase relative permeability. *Journal of Petroleum Technology*, 8(11):63–65.

Delshad, M. and Pope, G. (1989). Comparison of the three-phase oil relative permeability models. *Transport in Porous Media*, 4(1).

Dietrich, J. K. and Bondor, P. L. (1976). Three-phase oil relative permeability models. In *SPE Annual Fall Technical Conference and Exhibition*. Society of Petroleum Engineers.

Donaldson, E., Dean, G., and of Mines, U. S. B. (1966). *Two- and three-phase relative permeability studies*. Report of investigations. U.S. Dept. of the Interior, Bureau of Mines.

Fassihi, M. and Gillham, T. (1993). The use of air injection to improve the double displacement processes. In *SPE Annual Technical Conference and Exhibition*. Society of Petroleum Engineers.

Hustad, O. and Holt, T. (1992). Gravity stable displacement of oil by hydrocarbon gas after waterflooding. In *SPE/DOE Enhanced Oil Recovery Symposium*. Society of Petroleum Engineers.

Hustad, O. S. (2007). Modeling laboratory displacement experiments. Powerpoint Presentation.

Hustad, O. S. and Browning, D. J. (2010). A fully coupled three-phase model for capillary pressure and relative permeability for implicit compositional reservoir simulation. *SPE Journal*, 15(04):1003–1019.

Kantzas, A., Chatzis, I., and Dullien, F. (1988). Enhanced oil recovery by inert gas injection. In *SPE Enhanced Oil Recovery Symposium*. Society of Petroleum Engineers.

Kleppe, J. (2017). Review of relative permeabilities and capillary pressures. Handout.

Kokal, S. and Maini, B. B. (1990). An improved model for estimating three-phase oil-water-gas relative permeabilities from two-phase oil-water and oil-gas data. *Journal of Canadian Petroleum Technology*, 29(02).

Kostelnik, K., Arredondo, P., and Montenegro, A. (2017). A case history on california immiscible gas injection, elk hills field. In *SPE Western Regional Meeting*. Society of Petroleum Engineers.

Lake, L. W. (1996). *Enhanced Oil Recovery*. Prentice Hall.

Land, C. S. (1968). Calculation of imbibition relative permeability for two- and three-phase flow from rock properties. *Society of Petroleum Engineers Journal*, 8(02):149–156.

Leverett, M. and Lewis, W. (1941). Steady flow of gas-oil-water mixtures through unconsolidated sands. *Transactions of the AIME*, 142(01):107–116.

Madathil, A., Azrak, O., Pearce, A., Amrie, O. A., Gunasan, E., and Blondeau, C. (2015). 24 years of successful EOR through immiscible tertiary gas injection. In *Abu Dhabi International Petroleum Exhibition and Conference*. Society of Petroleum Engineers.

Maini, B., for Mineral, C. C., Technology, E., Canada. Energy, M., Canada, R., Institute, P. R., Energy, M., Program, R. C. S. E. C., on Energy Research, F. P., and (Canada), D. (1990). *Measurements and Estimation of Three-phase Relative Permeability: Final Report*. Petroleum Recovery Institute.

Manjnath, A. and Honarpour, M. (1984). An investigation of three-phase relative permeability. In *SPE Rocky Mountain Regional Meeting*. Society of Petroleum Engineers.

Naar, J. and Wygal, R. (1961). Three-phase imbibition relative permeability. *Society of Petroleum Engineers Journal*, 1(04):254–258.

Oak, M. (1990). Three-phase relative permeability of water-wet berea. In *SPE/DOE Enhanced Oil Recovery Symposium*. Society of Petroleum Engineers.

Pearce, A., Madathil, A., and Blondeau, C. (2013). A case study of effective immiscible hydrocarbon injection for enhancing oil recovery in a mature oil field. In *SPE Middle East Oil and Gas Show and Conference*. Society of Petroleum Engineers.

Pejic, D. and Maini, B. B. (2003). Three-phase relative permeability of petroleum reservoirs. In *SPE Latin American and Caribbean Petroleum Engineering Conference*. Society of Petroleum Engineers.

Peng, D.-Y. and Robinson, D. B. (1976). A new two-constant equation of state. *Industrial & Engineering Chemistry Fundamentals*, 15(1):59–64.

PERM Inc.

PERM Inc.

PERM Inc.

Pitzer, K. S., Lippmann, D. Z., Curl, R. F., Huggins, C. M., and Petersen, D. E. (1955). The volumetric and thermodynamic properties of fluids. II. compressibility factor, vapor pressure and entropy of vaporization1. *Journal of the American Chemical Society*, 77(13):3433–3440.

Redlich, O. and Kwong, J. N. S. (1949). On the thermodynamics of solutions. v. an equation of state. fugacities of gaseous solutions. *Chemical Reviews*, 44(1):233–244.

Reid, A. (1956). *The flow of three immiscible fluids in porous media*. PhD thesis, The University of Birmingham.

Ren, W., Bentsen, R., and Cunha, L. (2005). A study of the gravity assisted tertiary gas injection processes. *Journal of Canadian Petroleum Technology*, 44(02).

Rowlinson, J. S. (1988). *J.D. Van Der Waals: On the Continuity of the Gaseous and Liquid States (Studies in Statistical Mechanics, Vol 14)*. North-Holland.

Saraf, D. and Fatt, I. (1967). Three-phase relative permeability measurement using a nuclear magnetic resonance technique for estimating fluid saturation. *Society of Petroleum Engineers Journal*, 7(03):235–242.

Satter, A. and Iqbal, G. M. (2015). *Reservoir Engineering: The Fundamentals, Simulation, and Management of Conventional and Unconventional Recoveries*. Gulf Professional Publishing.

Schlumberger (2016a). *Reference Manual*. Schlumberger, 2016.2 edition.

Schlumberger (2016b). *Technical Description*. Schlumberger, 2016.2 edition.

Soave, G. (1972). Equilibrium constants from a modified redlich-kwong equation of state. *Chemical Engineering Science*, 27(6):1197–1203.

Spronsen, E. V. (1982). Three-phase relative permeability measurements using the centrifuge method. In *SPE Enhanced Oil Recovery Symposium*. Society of Petroleum Engineers.

Stone, H. (1970). Probability model for estimating three-phase relative permeability. *Journal of Petroleum Technology*, 22(02):214–218.

Stone, H. (1973). Estimation of three-phase relative permeability and residual oil data. *Journal of Canadian Petroleum Technology*, 12(04).

Whitson, C. H. and Brule, M. R. (2000). *Phase Behavior (Henry L. Doherty series)*. Society of Petroleum Engineers.

Appendix A

Eclipse data files

A.1 Eclipse data file for Experiment 1

```
-------
RUNSPEC
-------

TITLE
Equilibrium gas injection, Experiment 1, of SPE 24116 using Extended
Stone 1

NOECHO

START
 1 JUN 2009 /

LAB

OIL

WATER

GAS

COMPS
6 /

DIMENS
 1 1 74 /

TABDIMS
--NTSFUN NTPVT NSSFUN NPPVT NTFIP
     2      1      50     1*    2  /

EQLDIMS
 1 200 /

WELLDIMS
   4   2 /

-- FMTIN

-- FMTOUT

-- FMTSAVE

UNIFOUT

UNIFOUTS

NOMIX

CPR
/

--IMPES
FULLIMP
--AIM
-- IMPSAT
```

```
----
GRID
----

-- Request output of init file
INIT

-- Core diameter is 3.78 cm
DX
74*3.34993
/

DY
74*3.34993
/

DZ
-- core length 122.6
1*4.37857
8*0.54732125
4*1.0946425
48*2.189285
4*1.0946425
8*0.54732125
1*4.37857
/

NTG
74*1.0
/

TOPS
0.0
   4.37857     4.92589125  5.4732125    6.02053375 6.567855
7.11517625
   7.6624975    8.20981875  8.75714
   9.8517825   10.946425   12.0410625   13.13571
  15.324995    17.51428    19.703565    21.89285     24.082135
26.27142
  28.460705    30.64999    32.839275    35.02856     37.217845
39.40713
  41.596415    43.7857     45.974985    48.16427     50.353555
52.54284
  54.732125    56.92141    59.110695    61.29998     63.489265
65.67855
  67.867835    70.05712    72.246405    74.43569     76.624975
78.81426
  81.003545    83.19283    85.382115    87.5714      89.760685
91.94997
  94.139255    96.32854    98.517825   100.70711    102.896395
105.08568
 107.274965   109.46425   111.653535   113.84282    116.032105
118.22139
```

```
119.3160325  120.410675  121.5053175  122.59996
123.14728125 123.6946025 124.24192375 124.789245 125.33656625
125.8838875
126.43120875 126.97853
/

PERMX
74*2566.0
/

PERMY
74*2566.0
/

PERMZ
74*2566.0
/

-- Bulk volume first and last gridblock is 19.1390975108 cm3
-- Dead end volume top is 11.1717609878 cm3, which gives porosity of
0.583714095269
-- Dead end volume bottom is 1.00004486023 cm3, which gives porosity
of 0.0522514115238
PORO
0.02035 72*0.227 0.02035
/


RPTGRID
TOPS DX DY DZ NTG PERMX PERMY PERMZ PORO
/

-----
PROPS
-----

ZI
0.51639 0.14067 0.06116 0.16916 0.06848 0.04414
/

EOS
SRK
/

RTEMP
-- E300 Units are Celcius
91.9
/

CNAMES
HC1
HC2
HC5
HC9
HC21
HC40
```

```
  /


  MW
  16.236
  36.139
  68.592
  135.992
  279.089
  607.199
  /


  PCRIT
  -- Atm
  45.39847
  45.67481
  33.55539
  25.22576
  15.04071
  13.01752
  /


  VCRIT
  85.93
  150.22
  278.24
  460.17
  1045.56
  1548.19
  /


  TCRIT
  --   K
  190.17
  334.46
  455.12
  565.87
  766.6
  982.43
  /


  ACF
  0.0078
  0.1349
  0.2380
  0.5913
  1.0133
  1.2781
  /


  BIC
  0.0
  0.0   0.0
  0.0   0.0   0.0
  0.0   0.0   0.0   0.0
  0.0   0.0   0.0   0.0   0.0
```

```
 /

 ---SURFACE EOS
 EOSS
 SRK
 /



 MWS
 16.236
 36.139
 68.592
 135.992
 279.089
 607.199
 /

 PCRITS
 -- Atm
 46.44406
 46.72677
 34.32822
 25.47511
 15.18938
 13.14619
 /

 VCRITS
 85.93
 150.22
 278.24
 460.17
 1045.56
 1548.19
 /

 TCRITS
 --   K
 182.3135
 320.6425
 436.3177
 571.3027
 773.9598
 991.8619
 /

 ACFS
 0.00777
 0.134386
 0.237093
 0.591657
 1.013912
 1.278872
 /
```

```
BICS
0.0
0.0  0.0
0.0  0.0  0.0
0.0  0.0  0.0  0.0
0.0  0.0  0.0  0.0  0.0
/




PARACHOR

-- Pi = 59.3+2.34*MWi
  97.29224
 143.86526
 219.80528
 377.52128
 712.36826
1480.14566
/

LBCCOEF
 0.1023 0.023364 0.058533 -0.040758 0.0127642  /

STCOND
--std. temp. std. pres. (atm)
   15.0       0.986923 /

DENSITY
   1* 1.0 1* /
/

PVTW
-- Ref       Water    Water       Water   Water
-- Press     FVF      Comp        Visc Viscob
   309.8939 1.02187 4.40865E-05   0.305      1* / -- Pressure and
1/pressure in atm and 1/atm
/



ROCK
--    Value for rock reference pressure
--    Ref      Rock
--    Press    Comp
-- rock type 1
   309.8939   4.40865E-05   -- Pressure and 1/pressure in atm and
1/atm
/

SWOF
--   SW          KRW           KROW            PCOW (scaled atm)
0.04744         9.00E-07       0.92        0.355842
0.047764        9.00E-07       0.92        0.083883
0.048           0.000001       0.92        0.049888
0.06            0.000002       0.92        0.03629
```

```
0.075             0.000004        0.92        0.03289
0.098296          0.00001         0.92        0.031871
0.115             0.00002         0.92        0.031531
0.12              0.000025        0.915       0.031463
0.13              0.00004         0.9         0.031395
0.145             0.00006         0.885       0.031327
0.16              0.0001          0.852       0.031259
0.17              0.00015         0.83        0.031191
0.18              0.0002          0.8         0.031123
0.19              0.0003          0.75        0.031102
0.2               0.0004          0.7         0.031091
0.22              0.0006          0.595       0.028607
0.24              0.0009          0.565       0.026488
0.26              0.0015          0.52        0.024369
0.285049          0.0025          0.46        0.021191
0.32              0.00559         0.365       0.017934
0.4               0.0167          0.213       0.013798
0.48              0.04            0.103       0.011254
0.52              0.06            0.0554      0.010378
0.56              0.085           0.022       0.009662
0.58              0.098           0.0101      0.009384
0.61              0.123           0.002       0.009066
0.616             0.128           0.0015      0.008986
0.7               0.23            0.0001      0.008112
0.8               0.42            0           0.007396
0.95              0.82            0           0.006601
1                 1               0           0.006402
/
0.0000    0.0000              1.0000          0.0
1.0000    1.0000              0.0000          0.0
/

SGOF
-- SG      KRG         KROG        PCOG (scaled atm)
0          0           0.92        0.000194411
0.16       1.21E-03    0.438       0.00022592
0.18       5.63E-03    0.38        0.000230612
0.22       1.00E-02    0.31        0.000239327
0.26       2.00E-02    0.252       0.000250053
0.34       4.89E-02    0.151       0.000272846
0.38       7.53E-02    0.112       0.000284913
0.44       0.121       0.065       0.000308377
0.5        0.184       0.029       0.000337874
0.54       0.229       0.012       0.000361337
0.56       0.26        0.005       0.000373404
0.57       0.275       0.002       0.000381449
0.58       0.29        0.0005      0.000388153
0.59       0.305       1.00E-05    0.000394856
0.617      0.35        0           0.000414968
0.95256    1           0           0.067038431
/
0.0000    0.0000              1.0000          0.0
1.0000    1.0000              0.0000          0.0
/
```

```
STONE1

STONE1EX
  4.0  /
  1.0  /

-------
REGIONS
-------

PVTNUM
  74*1
/

FIPNUM
 2  72*1  2
/

SATNUM
 2  72*1  2
/

RPTREGS
PSTNUM ISTNUM DSTNUM
SDRGO SDROG SDROW SDRWO SDRGW SDRWG

RPTREGS
SDRGO SDROG SDROW SDRWO SDRGW SDRWG
/

--------
SOLUTION
--------

-- The end gridblocks has volume of 11.1717591644 cm3
-- inlet volume is set to 1 cm3 of water
SWAT
 0.01 72*0.616  0.999 /


SOIL
  0.01  72*0.384  0.001 /


PRESSURE
  74*309.8939  / --314 bar = 309.8939 atm

NEI
0.51639 0.14067 0.06116 0.16916 0.06848 0.04414 /

FIELDSEP
  1  15.0   0.986923  /
/

RPTSOL
 PRESSURE SWAT SOIL SGAS
```

```
 /

 RPTRST
 -- BASIC=2 KRO KRW KRG PCOW PCOG PCGW SOIL SWAT SGAS
  BASIC=2 KRO KRW KRG PCOW PCOG SOIL SWAT SGAS
  /

 -------
 SUMMARY
 -------

 RUNSUM

 --INCLUDE

 FPR
 FOPR
 FOPT
 FWPR
 FWPT
 FWIR
 FWIT
 FGIR
 FGPT
 FGPR
 FGPT
 FGOR
 FODN
 FGDN
 /

 BSWAT
 1  1  10   /
 1  1  70   /
 1  1  72   /
 1  1  35   /
 1  1  2    /
 1  1  5    /
 /

 BSOIL
 1  1  10   /
 1  1  70   /
 1  1  72   /
 1  1  35   /
 1  1  2    /
 1  1  5    /
 /

 BSGAS
 1  1  10   /
 1  1  70   /
 1  1  72   /
 1  1  35   /
 1  1  2    /
```

```
1  1  5     /
/

BWPC
1  1  10   /
1  1  70   /
1  1  72   /
1  1  35   /
1  1  2    /
1  1  5    /
/

BGPC
1  1  10   /
1  1  70   /
1  1  72   /
1  1  35   /
1  1  2    /
1  1  5    /
/

BPCO
1  1  10   /
1  1  70   /
1  1  72   /
1  1  35   /
1  1  2    /
1  1  5    /
/

BPCG
1  1  10   /
1  1  70   /
1  1  72   /
1  1  35   /
1  1  2    /
1  1  5    /
/

BPCW
1  1  10   /
1  1  70   /
1  1  72   /
1  1  35   /
1  1  2    /
1  1  5    /
/

--------
SCHEDULE
--------

CVCRIT
-- DPMAX MAX-NLI LSR MAX-LI MAX-FUG MIN-LI DVMAX DSPE MIN-NLI
   0.01  50      1*  150    1*      1*     1*    1*
/
```

```
TSCRIT
-- TsIni MinTs   MaxTs MaxTsDf MasTsIf TgtTTE MaxTTE TgtTPR MaxTPR
TgtSC
   0.0004  1.0E-10 0.01     1*      1*      1*      1*      0.0005
0.005   0.0250
/

WELLSTRE
'INJCOMP'
0.779171
0.13325
0.037295
0.047617
0.002618
5.01E-05
/
/

GRUPTREE
--'WFILL' 'FIELD' /
'GINJ'  'FIELD' /
 /

-- Define the E300 wells
WELSPECS
--
-- 1    2        3 4  5        6       7    8     9       10    11
12    13-15  16
--              BHP                    Inst            Pres Dens
Well
-- Wll  Group      Ref     Pref   Drng Infl  Auto    Xflow Tab
Calc        Model
-- Nme  Name    I J Dep     Phase Rad  Eqtn  Shut    Enabl Num
Type        Type
'TOP'    'GINJ'  1 1 0.85    'GAS'   1*  'STD' 'SHUT'  'NO'   1*
'SEG'  3*  'STD' /
'BOTTOM' 'GINJ'  1 1 125.15  'OIL'   1*  'STD' 'SHUT'  'NO'   1*
'SEG'  3*  'STD' /
/

COMPDAT
-- 1    2 3 4 5     6      7    8     9      10   11    12    13
14
--                       Sat  Con
Pres
-- Wl   I J K1             Tab  Trans Bore   Eff  Skin  D
Equiv
-- Nm         K2  Status Num  Fact  Diam   Kh   Fact  Fact  Dir
Rad
'TOP'    1 1  1  1 'OPEN'  2   1*  0.004297  1*   1*    1*   'Z'
1* /
'BOTTOM' 1 1 74 74 'OPEN'  2   1*  0.004297  1*   1*    1*   'Z'
1* /
/
```

```
WCONINJE
--    1    2      3      4     5    6     7
--        Inj            Cntl  Surf Res   BHP
--        Type    Status Mode  Rate Rate  Lim
   'TOP'  'GAS'   'OPEN' 'RESV' 1*   2.47  800.0  / -- BHP atm
/

-- Define injected composition
WINJGAS
'TOP' 'STREAM' 'INJCOMP'  /
/

WCONPROD
--    1     2     3     4    5    6    7    8     9
--                                         Res
--              Cntl  Oil  Wat  Gas  Liq  Vol  BHP
--       Status Mode  Rate Rate Rate Rate Rate Lim
   'BOTTOM' 'OPEN' 'BHP' 1*  1*   1*   1*   1*   309.4  / -- BHP
atm
/

SEPCOND
 'SEPARGAS' 'FIELD' 1  15.0  0.986923  3* /
 /

WSEPCOND
 'TOP'     'SEPARGAS' /
 'BOTTOM' 'SEPARGAS' /
/

TIME
0.0001
/

RPTSCHED
--PRESSURE SOIL SWAT SGAS KRO KRW KRG PCOG PCOW PCGW IFTGO IFTGW
IFTOW /
--PRESSURE SOIL SWAT SGAS KRO KRW KRG PCOG PCOW PCGW /
PRESSURE SOIL SWAT SGAS PCOG PCOW /

TIME
0.42743
/

TIME
1.0
/

TIME
5.2121
/

TIME
13.2121
/
```

```
TIME
21.2121
/

TIME
29.2121
/

TIME
37.2121
/

TIME
39.0
/

TIME
39.5
/

TIME
41.03126
/

TIME
45.2121
/

TIME
53.2121
/

TIME
59.39401
/

TIME
61.2121
/

TIME
63.5
/

TIME
64.0
/

TIME
69.2121
/

TIME
77.2121
/
```

```
TIME
85.2121
/

TIME
93.2121
/

TIME
101.2121
/

TIME
109.2121
/

TIME
113.2121
/

TIME
117.2121
/

TIME
125.2121
/

TIME
141.2121
/

TIME
169.2121
/

TIME
203.2121
/

TIME
212.5121
/


END
```

A.2   Eclipse data file for Experiment 2

```
-------
RUNSPEC
-------

TITLE
Dry separator gas injection, Experiment 2, of SPE 24116 using
Extended Stone 1
NOECHO

START
 1 JUN 2009 /

LAB

OIL

WATER

GAS

COMPS
6 /

DIMENS
 1 1 74 /

TABDIMS
--NTSFUN NTPVT NSSFUN NPPVT NTFIP
     2      1     50    1*     2  /

EQLDIMS
2 200 /

WELLDIMS
   4  2 /

-- FMTIN

-- FMTOUT

-- FMTSAVE

UNIFOUT

UNIFOUTS

-- Select nomixing of Kro/Krg for ODD3P
-- This option is selected by default if ODD3P specified in PROPS
Sect.
NOMIX

CPR
/

--IMPES
```

```
FULLIMP
--AIM
-- IMPSAT

--NOSIM

----
GRID
----

-- Request output of init file
INIT

-- Core diameter is 3.77 cm
DX
74*3.34104278615179
/

DY
74*3.34104278615179
/

DZ
-- core length 122.1 cm
1*4.37857
8*0.545089
4*1.0901786
48*2.180357
4*1.0901786
8*0.545089
1*4.37857
/

NTG
74*1.0
/

TOPS
0    4.36071429 4.90580358 5.45089287 5.99598216 6.54107145
7.08616074 7.63125003 8.17633932 8.72142861 9.81160718 10.90178575
11.99196432     13.08214289     15.26250003     17.44285717
     19.62321431     21.80357145
23.98392859     26.16428573     28.34464287     30.52500001
     32.70535715     34.88571429
37.06607143     39.24642857     41.42678571     43.60714285
     45.78749999     47.96785713
50.14821427     52.32857141     54.50892855     56.68928569
     58.86964283     61.04999997
63.23035711     65.41071425     67.59107139     69.77142853
     71.95178567     74.13214281
76.31249995     78.49285709     80.67321423     82.85357137
     85.03392851     87.21428565
89.39464279     91.57499993     93.75535707     95.93571421
     98.11607135     100.2964285
102.4767856     104.6571428     106.8374999     109.0178571
     111.1982142     113.3785713
```

```
115.5589285      117.7392856      118.8294642      119.9196428
       121.0098213      122.0999999
122.6450892      123.1901785      123.7352678      124.2803571
       124.8254463      125.3705356
125.9156249      126.4607142
/

PERMX
74*2645.0
/

PERMY
74*2645.0
/

PERMZ
74*2645.0
/

PORO
0.0204599057211339    72*0.233    0.0204599057211339

/


RPTGRID
TOPS DX DX DZ NTG PERMX PERMY PERMZ PORO
/

-----
PROPS
-----

ZI
0.488001427
0.13596298
0.080436444
0.187865683
0.070975213
0.036758252
/

EOS
SRK
/

RTEMP
-- E300 Units are Celcius
99.0
/

CNAMES
HC1
HC2
HC5
HC9
```

```
HC21
HC40
/

MW
16.236
36.139
68.592
135.992
279.089
607.199
/

PCRIT
-- Atm
45.39847
45.67481
33.55539
25.22576
15.04071
13.01752
/

VCRIT
85.93
150.22
278.24
460.17
1045.56
1548.19
/

TCRIT
--  K
190.17
334.46
455.12
565.87
766.6
982.43
/

ACF
0.0078
0.1349
0.2380
0.5913
1.0133
1.2781
/

BIC
0.0
0.0  0.0
0.0  0.0  0.0
0.0  0.0  0.0  0.0
```

```
 0.0   0.0   0.0   0.0   0.0
 /

 ---SURFACE EOS
 EOSS
 SRK
 /


 MWS
 16.236
 36.139
 68.592
 135.992
 279.089
 607.199
 /

 PCRITS
 -- Atm
 45.59770595
 45.87525869
 33.70265135
 23.97880439
 14.2972201
 12.3740401
 /

 VCRITS
 85.93
 150.22
 278.24
 460.17
 1045.56
 1548.19
 /

 TCRITS
 --   K
 175.8627868
 309.2973006
 420.8795894
 527.7119904
 714.9062715
 916.1823223
 /

 ACFS
 0.008399998
 0.145276884
 0.256307623
 0.636157078
 1.090170754
 1.375058957
 /
```

```
BICS
0.0
0.0  0.0
0.0  0.0  0.0
0.0  0.0  0.0  0.0
0.0  0.0  0.0  0.0  0.0
/



PARACHOR
-- Pi = 59.3+2.34*MWi
97.29224
143.86526
219.80528
377.52128
712.36826
1480.14566
/

LBCCOEF
 0.1023 0.023364 0.058533 -0.040758 0.0127642  /

STCOND
--std. temp. std. pres. (atm)
   15.0       0.986923 /

DENSITY
   1* 1.0 1* /
--/

PVTW
-- Ref       Water     Water       Water    Water
-- Press      FVF      Comp        Visc  Viscob
   309.8939 1.02187 4.40865E-05   0.305      1* / -- Pressure and
1/pressure in atm and 1/atm
--/


ROCK
--   Value for rock reference pressure
--   Ref       Rock
--   Press     Comp
-- rock type 1
   309.8939   4.40865E-05   -- Pressure and 1/pressure in atm and
1/atm
/

SWOF
--SW         KRW              KROW        PCOW (scaled atm)
0.04744    9.00E-07         0.92        0.355842
0.047764   9.00E-07         0.92        0.083883
0.048      0.000001         0.92        0.049888
0.06       0.000002         0.92        0.03629
0.075      0.000004         0.92        0.03289
0.098296   0.00001          0.92        0.031871
```

```
0.115      0.00002    0.92       0.031531
0.12       0.000025   0.915      0.031463
0.13       0.00004    0.9        0.031395
0.145      0.00006    0.885      0.031327
0.16       0.0001     0.852      0.031259
0.17       0.00015    0.83       0.031191
0.18       0.0002     0.8        0.031123
0.19       0.0003     0.75       0.031102
0.2        0.0004     0.7        0.031091
0.22       0.0006     0.595      0.028607
0.24       0.0009     0.565      0.026488
0.26       0.0015     0.52       0.024369
0.285049   0.0025     0.46       0.021191
0.32       0.00559    0.365      0.017934
0.4        0.0167     0.213      0.013798
0.48       0.04       0.103      0.011254
0.52       0.06       0.0554     0.010378
0.56       0.085      0.022      0.009662
0.58       0.098      0.0101     0.009384
0.61       0.123      0.002      0.009066
0.616      0.128      0.0015     0.008986
0.7        0.23       0.0001     0.008112
0.8        0.42       0          0.007396
0.95       0.82       0          0.006601
1          1          0          0.006402
/
0.0000     0.0000         1.0000     0.0
1.0000     1.0000         0.0000     0.0
/

SGOF
--SG       KRG              KROG       PCOG (scaled atm)
0          0                0.92       1.42E-04
0.16       1.21E-03         0.438      1.64E-04
0.18       5.63E-03         0.38       1.68E-04
0.22       1.00E-02         0.31       1.74E-04
0.26       2.00E-02         0.252      1.82E-04
0.34       4.89E-02         0.151      1.99E-04
0.38       7.53E-02         0.112      2.07E-04
0.44       0.121            0.065      2.24E-04
0.5        0.184            0.029      2.46E-04
0.54       0.229            0.012      2.63E-04
0.56       0.26             0.005      2.72E-04
0.57       0.275            0.002      2.78E-04
0.58       0.29             0.0005     2.83E-04
0.59       0.305            1.00E-05   2.87E-04
0.617      0.35             0          3.02E-04
0.95256    1                0          1*
/
   0.0000   0.0000      1.0000          0.0
   1.0000   1.0000      0.0000          0.0
/

STONE1

STONE1EX
```

```
  4.0  /
  1.0  /

 -------
 REGIONS
 -------

 PVTNUM
  74*1
 /

 FIPNUM
  2  72*1  2
 /

 SATNUM
  2  72*1  2
 /

 EQLNUM
   1  73*2  /

 RPTREGS
 PSTNUM ISTNUM DSTNUM
 SDRGO SDROG SDROW SDRWO SDRGW SDRWG

 RPTREGS
 SDRGO SDROG SDROW SDRWO SDRGW SDRWG
 /

 --------
 SOLUTION
 --------

 EQUIL
 --   1            2           3        4       5       6   7  8   9
 10
 -- Datum      Pressure      WOC     Pcow    GOC    Pcgo
 -- depth                    depth   WOC   depth   GOC
   2.37857    310.880829 / -- 126.4785458  0.0  4.37857   0.0   1* 1*
 0   2  /
 126.4785458  310.880829 / -- 126.4785458  0.0  4.37857   0.0   1* 1*
 0   1  /

 -- The end gridblocks has volume of 11.1717591644 cm3
 -- inlet volume is set to 1 cm3 of water
 SWAT
      0.0001 72*0.616  0.9999 /


 SOIL
      0.0   72*0.384  0.0001 /

 PRESSURE
   74*310.880829   / --315 bar = 310.880829 atm
```

```
NEI
0.8198
0.14712
0.02949
0.00359
0.0
0.0 /
0.488001427
0.13596298
0.080436444
0.187865683
0.070975213
0.036758252 /

FIELDSEP
  1  15.0   0.986923  /
/

RPTSOL
 PRESSURE SWAT SOIL SGAS
/

RPTRST
 BASIC=2 KRO KRW KRG PCOW PCOG SOIL SWAT SGAS
 /

-------
SUMMARY
-------

RUNSUM

--INCLUDE

FPR
FOPR
FOPT
FWPR
FWPT
FWIR
FWIT
FGIR
FGPT
FGPR
FGPT
FGOR
FODN
FGDN
FYMF
/
BDENO
1 1 10 /
1 1 20 /
1 1 40 /
/
BDENG
```

```
1 1 10 /
1 1 20 /
1 1 40 /
/

BSWAT
1  1  10   /
1  1  70   /
1  1  72   /
1  1  35   /
1  1  2    /
1  1  5    /
/

BWPC
1  1  10   /
1  1  70   /
1  1  72   /
1  1  35   /
1  1  2    /
1  1  5    /
/

BGPC
1  1  10   /
1  1  70   /
1  1  72   /
1  1  35   /
1  1  2    /
1  1  5    /
/

BPCO
1  1  10   /
1  1  70   /
1  1  72   /
1  1  35   /
1  1  2    /
1  1  5    /
/

BPCG
1  1  10   /
1  1  70   /
1  1  72   /
1  1  35   /
1  1  2    /
1  1  5    /
/

BPCW
1  1  10   /
1  1  70   /
1  1  72   /
1  1  35   /
1  1  2    /
```

```
1  1  5    /
/

-------
SCHEDULE
--------

CVCRIT
-- DPMAX MAX-NLI LSR MAX-LI MAX-FUG MIN-LI DVMAX DSPE MIN-NLI
   0.01  50       1*  150    1*      1*    1*    1*
/

TSCRIT
-- TsIni MinTs   MaxTs MaxTsDf MasTsIf TgtTTE MaxTTE TgtTPR MaxTPR
TgtSC
   0.0004  1.0E-10 0.01  1*      1*      1*      1*     0.0005
0.005   0.0250
/

WELLSTRE
'INJCOMP'
8.20E-01
1.47E-01
2.95E-02
3.59E-03
0.00E+00
0.00E+00
/
/

GRUPTREE
--'WFILL' 'FIELD' /
'GINJ'  'FIELD' /
 /

-- Define the E300 wells
WELSPECS
--
-- 1    2       3 4 5      6      7    8     9      10    11
12    13-15  16
--               BHP               Inst         Pres Dens
Well
-- Wll  Group      Ref     Pref   Drng Infl  Auto   Xflow  Tab
Calc       Model
-- Nme  Name    I J Dep     Phase  Rad  Eqtn  Shut   Enabl  Num
Type       Type
'TOP'     'GINJ'  1 1 0.85    'GAS'   1*  'STD' 'SHUT' 'NO'   1*
'SEG'  3*  'STD' /
'BOTTOM' 'GINJ'  1 1 125.15  'OIL'   1*  'STD' 'SHUT' 'NO'   1*
'SEG'  3*  'STD' /
/

COMPDAT
-- 1     2 3 4 5     6      7    8     9       10   11    12    13
14
```

```
--                       Sat  Con
Pres
-- Wl    I J K1          Tab  Trans Bore   Eff  Skin  D
Equiv
-- Nm           K2    Status Num  Fact  Diam      Kh   Fact Fact Dir
Rad
'TOP'    1 1  1  1   'OPEN'  2   1*   0.004297  1*   1*   1*     'Z'
1* /
'BOTTOM' 1 1 74 74   'OPEN'  2   1*   0.004297  1*   1*   1*     'Z'
1* /
/

WCONINJE
--    1     2      3       4     5     6      7
--       Inj              Cntl  Surf  Res   BHP
--       Type     Status  Mode  Rate  Rate  Lim
   'TOP'  'GAS'   'OPEN'  'RESV' 1*    2.58  800.0/ -- BHP atm

/

-- Define injected composition
WINJGAS
'TOP' 'STREAM' 'INJCOMP'  /
/

WCONPROD
--    1     2      3     4     5     6     7     8      9
--                                         Res
--              Cntl  Oil   Wat   Gas   Liq   Vol  BHP
--       Status Mode  Rate  Rate  Rate  Rate  Rate Lim
   'BOTTOM' 'OPEN' 'BHP' 1*  1*    1*    1*    1*   310.880829  /  --
BHP atm
/

SEPCOND
 'SEPARGAS' 'FIELD' 1  15.0  0.986923  3* /
 /

WSEPCOND
 'TOP'    'SEPARGAS' /
 'BOTTOM' 'SEPARGAS' /
/

TIME
0.0001
/

RPTSCHED
PRESSURE SOIL SWAT SGAS PCOG PCOW KRO KRW KRG/

TIME
0.42743
/

TIME
1.0
```

```
/

TIME
5.2121
/

TIME
13.2121
/

TIME
21.2121
/

TIME
29.2121
/

TIME
37.2121
/

TIME
39.0
/

TIME
39.5
/

TIME
41.03126
/

TIME
45.2121
/

TIME
53.2121
/

TIME
59.39401
/

TIME
61.2121
/

TIME
63.5
/

TIME
64.0
```

```
/

TIME
69.2121
/

TIME
77.2121
/

TIME
85.2121
/

TIME
93.2121
/

TIME
101.2121
/

TIME
109.2121
/

TIME
113.2121
/

TIME
117.2121
/

TIME
125.2121
/

TIME
141.2121
/

TIME
169.2121
/

TIME
203.2121
/

TIME
212.2121
/

TIME
253.2121
```

```
/

TIME
303.243
/
TIME
418
/

END
```